5-1-2012

Decellularized Porcine Myocardium as a Scaffold for Cardiac Tissue Engineering

Bo Wang

DECELLULARIZED PORCINE MYOCARDIUM AS A SCAFFOLD FOR CARDIAC TISSUE ENGINEERING

By

Bo Wang

A Dissertation
Submitted to the Faculty of
Mississippi State University
in Partial Fulfillment of the Requirements
for the Degree of Doctor of Philosophy
in Biomedical Engineering
in the Department of Agricultural and Biological Engineering

Mississippi State, Mississippi

May 2012

DECELLULARIZED PORCINE MYOCARDIUM AS A SCAFFOLD FOR CARDIAC TISSUE ENGINEERING

By

Bo Wang

Approved:

Jun Liao Assistant Professor of Biomedical Engineering (Major Professor and Director of Dissertation)	Steven H. Elder Professor of Biomedical Engineering (Committee Member)
Jim Cooley Professor of Pathobiology and Population Medicine (Committee Member)	Lakiesha N Williams Assistant Professor of Biomedical Engineering (Committee Member)
S. D. Filip To Associate Professor of Agricultural and Biological Engineering (Committee Member)	Steven H. Elder Professor and Graduate Coordinator of Biomedical Engineering
Sarah A. Rajala Dean of Engineering	

Name: Bo Wang

Date of Degree: May 11, 2012

Institution: Mississippi State University

Major Field: Biomedical Engineering

Major Professor: Dr. Jun Liao

Title of Study: DECELLULARIZED PORCINE MYOCARDIUM AS A SCAFFOLD FOR CARDIAC TISSUE ENGINEERING

Pages in Study: 122

Candidate for Degree of Doctor of Philosophy

Myocardial infarction (MI) and heart failure are leading causes of mortality globally. Recently, cardiac tissue engineering has become an attractive option for MI treatment due to the following advantages: it might provide optimal tissue performance maintained by viable transplanted cells, and might also stimulate the formation of vasculature supplying oxygen and nutrients in the patched region. However, fabrication of a thick viable cardiac patch with 3D scaffolds that are thoroughly recellularized with desired cells remains a challenge.

We hypothesize that the decellularized porcine myocardium scaffold can preserve natural extracellular matrix (ECM) structure, cardiomyocyte lacunae, mechanical properties, and vasculature templates that are able to facilitate stem cell reseeding, proliferation, cardiomyocyte differentiation, and angiogenesis. In this dissertation, we have (i) assessed the potential of the decellularized porcine myocardium as a scaffold for thick cardiac patch tissue engineering; (ii) thoroughly characterized the structural and biomechanical properties of the myocardial ECM; (iii) designed and built a novel bioreactor that could provide coordinated mechanical and electrical stimulations, and (iv)

evaluated the efficiency of the multi-stimulations on the development of a cardiac tissue construct.

An optimized decellularization protocol has been identified to obtain the acellular myocardial scaffold that preserves subtle ECM composition and ultrastructure. We recellularized the acellular scaffold with bone marrow mononuclear cells using a rotating bioreactor and observed successful recellularization with good cell viability, proliferation, and differentiation in a 2-week culture time. Furthermore, we have successfully built a novel bioreactor that is able to provide coordinated mechanical and electrical stimulations for facilitating stem cell differentiation and tissue construct development. We found that cardiomyocyte differentiation and tissue remodeling were more effectively and efficiently promoted with the coordinated simulations, evidenced by good cell viability, proliferation, differentiation, positive tissue remodeling, and a trend of angiogenesis in a short period of time (2 - 4 days).

The clinical product that we envision will benefit from the natural architecture of myocardial ECM, which has the potential to promote stem cell differentiation, cardiac regeneration, and angiogenesis. The hopes are that our novel approach will ultimately impact thousands of patients who have suffered significant damage from a prior myocardial infarction.

DEDICATION

This work is dedicated to my parents and my whole family in China. They are my spirit support and indeed the source of my inspiration.

ACKNOWLEDGEMENTS

I would like to thank my advisor, Dr. Jun Liao, for his indispensable knowledge, experience, guidance, and support during the past five years. The opportunities he has offered to me have been both valuable and enjoyable in regards to not only my professional progress, but growth as a person. I would also like to thank Dr. Filip To for his kind help in guiding me to finish the bioreactor fabricating and programming. Thanks also to my other committee members, Dr. Steve Elder, Dr. Lakiesha Williams, and Dr. Jim Cooley, for their expertise, and making my learning experience even more valuable. I have learned so much from the above mentioned mentors and could not have been blessed with better people to work with.

In addition, I would to thank all of the past and present members of the Tissue Bioengineering Laboratory and Tissue Engineering Research Center, Ali Borazjani, Ben Weed, Mina Tahai, Joseph Chen, Lauren B. Priddy, Robbin Bertucci, Sourav Patnaik, and Katherine Gilbert. I greatly appreciated all supports and helps from the Department of Biological Engineering during my study here. I would like to thank Bill Monroe and Amanda Lawrence at the Electron Microscope Center for their help in image observation. Support from Sansing Meat Service (Maben, MS) is also greatly appreciated. I would also like to acknowledge my project collaborators, Dr. Mary Tedder and Dr. Dan T. Simionescu in Clemson University, and Ms. Alayne White and Dr. Amy L de Jongh Curry in Memphis University, whom deserve special recognition for their dedication and effort.

At last, I would like to acknowledge the financial support provided by the following grants from the NIH National Heart, Lung, and Blood Institute (HL097321), Health Resources and Services Administration (HRSA) (DHHS R1CRH10429-01-00) and the MAFES Strategic Research Initiative Funding (CRESS MIS-741110).

TABLE OF CONTENTS

LIST OF TABLES

LIST OF FIGURES

LIST OF ABBREVIATIONS

Myocardial Infarction (MI)

Three-Dimensional (3-D)

Mitral Valve (MV)

Tricuspid Valve (TV)

Aortic Valve (AV)

Pulmonary Valve (PV)

Left Ventricular (LV)

Embryonic Stem Cells (ESCs)

Induced Pluripotent Stem Cells (iPS)

Bone Marrow Mesenchymal Stem Cells (MSCs)

Polyglycolic Acid (PGA)

Polylactic Acid (PLLA),

Poly (Caprolactone) (PCL),

Poly(Ethylene Oxide) (PEO)

Poly(Vinyl Alcohol) (PVA)

Extracellular Matrix (ECM)

Small Intestine Submucosa (SIS)

U S Food and Drug Administration (FDA)

Polytetrafluoroethylene (ePTFE)

Bone Marrow Mononuclear Cells (BMMCs)

Phosphate Buffered Saline (PBS)

Sodium Dodecyl Sulfate (SDS)

Phenylmethylsulfonylfluoride (PMSF)

Antibiotics/Antimycotics (ABAM)

Low-glucose Dulbecco's Modified Eagle's Medium (L-DMEM)

Fetal Bovine Serum (FBS)

Hematoxylin and Eosin (H&E)

Von Willebrand Factor (vWF)

Myosin Heavy Chain (MHC)

Muscle/Scaffold Fiber Preferred Direction (PD)

Cross Preferred Direction (XD)

One Way Analysis of Variances (ANOVA)

CHAPTER I

INTRODUCTION

1.1 Human Heart

The basic function of the human heart is to circulate blood, which carries vital supplies throughout the whole body. A four-chambered muscular pump design helps the heart realize its function with the assistance of four heart valves that direct blood flow in only one direction through the heart.

The heart has two upper chambers named as right and left atria tasked with the function of accepting blood and two lower chambers known as right and left ventricles tasked with the function of expelling blood (Figure 1.1). The blood flow begins from the right atrium, in which blood is received from the whole body, and in turn directs blood flow into the right ventricle. The right ventricle then pumps the blood through the pulmonary artery to the lungs to be reoxygenated. The left atrium receives oxygenated blood from the lungs and then directs the blood into the left ventricle, which pumps it out to the body via the aorta. The human heart is a special organ with unique pumping function, which is largely made possible by the cardiac muscles.

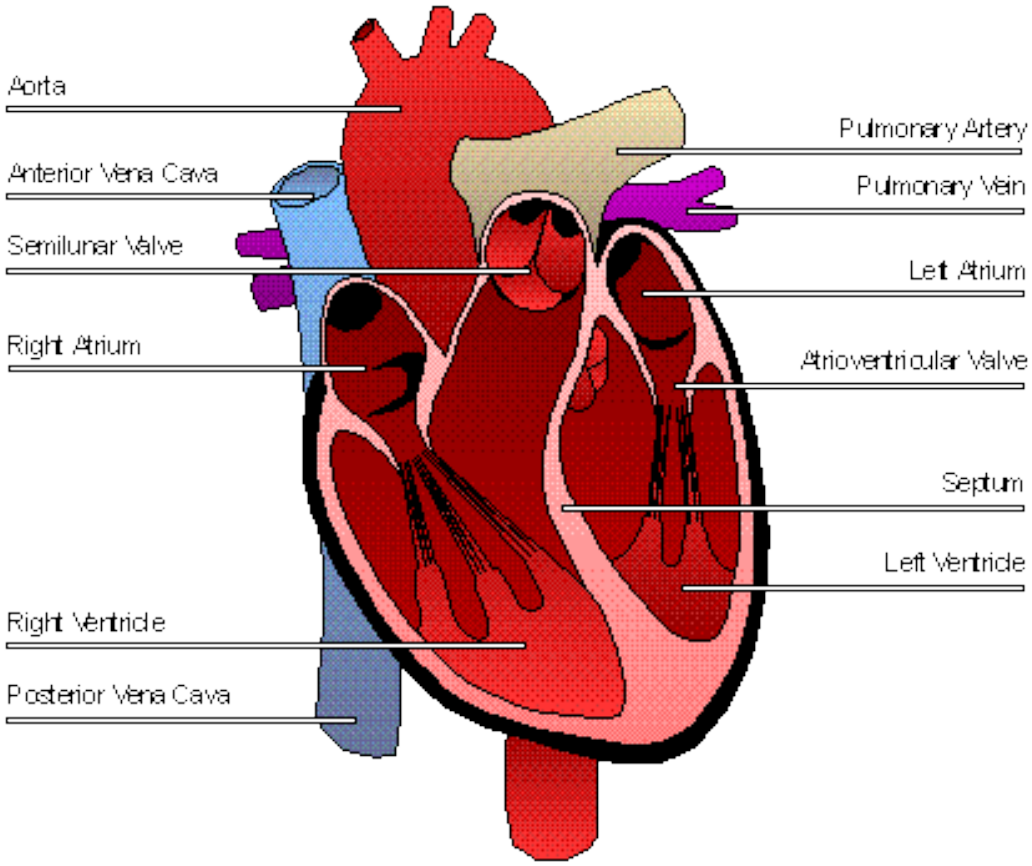

Figure 1.1 The anatomy of the human heart. From http://www.worldinvisible.com/apologet/humbody/heart.htm

1.2 Heart Muscle: Structure and Function

Cardiac muscles are special muscles which construct the heart walls, and they resemble skeletal muscles in some respects: they are striated, and each cell contains sarcomeres with sliding filaments of actin and myosin (Figure 1.2).

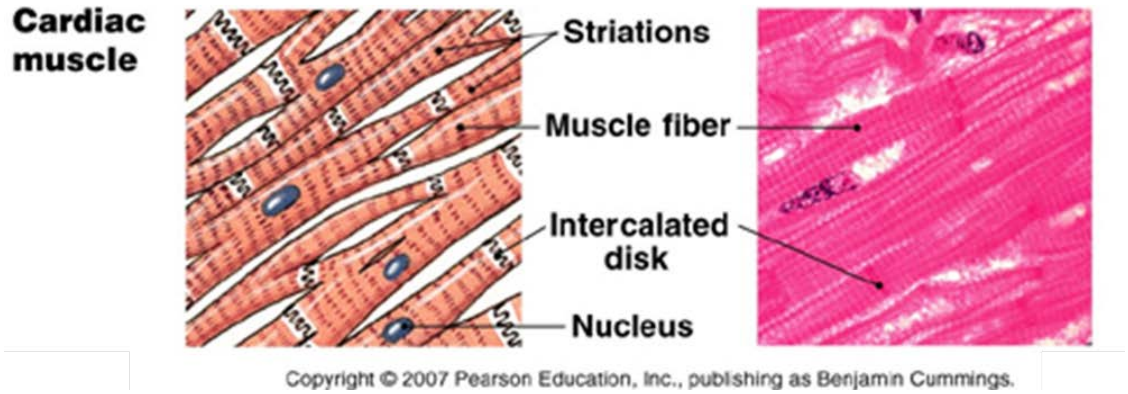

Figure 1.2 Structure of myocardium. 2007 Pearson Education, Inc,. publishing as Benjamn Cummings

Cardiac muscles have several unique features that reflect their function of pumping blood. One of the distinct features is that they are branched with alternate thick (myosin) and thin (actin) protein filaments. Myosin and actin are the two key proteins of the cardiac muscle fibers known as myofibrils. Sarcomeres are the sub-units of myofibrils that generate the contractile forces. Actin molecules all attach to the Z lines (Z-discs), which separate the adjacent sarcomeres and show the dark lines perpendicular to the muscle fiber length under TEM (Figure 1.4). The Z-lines are important connections where muscle contraction signals and forces are being transferred. Among muscle fibers, are electrical gap junctions that enable the action potential that drives contraction of the heart which passes from fiber to fiber. Moreover, the adjacent myofibril branches are connected with adherens junctions that provide strong mechanical coupling and attachments and transfer forces, which enables the heart to contract and expand in a coordinated fashion.

The heart muscles have a well-organized multilayered helical architecture as shown by the Diffusion Tensor-Magnetic Resonance Image (DT-MRI, Figure 1.3-a). The multilayered helical structure has been found essential for global heart contraction, and

this muscle architecture is mediated by a complicated 3D myocardial ECM. Besides, cardiac muscles have an abundant blood supply and a much richer supply of mitochondria than skeletal muscles that cause them to have a greater dependence on cellular respiration for ATP (Figure 1.3-a). The above structures allow the heart to easily contract and expand with the action potential signal spreading through it periodically.[1] However, the heart muscles die easily when the oxygen supply is low, as in the case of a heart attack and myocardial infarction usually happens.[2]

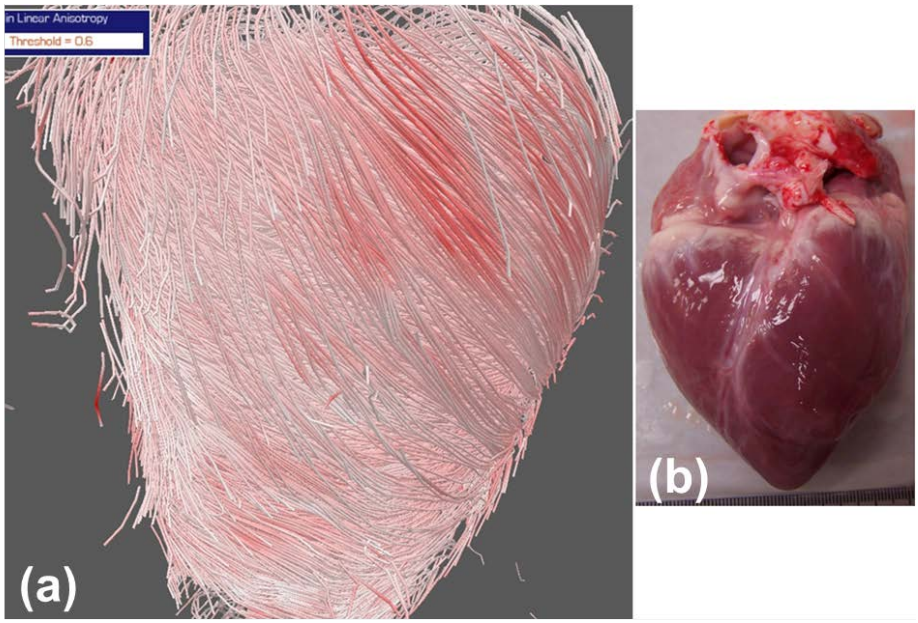

Figure 1.3 (a) Heart muscles have well-organized multilayered helical architecture, which is mediated by 3D ECM (Diffusion Tensor MRI image by Zhang and Liao, 2008); (b) Porcine heart used for DT-MRI image shown in panel (a).

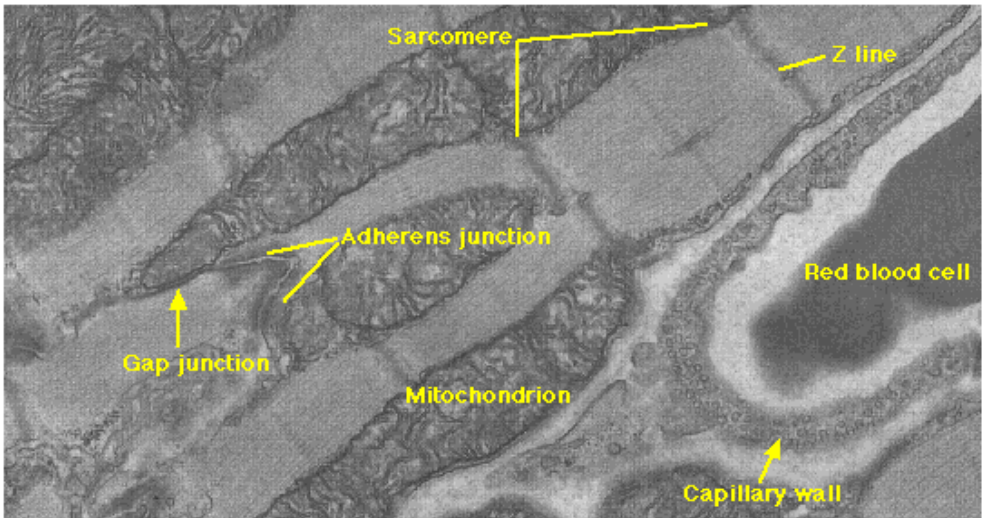

Figure 1.4 Electron micrograph of myocardium.(Keith R. Porter and Mary A. Bonneville, An Introduction to the Fine Structure of Cells and Tissues, 4th ed, Lea&Febiger, Philadephia, 1973)

1.3 Myocardial Infarction and Treatments

1.3.1 Myocardial infarction (MI)

Myocardial infarction (MI) (Figure 1.5) and heart failure are the leading causes of mortality globally.[3] Each year, approximately one million Americans suffer from MI with a 10% in-hospital mortality rate.[4] Acute MI, which is characterized by necrosis of a portion of the heart muscle, is one of the most frequent causes of death in the United States and other developed countries (Figure 1.5). The progressive pathological changes of MI include an initial inflammatory response,[2] loss of cardiomyocytes,[5, 6] and degradation of the left ventricular (LV) extracellular matrix (ECM) by matrix metalloproteases,[7, 8] which lead to wall thinning, infarct expansion,[9, 10] scar tissue formation, LV dilatation, and decrease in cardiac function.[11] If the amount of myocardium loss as a result of the MI is large, significant mechanical complications such as left ventricular dilatation, arrhythmias, mitral regurgitation, and heart failure can occur, each of which can be fatal.[12, 13] [14]

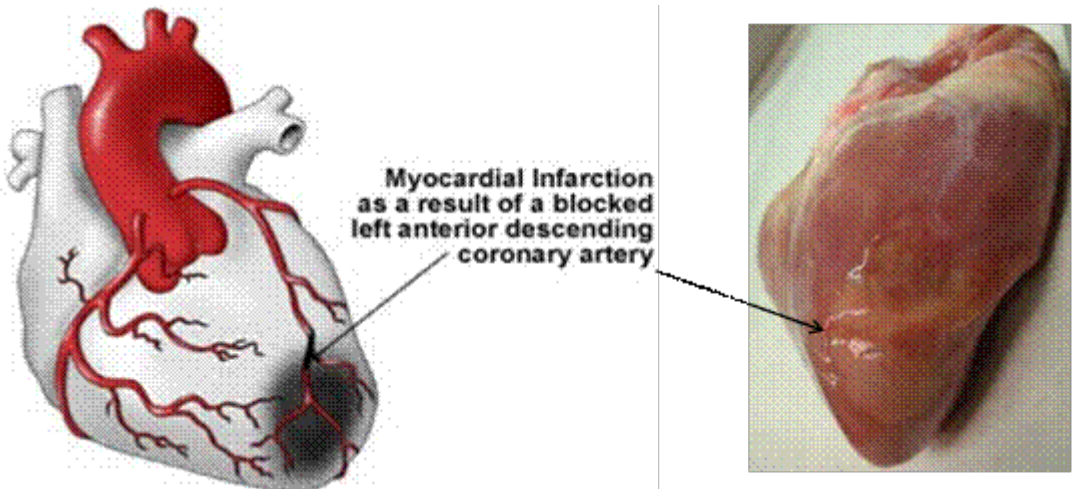

Figure 1.5 Myocardium infraction of a porcine heart after coronary artery blockage. If the amount of myocardium loss as a result of the MI is large, significant mechanical complications can occur.

1.3.2 Standard Treatments for MIs

The main goal of all the treatments to MIs is to prevent the adverse remodeling of the left ventricle that leads to heart failure.[15] Standard treatments of acute MI include prompting revascularization as complete as possible with a fibrinolytic agent and surgery therapy (angioplasty or coronary artery bypass grafting), which aim to limit the infarction size and prevent extension of the infarction. Other treatments include pain relief with morphine, anti-platelet medication, beta blockers, and angiotensin-converting enzyme inhibitors.[14] For end-stage heart failure, the only successful treatment currently is total heart transplantation. Unfortunately, there is limited availability of suitable heart donors for every patient who is progressing to a severe cardiomyopathy, and some people die while waiting for a heart transplant.

1.3.3 Newer Treatment for MIs

Current studies have demonstrated that the adult heart lacks self-healing ability by any native processes for the reason that cardiac myocytes have limited regeneration

abilities to replace the injured cells.[16-18] Recent researches on MI treatment are focusing on either avoiding scar formation,[19] or replacing formed scar tissue with functioning cardiac muscle.[20, 21] Newer strategies have come to the forefront as viable alternatives, such as cellular transplantation (myoblast/stem cell injection), intramyocardial gene transfer, and cardiac tissue engineering.[22, 23] [24] The ultimate goal of interventions is to prevent further left ventricular dilation and pathological remodeling. Among those newer treatments, cellular transplantation [22] and cardiac tissue engineering are two commonly studied approaches for cardiac tissue regeneration therapy.[23, 24]

For the *in situ* cellular transplantation therapy, new cells are injected into the infarction region in order to replace the damaged cells and improve the cardiac tissue function.[25-27] However, this cell therapy has met with limited success due to the lack of an appropriate extracellular environment for the retention of transplanted cells; the lack of extracellular environment also impedes the integration of the repair region with the host tissue both structurally and biomechanically.[28, 29] Cardiac patch tissue engineering is another strategy that aims at fabricating tissue constructs that can restore basic cardiac function by integrating cellular components within scaffolds that serve as a structural guide.[30-33]

1.4 Tissue Engineered Cardiac Patch

The tissue engineered cardiac patch has been developed to repair an injured heart and restore cardiac function. Polymeric and tissue derived materials such as polytetrafluoroethylene (ePTFE), Dacron, and chemical treated pericardium have been used as patch material.[34, 35] However, nonviable patches have limitations including

an inflammatory response, mismatched mechanical properties, and thrombosis.[35] Recently, the tissue engineering approach has attracted significant interest.[30-33] The ideal tissue engineered cardiac patch would provide optimal structural, mechanical, and electrophysiological properties maintained by viable transplanted cells, and might also stimulate the formation of vasculature that can supply oxygen and nutrients.[36] Currently, two major approaches have been investigated intensively to identify the ideal scaffolds: one is to use synthetic biodegradable material and the other is to use tissue-derived acellular scaffolds.[10, 11][4, 16, 17]

1.4.1 Synthetic Biodegradable Polymers

Synthetic biodegradable polymers, such as polyglycolic acid (PGA), polylactic acid (PLLA), poly ester (urethane urea), poly (caprolactone) (PCL), poly (ethylene oxide) (PEO), and poly (vinyl alcohol) (PVA), have been used as scaffold materials.[34, 35, 37-40] The advantages of polymeric materials include that they are biodegradable, and can be made reproducibly with certain material and structural properties.[37, 41, 42] However, the synthetic polymeric approach is still facing issues such as inflammatory response, mismatched material properties, nonpliability, and challenges in controlling the degradation rates.[34] [43, 44]

1.4.2 Tissue-derived Acellular Scaffolds

Recently, decellularized scaffolds derived from native tissues have gained significant attentions.[34, 45-53] The basic concept of decellularization is to remove all cellular and nuclear components from a tissue or an organ, thus leaving the complex mixture of structural and functional proteins that constitute the ECM.[48, 54-56] The major advantage of the decellularization approach is that the mechanical and biological

properties of the ECM can be well preserved.[48, 54-56] The most robust and effective decellularization methods include a combination of physical, chemical, and enzymatic approaches. The working principle of these methods is that the cell membrane was disrupted and the cell contents were released and rinsed away.[27] The removal of cellular content and antigens reduces foreign body reaction, inflammation, and potential immune rejection.[48] Various decellularized ECMs, including small intestine submucosa (SIS), pericardium, skin, and heart valves, have gotten US Food and Drug Administration (FDA) approval and have been successfully used in both pre-clinical animal studies and in human clinical applications.[57] In short, the advantages of the decellularization approach are (i) efficient removal of all cellular and nuclear content and (ii) preservation of ECM composition, biologic activity, and mechanical integrity.[48] We hence take the decellularization approach in the dissertating research.

1.4.3 Cardiac ECM Structure

Myocardial ECM is an intriguing network that mediates complex muscle fiber architecture and maintains unique cell to cell interconnections.[58-61] Composed of collagen (type I and III) fiber network, elastin, proteoglycans, and glycosaminoglycans (GAGs).[58-61] The intriguing myocardial ECM network provides important functions in maintaining structural integrity, tethering myocytes and mediating their contraction/relaxation, and preventing excessive stretching.[62-64] Macchiarelli and Ohtani digested the native myocardium with NaOH and revealed the lacuna morphology and ultrastructure in the cardiac ECM by SEM (Figure 1.5).[61] This cardiac ECM structure revealed by Macchiarelli and Ohtani showed the challenges of scaffold fabrication or preparation, i.e., how to obtain interconnecting open pores that will later

house the reseeded cells and provide structural and mechanical cues for cardiomyocyte differentiation/functioning.

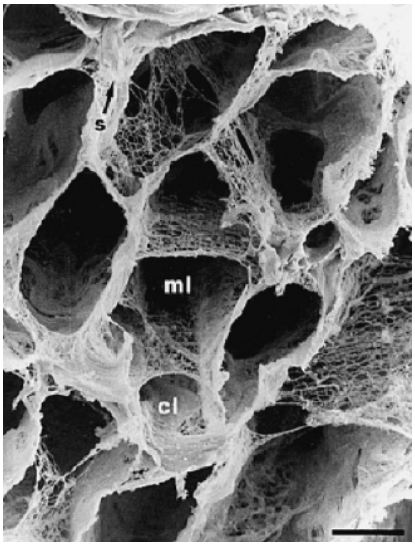

Figure 1.6 SEM of cardiac ECM ultrastructure showed the morphology of cardiomyocyte lacunae. Native myocardium was digested with NaOH to expose the ECM structure (Macchiarelli and Ohtani, 2001).

1.4.4 Cardiac Tissue Engineering using Decellularized Myocardium

As milestone study, Ott et al. showed a revitalized beating rat heart by recellularizing a decelluarized intact rat heart with cardiac and endothelial cells via a perfusion bioreactor.[65] Ott et al. found that the decellularization was able to thoroughly remove cells/cell debris and retain perfusable vascular architecture, competent acellular valves and intact chamber geometry.[65] A pump function similar to 2% of adult or 25% of 16-week fetal heart was observed under a physiological load and electrical stimulation. Ott's study revealed that acellular myocardial ECM itself might provide the most optimal ECM environment for cardiac tissue engineering.

Another approach, currently undertaken by Badylak laboratory [66] and Taylor laboratory, is to scale up whole heart tissue engineering from rat heart to pig heart.

Apparently, many questions and technique hurdles, such as the reseeding of thick tissue scaffold, feasibility of using existing vasculature network, and angiogenesis in thick tissues, need to be addressed before any scaling up attempts. We hence set up our current research goals on the decellularized porcine myocardium at patch scale.

1.5 Cell Sources

1.5.1 Cell Sources in Cardiac Tissue Engineering

Various cell types, such as bone marrow stem cells, umbilical stem cells, embryonic stem cells, cardiac stem cells, induced pluripotent cells, fetal cardiomyocytes, and skeletal myoblasts, have been investigated as cell sources for cardiac recellularization (Table 1.1).[67-71]

Skeletal myoblasts have advantages such as their capability of regeneration and differentiation into 'cardiac-like'' myocytes and low risk of tumor formation.[72] Nevertheless, the limitation of skeletal myoblasts is that they do not synthesize gap junctions and often cause ventricular arrhythmias in clinical trials.[72] Cardiac stem cells are able to self-renew, expand, and differentiate into both cardiomyocyte and vascular lineages.[73] However, cardiac stem cells isolated from an aging heart may not be able to improve cardiac function sufficiently. Embryonic stem cells (ESCs) can be isolated directly from the inner cell mass of embryos at the blastocyst stage.[74] They can divide for unlimited passages in culture and can be differentiated into cardiomyocytes[74][74] [27, 40, 57, 75] by forming embryoid bodies.[76] Nevertheless, the major ethical conflict and the possibility of teratoma formation are currently the major considerations.[76] After reprogramming, induced pluripotent stem (iPS) cells provide autologous patient-specific pluripotent cell lines, which can be directed into specific cell lineages.[77] They

have potential to differentiate into beating cardiomyocytes, smooth muscle cells, and endothelial cells, yet the fate of iPS cells still need to be better understood.[78] Lastly, bone marrow mesenchymal stem cells (MSCs) have also been found to have the capacity to regenerate myocardium, induction of angiogenesis, and they are free from ethical issues.[22, 71, 79, 80]

Table 1.1 Cell source being studied for myocardial regeneration. [72]

Cell Type	Advantages	Disadvantages
Skeletal myoblasts	Capability of differentiation into 'cardiac-like" myocytes low risk of tumor formation	Do not synthesize gap junctions
Cardiac stem cells	Can be self-renewed, expanded, and capable of differentiating into both cardiomyocyte and vascular lineages	Cells isolated from aging hearts may not capable to improve cardiac function sufficiently
Embryonic stem cells	Divide for unlimited passages in culture and can be differentiated into cardiomyocytes	Ethical conflict and possibility of teratoma formation
Induced pluripotent cells	Have potential to differentiate into beating cardiomyocytes, smooth muscle cells, and endothelial cells	
Mesenchymal stem cells	Be able to regenerate myocardium, induction of angiogenesis, and free from ethical issues	Limited success in clinical trials

1.5.2 Bone Marrow MSCs

Bone marrow MSCs are one of the good candidates for cell therapy of MIs for the reason that they maintain cell biological properties typically associated with stem cells including continuous self-renewal ability and the multipotency of differentiation.[81, 82] Besides, MSCs are relatively easy to isolate, expand, and genetically modify *in vitro*, and they are free from ethical issues.[83, 84] Based on these unique properties, MSCs have

been applied as a therapeutic cell source for a large variety of applications. The first use of MSCs in humans is the adjunct therapy to hasten and improve engraftment in the 1990s.[85] Since then, MSCs have been used in therapies and researches including inflammatory diseases,[86, 87] gene therapies,[88] and tumor treatments.[89]

Most recently, MSCs have been wildly used in tissue engineering applications, which utilized their capacity to differentiate into adipose cells, bone cells, chondrocytes,[81, 90-93] endothelial cells,[82] cardiac cells,[94] neurogenic cells,[95-97] and neovascular cells (Figure 1.6).[98-100] In the field of cardiovascular tissue regeneration, MSCs have also been widely applied in both clinical treatment and researches. Animal experiments demonstrated that MSCs transplantation can reduce myocardial infarction size, improve left ventricular function, and increase vascular density and myocardial perfusion.[75, 101-104].[105]

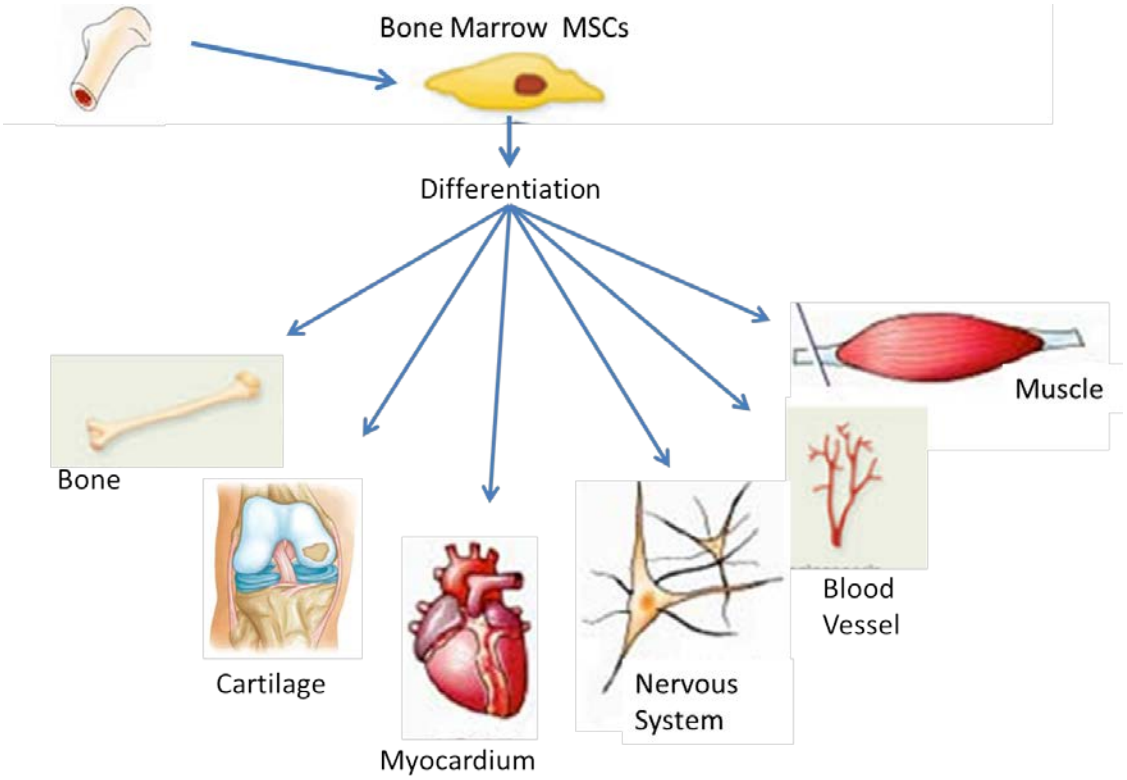

Figure 1.7 Multipotency of bone marrow MSCs.[105]

1.6 Specific Aims

In this project, we propose to investigate the decellularized porcine myocardial scaffold as a potential template for tissue engineering of thick cardiac patch. The acellular myocardial scaffold can be perceived as a means of mechanical restoration, as well as a facilitator for stem cell differentiation and a cell delivery vehicle.

We hypothesize that (i) the decellularized porcine myocardium scaffold will preserve natural ultrastructural, mechanical, and compositional cues for cardiac tissue regeneration and (ii) the 3D porous ECM structure and vasculature templates will provide optimal microenvironments for stem cell reseeding, cardiomyocyte differentiation, and angiogenesis. A novel bioreactor, which provides coordinated mechanical and electrical

stimulations, will be developed to facilitate *in vitro* conditioning of the tissue constructs. The hypotheses will be addressed in the following aims:

Specific Aim 1: Develop optimal decellularization and recellularization protocols for porcine myocardium to generate a thoroughly reseeded construct (Chapter 2 and 3). Different decellularization and recellularization protocols will be evaluated to determine the optimal approach that generates a 3D open porous scaffold with natural structural, mechanical, and ECM cues, and later thorough cell reseeding. The structural and biomechanical properties of the acellular myocardial ECM will also be characterized in great detail. The endpoint of this aim will be to identify the scaffold engineering and reseeding protocols that provide a construct with optimal recellularization (good viability, high density, and thorough reseeding).

Specific Aim 2: Fabricate a novel bioreactor that provides coordinated mechanical and electrical stimulations to facilitate stem cell differentiation (Chapter 4 and 5).

In the *in vitro* bioreactor conditioning procedure, an electrical stimulus, along with mechanical signaling, will be applied when each unloading cycle starts. Static cell culture, mechanical stimulation alone, and electrical stimulation alone will be used as controls. Biochemical cues to promote cardiomyocyte differentiation will be delivered correspondingly. The endpoint of this aim will be to assess whether the coordinated mechanical and electrical stimulations more efficiently and effectively promote MSCs to differentiate towards a cardiomyocyte phenotype.

1.7 References

1. Walker, C.A. and F.G. Spinale, The structure and function of the cardiac myocyte: a review of fundamental concepts. J Thorac Cardiovasc Surg, 1999. 118(2): p. 375-82.

2. Raab, W., The Nonvascular Metabolic Myocardial Vulnerability Factor in "Coronary Heart Disease". Fundamentals of Pathogenesis, Treatment, and Prevention. Am Heart J, 1963. 66: p. 685-706.

3. Rosamond, W., et al., Heart disease and stroke statistics--2007 update: a report from the American Heart Association Statistics Committee and Stroke Statistics Subcommittee. Circulation, 2007. 115(5): p. e69-171.

4. Heart and stroke statistical update, American Heart Association, in American Heart Association. 2002: Dallas [TX].

5. Baroldi, G., Coronary heart disease: significance of the morphologic lesions. Am Heart J, 1973. 85(1): p. 1-5.

6. Baroldi, G., Acute coronary occlusion as a cause of myocardial infarct and sudden coronary heart death. Am J Cardiol, 1965. 16(6): p. 859-80.

7. Erhardt, L.R., G. Unge, and G. Boman, Formation of coronary arterial thrombi in relation to onset of necrosis in acute myocardial infarction in man. A clinical and autoradiographic study. Am Heart J, 1976. 91(5): p. 592-8.

8. Reichenbach, D.D. and N.S. Moss, Myocardial cell necrosis and sudden death in humans. Circulation, 1975. 52(6 Suppl): p. III60-2.

9. Silver, M.D., et al., Letter: Nutritional muscular dystrophy and human myocardial infarction. Lancet, 1973. 2(7834): p. 912-3.

10. Narula, J., et al., Apoptosis in myocytes in end-stage heart failure. N Engl J Med, 1996. 335(16): p. 1182-9.

11. Robin, E.D., Special report: dysoxia. Abnormal tissue oxygen utilization. Arch Intern Med, 1977. 137(7): p. 905-10.

12. Cleutjens, J.P., et al., The infarcted myocardium: simply dead tissue, or a lively target for therapeutic interventions. Cardiovasc Res, 1999. 44(2): p. 232-41.

13. De Celle, T., et al., Long-term structural and functional consequences of cardiac ischaemia-reperfusion injury *in vivo* in mice. Exp Physiol, 2004. 89(5): p. 605-15.

14. Gaby, A.R., Nutritional treatments for acute myocardial infarction. Altern Med Rev. 15(2): p. 113-23.

15. Topol, E.J., Current status and future prospects for acute myocardial infarction therapy. Circulation, 2003. 108(16 Suppl 1): p. III6-13.

16. Dowell, J.D., L.J. Field, and K.B. Pasumarthi, Cell cycle regulation to repair the infarcted myocardium. Heart Fail Rev, 2003. 8(3): p. 293-303.

17. Pasumarthi, K.B. and L.J. Field, Cardiomyocyte cell cycle regulation. Circ Res, 2002. 90(10): p. 1044-54.

18. McMahon, J.T. and N.B. Ratliff, Regeneration of adult human myocardium after acute heart transplant rejection. J Heart Transplant, 1990. 9(5): p. 554-67.

19. Laflamme, M.A., et al., Cell-based therapy for myocardial ischemia and infarction: pathophysiological mechanisms. Annu Rev Pathol, 2007. 2: p. 307-39.

20. Kreutziger, K.L. and C.E. Murry, Engineered human cardiac tissue. Pediatr Cardiol. 32(3): p. 334-41.

21. Ye, K.Y. and L.D. Black, 3rd, Strategies for tissue engineering cardiac constructs to affect functional repair following myocardial infarction. J Cardiovasc Transl Res. 4(5): p. 575-91.

22. Sharma, R. and R. Raghubir, Stem cell therapy: a hope for dying hearts. Stem Cells Dev, 2007. 16(4): p. 517-36.

23. Grauss, R.W., et al., Mesenchymal stem cells from ischemic heart disease patients improve left ventricular function after acute myocardial infarction. Am J Physiol Heart Circ Physiol, 2007. 293(4): p. H2438-47.

24. Strauer, B.E. and R. Kornowski, Stem cell therapy in perspective. Circulation, 2003. 107(7): p. 929-34.

25. Pfeffer, M.A. and E. Braunwald, Ventricular remodeling after myocardial infarction. Experimental observations and clinical implications. Circulation, 1990. 81(4): p. 1161-72.

26. Beitnes, J.O., et al., Long-term results after intracoronary injection of autologous mononuclear bone marrow cells in acute myocardial infarction: the ASTAMI randomised, controlled study. Heart, 2009. 95(24): p. 1983-9.

27. Schachinger, V., et al., Intracoronary infusion of bone marrow-derived mononuclear cells abrogates adverse left ventricular remodelling post-acute myocardial infarction: insights from the reinfusion of enriched progenitor cells and infarct remodelling in acute myocardial infarction (REPAIR-AMI) trial. Eur J Heart Fail, 2009. 11(10): p. 973-9.

28. Murry, C.E., et al., Haematopoietic stem cells do not transdifferentiate into cardiac myocytes in myocardial infarcts. Nature, 2004. 428(6983): p. 664-8.

29. Zenovich, A.G., B.H. Davis, and D.A. Taylor, Comparison of intracardiac cell transplantation: autologous skeletal myoblasts versus bone marrow cells. Handb Exp Pharmacol, 2007(180): p. 117-65.

30. Langer, R. and J.P. Vacanti, Tissue Engineering. Science, 1993. 260: p. 920-926.

31. Zimmermann, W.H., I. Melnychenko, and T. Eschenhagen, Engineered heart tissue for regeneration of diseased hearts. Biomaterials, 2004. 25(9): p. 1639-47.

32. Thompson, R.B., et al., Comparison of intracardiac cell transplantation: autologous skeletal myoblasts versus bone marrow cells. Circulation, 2003. 108 Suppl 1: p. II264-71.

33. Bursac, N., et al., Cardiac muscle tissue engineering: toward an *in vitro* model for electrophysiological studies. Am J Physiol, 1999. 277(2 Pt 2): p. H433-44.

34. Ozawa, T., et al., Optimal biomaterial for creation of autologous cardiac grafts. Circulation, 2002. 106(12 Suppl 1): p. I176-82.

35. Ozawa, T., et al., Histologic changes of nonbiodegradable and biodegradable biomaterials used to repair right ventricular heart defects in rats. J Thorac Cardiovasc Surg, 2002. 124(6): p. 1157-64.

36. Kellar, R.S., et al., Cardiac patch constructed from human fibroblasts attenuates reduction in cardiac function after acute infarct. Tissue Eng, 2005. 11(11-12): p. 1678-87.

37. Fujimoto, K.L., et al., *In vivo* evaluation of a porous, elastic, biodegradable patch for reconstructive cardiac procedures. Ann Thorac Surg, 2007. 83(2): p. 648-54.

38. Fujimoto, K.L., et al., An elastic, biodegradable cardiac patch induces contractile smooth muscle and improves cardiac remodeling and function in subacute myocardial infarction. J Am Coll Cardiol, 2007. 49(23): p. 2292-300.

39. Li, W.J., et al., Electrospun nanofibrous structure: a novel scaffold for tissue engineering. J Biomed Mater Res, 2002. 60(4): p. 613-21.

40. Smith, I.O., et al., Nanostructured polymer scaffolds for tissue engineering and regenerative medicine. Wiley Interdiscip Rev Nanomed Nanobiotechnol, 2009. 1(2): p. 226-36.

41. Hutmacher, D.W., J.C. Goh, and S.H. Teoh, An introduction to biodegradable materials for tissue engineering applications. Ann Acad Med Singapore, 2001. 30(2): p. 183-91.

42. Hutmacher, D.W., Scaffold design and fabrication technologies for engineering tissues--state of the art and future perspectives. J Biomater Sci Polym Ed, 2001. 12(1): p. 107-24.

43. Grad, S., et al., Chondrocytes seeded onto poly (L/DL-lactide) 80%/20% porous scaffolds: a biochemical evaluation. J Biomed Mater Res A, 2003. 66(3): p. 571-9.

44. Weber, B., et al., Tissue engineering on matrix: future of autologous tissue replacement. Semin Immunopathol. 33(3): p. 307-15.

45. Hodde, J., Naturally occurring scaffolds for soft tissue repair and regeneration. Tissue Eng, 2002. 8(2): p. 295-308.

46. Atala, A., et al., Tissue-engineered autologous bladders for patients needing cystoplasty. Lancet, 2006. 367(9518): p. 1241-6.

47. Wang, X., et al., Development of small-diameter vascular grafts. World J Surg, 2007. 31(4): p. 682-9.

48. Gilbert, T.W., T.L. Sellaro, and S.F. Badylak, Decellularization of tissues and organs. Biomaterials, 2006. 27(19): p. 3675-83.

49. Liao, J., E.M. Joyce, and M.S. Sacks, Effects of decellularization on mechanical and structural properties of the porcine aortic valve leaflets. Biomaterials, 2008. 29(8): p. 1065-74.

50. Borschel, G.H., et al., Tissue engineering of recellularized small-diameter vascular grafts. Tissue Eng, 2005. 11(5-6): p. 778-86.

51. Borschel, G.H., R.G. Dennis, and W.M. Kuzon, Jr., Contractile skeletal muscle tissue-engineered on an acellular scaffold. Plast Reconstr Surg, 2004. 113(2): p. 595-602; discussion 603-4.

52. Badylak, S.F., et al., The use of xenogeneic small intestinal submucosa as a biomaterial for Achilles tendon repair in a dog model. J Biomed Mater Res, 1995. 29(8): p. 977-85.

53. Leor, J., et al., Bioengineered cardiac grafts: A new approach to repair the infarcted myocardium? Circulation, 2000. 102(19 Suppl 3): p. III56-61.

54. Badylak, S.F., Xenogeneic extracellular matrix as a scaffold for tissue reconstruction. Transpl Immunol, 2004. 12(3-4): p. 367-77.

55. Hoshiba, T., et al., Decellularized matrices for tissue engineering. Expert Opin Biol Ther. 10(12): p. 1717-28.

56. Knight, R.L., et al., The use of acellular matrices for the tissue engineering of cardiac valves. Proc Inst Mech Eng H, 2008. 222(1): p. 129-43.

57. Badylak, S.F., D.O. Freytes, and T.W. Gilbert, Extracellular matrix as a biological scaffold material: Structure and function. Acta Biomater, 2009. 5(1): p. 1-13.

58. Streeter, D., et al., Three-Dimensional Fiber Orientation in the Mammalian Left Ventricular Wall, in Cardiovascular System Dynamics. 1978, M.I.T Press. p. 73.

59. Streeter, D.D., Jr. and W.T. Hanna, Engineering mechanics for successive states in canine left ventricular myocardium. II. Fiber angle and sarcomere length. Circ Res, 1973. 33(6): p. 656-64.

60. Streeter, D.D., Jr., et al., Fiber orientation in the canine left ventricle during diastole and systole. Circ Res, 1969. 24(3): p. 339-47.

61. Macchiarelli, G. and O. Ohtani, Endomysium in left ventricle. Heart, 2001. 86(4): p. 416.

62. Weber, K.T., Cardiac interstitium in health and disease: the fibrillar collagen network. J Am Coll Cardiol, 1989. 13(7): p. 1637-52.

63. Holmes, J.W., T.K. Borg, and J.W. Covell, Structure and mechanics of healing myocardial infarcts. Annu Rev Biomed Eng, 2005. 7: p. 223-53.

64. Humphery, J.D., Cardiovascular Solid Mechanics. 2002: Springer Verlag.

65. Ott, H.C., et al., Perfusion-decellularized matrix: using nature's platform to engineer a bioartificial heart. Nat Med, 2008. 14(2): p. 213-21.

66. Crapo, P.M., T.W. Gilbert, and S.F. Badylak, An overview of tissue and whole organ decellularization processes. Biomaterials. 32(12): p. 3233-43.

67. Carrier, R.L., et al., Cardiac tissue engineering: cell seeding, cultivation parameters, and tissue construct characterization. Biotechnol Bioeng, 1999. 64(5): p. 580-9.

68. Birla, R.K., et al., Myocardial engineering *in vivo*: formation and characterization of contractile, vascularized three-dimensional cardiac tissue. Tissue Eng, 2005. 11(5-6): p. 803-13.

69. Birla, R.K., G.H. Borschel, and R.G. Dennis, *In vivo* conditioning of tissue-engineered heart muscle improves contractile performance. Artif Organs, 2005. 29(11): p. 866-75.

70. Borschel, G.H., et al., Tissue-engineered axially vascularized contractile skeletal muscle. Plast Reconstr Surg, 2006. 117(7): p. 2235-42.

71. Vouyouka, A.G., et al., Ambient pulsatile pressure modulates endothelial cell proliferation. J Mol Cell Cardiol, 1998. 30(3): p. 609-15.

72. Campion, D.R., The muscle satellite cell: a review. Int Rev Cytol, 1984. 87: p. 225-51.

73. Beltrami, A.P., et al., Evidence that human cardiac myocytes divide after myocardial infarction. N Engl J Med, 2001. 344(23): p. 1750-7.

74. Shamblott, M.J., et al., Human embryonic germ cell derivatives express a broad range of developmentally distinct markers and proliferate extensively *in vitro*. Proc Natl Acad Sci U S A, 2001. 98(1): p. 113-8.

75. Schuleri, K.H., et al., Autologous mesenchymal stem cells produce reverse remodelling in chronic ischaemic cardiomyopathy. Eur Heart J, 2009. 30(22): p. 2722-32.

76. Kehat, I., et al., High-resolution electrophysiological assessment of human embryonic stem cell-derived cardiomyocytes: a novel *in vitro* model for the study of conduction. Circ Res, 2002. 91(8): p. 659-61.

77. Zhang, J., et al., Functional cardiomyocytes derived from human induced pluripotent stem cells. Circ Res, 2009. 104(4): p. e30-41.

78. Rangappa, S., R. Makkar, and J. Forrester, Review article: current status of myocardial regeneration: new cell sources and new strategies. J Cardiovasc Pharmacol Ther. 15(4): p. 338-43.

79. Kajstura, J., et al., Bone marrow cells differentiate in cardiac cell lineages after infarction independently of cell fusion. Circ Res, 2005. 96(1): p. 127-37.

80. Barandon, L., et al., Repair of myocardial infarction by epicardial deposition of bone-marrow-cell-coated muscle patch in a murine model. Ann Thorac Surg, 2004. 78(4): p. 1409-17.

81. Pittenger, M.F., et al., Multilineage potential of adult human mesenchymal stem cells. Science, 1999. 284(5411): p. 143-7.

82. Dennis, J.E., et al., A quadripotential mesenchymal progenitor cell isolated from the marrow of an adult mouse. J Bone Miner Res, 1999. 14(5): p. 700-9.

83. Angoulvant, D., et al., Cell-based gene therapy modifies matrix remodeling after a myocardial infarction in tissue inhibitor of matrix metalloproteinase-3-deficient mice. J Thorac Cardiovasc Surg, 2009. 137(2): p. 471-80.

84. Fedak, P.W., et al., Cell transplantation preserves matrix homeostasis: a novel paracrine mechanism. J Thorac Cardiovasc Surg, 2005. 130(5): p. 1430-9.

85. Lazarus, H.M., et al., Ex vivo expansion and subsequent infusion of human bone marrow-derived stromal progenitor cells (mesenchymal progenitor cells): implications for therapeutic use. Bone Marrow Transplant, 1995. 16(4): p. 557-64.

86. Nauta, A.J. and W.E. Fibbe, Immunomodulatory properties of mesenchymal stromal cells. Blood, 2007. 110(10): p. 3499-506.

87. Horwitz, E.M., et al., Transplantability and therapeutic effects of bone marrow-derived mesenchymal cells in children with osteogenesis imperfecta. Nat Med, 1999. 5(3): p. 309-13.

88. Eliopoulos, N., et al., Erythropoietin delivery by genetically engineered bone marrow stromal cells for correction of anemia in mice with chronic renal failure. J Am Soc Nephrol, 2006. 17(6): p. 1576-84.

89. Cogle, C.R., et al., Bone marrow contributes to epithelial cancers in mice and humans as developmental mimicry. Stem Cells, 2007. 25(8): p. 1881-7.

90. Bruder, S.P., et al., Bone regeneration by implantation of purified, culture-expanded human mesenchymal stem cells. J Orthop Res, 1998. 16(2): p. 155-62.

91. Johnstone, B., et al., *In vitro* chondrogenesis of bone marrow-derived mesenchymal progenitor cells. Exp Cell Res, 1998. 238(1): p. 265-72.

92. Haynesworth, S.E., et al., Characterization of cells with osteogenic potential from human marrow. Bone, 1992. 13(1): p. 81-8.

93. Yoo, J.U., et al., The chondrogenic potential of human bone-marrow-derived mesenchymal progenitor cells. J Bone Joint Surg Am, 1998. 80(12): p. 1745-57.

94. Gojo, S., et al., *In vivo* cardiovasculogenesis by direct injection of isolated adult mesenchymal stem cells. Exp Cell Res, 2003. 288(1): p. 51-9.

95. Sanchez-Ramos, J., et al., Adult bone marrow stromal cells differentiate into neural cells *in vitro*. Exp Neurol, 2000. 164(2): p. 247-56.

96. Woodbury, D., et al., Adult rat and human bone marrow stromal cells differentiate into neurons. J Neurosci Res, 2000. 61(4): p. 364-70.

97. Kohyama, J., et al., Brain from bone: efficient "meta-differentiation" of marrow stroma-derived mature osteoblasts to neurons with Noggin or a demethylating agent. Differentiation, 2001. 68(4-5): p. 235-44.

98. Kobayashi, T., et al., Enhancement of angiogenesis by the implantation of self bone marrow cells in a rat ischemic heart model. J Surg Res, 2000. 89(2): p. 189-95.

99. Tomita, S., et al., Autologous transplantation of bone marrow cells improves damaged heart function. Circulation, 1999. 100(19 Suppl): p. II247-56.

100. Sato, T., et al., Coronary vein infusion of multipotent stromal cells from bone marrow preserves cardiac function in swine ischemic cardiomyopathy via enhanced neovascularization. Lab Invest. 91(4): p. 553-64.

101. Amado, L.C., et al., Cardiac repair with intramyocardial injection of allogeneic mesenchymal stem cells after myocardial infarction. Proc Natl Acad Sci U S A, 2005. 102(32): p. 11474-9.

102. Toma, C., et al., Human mesenchymal stem cells differentiate to a cardiomyocyte phenotype in the adult murine heart. Circulation, 2002. 105(1): p. 93-8.

103. Valina, C., et al., Intracoronary administration of autologous adipose tissue-derived stem cells improves left ventricular function, perfusion, and remodelling after acute myocardial infarction. Eur Heart J, 2007. 28(21): p. 2667-77.

104. Shake, J.G., et al., Mesenchymal stem cell implantation in a swine myocardial infarct model: engraftment and functional effects. Ann Thorac Surg, 2002. 73(6): p. 1919-25; discussion 1926.

105. Kinkaid, H.Y., et al., What's new in cardiac cell therapy? Allogeneic bone marrow stromal cells as "universal donor cells". J Card Surg. 25(3): p. 359-66.

CHAPTER II

PORCINE MYOCARDIAL EXTRACELLULAR MATRIX: FABRICATION AND BIOMECHANICAL CHARACTERIZATION

2.1 Introduction

Myocardial ECM is an intriguing network that mediates complex muscle fiber architecture and maintains unique cell to cell interconnections.[1-4] The subtle 3D ultrastructure of myocardial ECM represents a challenge in the decellularization efforts. The first step of our research is thus to determine an optimized decellularization protocol that is able to (i) thoroughly remove the cardiomyocytes and other types of cells in the ECM and vasculature network and (ii) preserve the 3D myocardial ECM ultrastructure. Moreover, the decellularized myocardial scaffolds with well-preserved ECM components and 3D architecture offer an opportunity to examine the myocardial ECM in great detail.

As we discussed in Chapter 1, the goal of decellularization is to remove all the cellular and nuclear components from a tissue or an organ while reducing any undesirable effects on the composition, biological activity, and mechanical property of the remaining ECM.[5-7] Various decellularization protocols have been studied and each of these methods can affect the biochemical composition, ultrastructure, and mechanical behavior of the ECM scaffold materials at different levels.[5] The most commonly used decellularization methods involve physical treatment, chemical treatment, enzymatic treatment, and combination approaches of those treatments.[5] The effectiveness and

efficiency of the decellularization approach also depend on the tissue/organ factors such as tissue's size and thickness, cell density, and compositions.[8]

The most commonly applied physical treatments include snap freezing, direct pressure, sonication, and mechanical agitation.[5] Snap freezing can disrupt cellular membranes by forming intracellular ice crystals and cause cell lysis, and this method has been used frequently in tendinous tissue, ligamentous tissue,[9-13] and nerve [14] decellularization. Direct pressure can cause cell lysis; however, only tissues or organs with sparsely organized ECM structures can be effectively decellularized with this method.[5] Mechanical agitation and sonication have been applied along with chemical treatment to assist in cell lysis and cellular debris removal. Overall, physical treatment is insufficient to achieve thorough decellularization when applied alone, and must be combined with other chemical and/or enzymatic treatments.[5]

The most generally used chemical agents for decellularization include acids or bases, hypotonic or hypertonic solutions, and detergents.[8] Acids or bases cause hydrolytic degradation of biomolecules; however, they have disadvantages such as damaging ECM components and decreasing mechanical properties.[15-18] Hypertonic saline can cause DNA to be dissociated from proteins,[19] while hypotonic solutions can cause cell lysis by simple osmotic effect and thus better preserve the ECM architecture.[20].

Triton X-100 and Sodium dodecyl sulfate (SDS) are the most commonly used detergents for decellularization. Triton X-100 can remove cellular residues more successfully than the enzymatic or osmotic treatment.[21] Sodium dodecyl sulfate (SDS) shows more sufficient ability in removing nuclei from dense tissues and organs than the Triton X-100 while preserving the overall tissue dimension, ECM ultrastructure, and

mechanical behaviors.[22-24] Enzymatic treatments, including the use of trypsin, nucleases, collagenase, lipase, dispase, thermolysin, and a-galactosidase, can specifically remove cell residues or undesirable ECM constituents; nevertheless, enzymes are usually added in the mixed decellularization solution since enzymatic treatment alone is difficult to achieve complete cell removal.[8] In short, the method of combining multiple detergents and agents has been widely used; it has been found that the combination approach is more effective for cell removal [25] and ultrastructure preservation.[26]

In this chapter, we reported an optimized decellularization protocol that has been shown to remove cell and cell debris effectively and leave the delicate 3D myocardial ECM well preserved. We also carried out thorough structural and biomechanical characterizations on the acellular myocardial scaffolds.

The accurate assessments of the acellular scaffold enable us to better understand the intrinsic structural and mechanical characteristics of myocardial ECM. The knowledge gained in this research will (i) provide a baseline for cardiac tissue engineering that either partially or wholly utilizes acellular porcine myocardial scaffolds, (ii) serve as a reference for polymeric based cardiac scaffold design, and (iii) shed light on the biomechanical role of myocardial ECM in cardiac function.

2.2 Materials and Methods

2.2.1 Preparation of Porcine Myocardium

Thirty fresh porcine hearts were obtained from juvenile pigs (~6 months old) from a local abattoir and transported to the laboratory in PBS on ice. A myocardium square (20 × 20 × ~3 mm) or myocardium strip (30 × 10 × ~3 mm) was dissected from the middle region of the anterior left ventricular wall of the porcine heart (Figure 2.1-b). Square

samples were used for histological, structural, and biochemical characterizations, and the strip samples were used for uniaxial and shear testing. For the square samples, one edge was aligned along with the muscle fiber preferred direction (PD) that was determined by the overall fiber texture and heart anatomy. For the strip samples, the long edge either aligned along with the muscle fiber PD direction or aligned along with the cross-fiber preferred direction (XD).

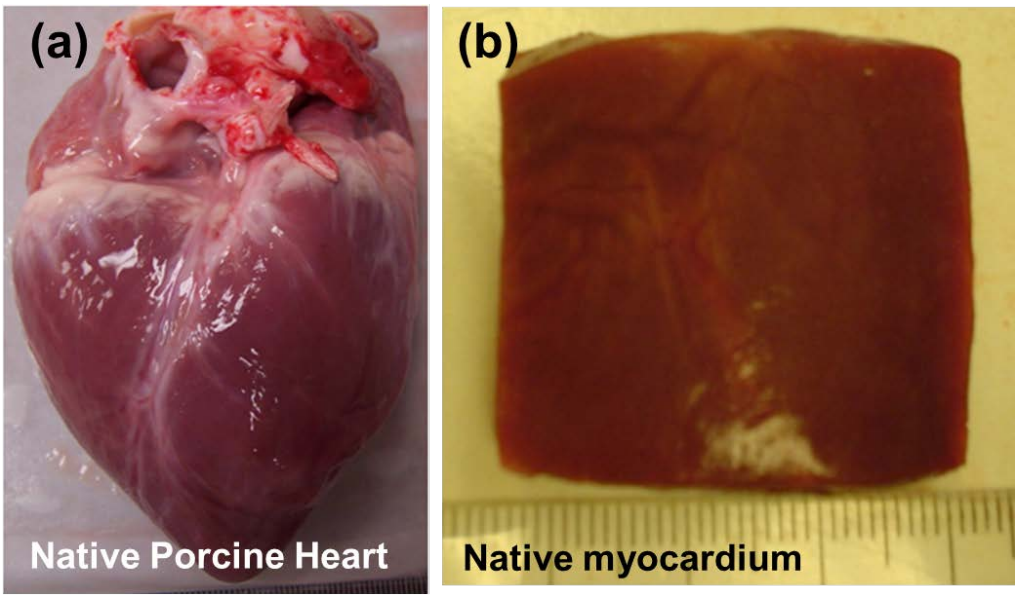

Figure 2.1 (a) Fresh porcine heart (b) Myocardium squares (20 × 20 × ~3 mm) were dissected from the middle region of the anterior left ventricular wall. One edge of the square sample was aligned along with the muscle fiber preferred direction (PD)

2.2.2 Optimized Decellularization Protocol for Fabricating Acellular Myocardial ECM

An optimized decellularization protocol is described as follows. A frame-pin supporting system was designed to better maintain tissue macrogeometry during decellularization (Fig. 2.2). Briefly, four corners of the myocardium sample were perforated with four 27G x 31/2" BD Quincke Spinal Needles, which were then mounted

onto custom made rectangular plastic frames. The myocardium was then decellularized in a rotating bioreactor using 0.1% sodium dodecyl sulfate (SDS) (Sigma) with 0.01% trypsin (VWR), 1 mM phenylmethylsulfonylfluoride (PMSF, protease inhibitor) (Sigma), 20 µg/ml RNase A (Sigma) and 0.2 mg/ml DNase (Sigma) at room temperature for 3 weeks. Ten-minute ultrasonic treatment (50 HZ, Branson, US) was applied each day, and the decellularization solution was changed every two days to avoid contamination and tissue deterioration.

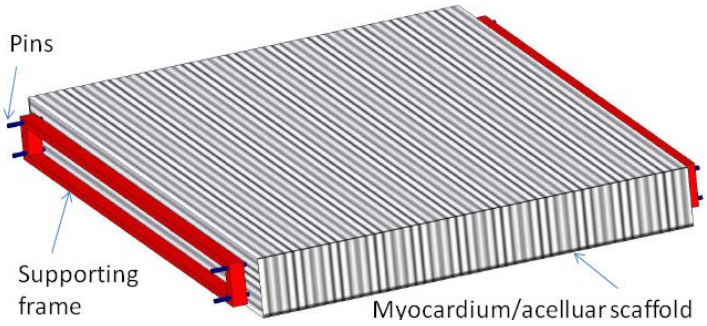

Figure 2.2 Frame-pin supporting system.

2.2.3 Morphology, Histology, and SEM

For estimating the dimensional changes, the thickness and surface area of native myocardium samples were measured using a caliper and a digital picture of the samples, respectively. After decellularization, the thickness and surface area of the acellular myocardial scaffolds were immediately measured in order to compare the dimensional alterations.

For histological analysis, samples were fixed in 2% paraformaldehyde in PBS at room temperature for 2 hours, dehydrated with graduated concentrations of ethanol and embedded in paraffin. Cross-sections of the myocardium were cut to 5 µm thick. To elucidate changes in tissue components, Masson's trichrome staining and Movat's

pentachrome staining were used to identify cardiomyocytes, collagen network, elastin, and proteoglycans. Stained tissue sections were imaged using bright field microscopy (Nikon EC600). Polarizing light imaging was also taken to reveal the light extinguishing patterns of the collagen network in both the acellular myocardial scaffolds and the native myocardium.

Scanning Electron Microscope (SEM), capable of showing 3D topography, was used to observe the cross section of the acellular scaffolds and the native myocardium. After fixation with 2.5% glutaraldehyde for 24 hours, the samples were dehydrated in a graded ethanol series. The samples were then processed with critical point drying (Polaron E 3000 CPD), sputter coated with gold-palladium, and observed with the SEM (JEOL JSM-6500 FE-SEM).

2.2.4 DNA Assay, DAPI Staining, and Griffonia Simplicifolia (GS) Lectin Immunohistochemistry

To test for the completeness of decellularization, both native myocardium and acellular scaffolds were weighed wet; DNA was extracted and purified with a specific kit (Qiagen, Valencia, CA). The amounts of DNA were quantified by reading absorbance at 260 nm, and quantities of DNA were normalized to the wet weight and expressed as ng/mg.

To further show effectiveness of DNA fragment removal, DAPI staining was carried out in the acellular myocardial scaffolds. For DAPI staining, after the tissue sections rehydration and antigen retrieval with 0.05% Trypsin for 10 min at 37ºC, sections were then stained with DAPI (Invitrogen) for cell nuclei. Immunohistological slides were observed with laser scanning confocal microscope (Zeiss LSM 510).

The major problem of xenografts transplantation is the hyperacute rejection which is mediated by natural antibodies in humans to pig antigens,[27] The Galα1-3Gal antigen (α-Gal) is the main target for human natural anti-pig xenoantibodies.[28, 29] To detect α-Gal after decellularization, biotinylated Griffonia simplicifolia (GS) lectin immunohistochemistry was performed, followed by ABC-peroxidase complex and DAB detection with haematoxylin counterstaining.[28, 29]

2.2.5 Differential Scanning Calorimetry, Water Content, and Collagen Stabilization Studies

Acellular myocardial scaffolds were subjected to differential scanning calorimetry (DSC, model 131 Setaram Instrumentation, Caluire, France) to determine the thermal denaturation temperature (T_d). Specimens were tested at a heating rate of 10 ºC/min from 24 °C to 100 °C in a N_2 gas environment (N = 4). T_d is defined as the temperature at the endothermic peak and is a well-known indicator of degree of collagen crosslinking.[30]

Water content was calculated as the percentage weight difference between wet and dry samples that was normalized to the wet weight. Both native myocardium and acellular scaffolds were cut into small pieces ($3 \times 3 \times 3$ mm^3) and the surfacing moisture was absorbed using filter paper. After measuring the wet weight, all the samples were put into a Freeze Dryer System (Cole-Parmer, Illinois) at -54°C. After samples were totally dried, the dry weights were immediately measured (N = 24 for each group).

To assess degradability of acellular myocardium scaffolds, collagenase treatment was applied as an accelerated degradation model.[30] After lyophilization, the dry weight of the samples were recorded (range from 10 to 15 mg) and samples were then incubated in 1 mL collagenase Type I (USB) solution (5 Units of collagenase/mL in 50 mM Tris, 1 mM $CaCl_2$, 0.02% N_3Na, pH=7.8). At 3 and 7 days, samples (N = 6 per time

point) were rinsed three times in ddH_2O by centrifugation at 12,000 rpm for 5 minutes, lyophilized, and weighed. Percent mass loss was calculated from the following equation: (scaffold weight before collagenase treatment - scaffold weight after collagenase treatment)/scaffold weight before collagenase treatment.

2.2.6 Mechanical Characterizations

Uniaxial Mechanical Testing. Uniaxial mechanical properties of acellular myocardial scaffolds were characterized with a uniaxial testing machine (Mach-1, Biosyntech, MN) (Figure 2.3). Dogbone-shaped tissue strips were trimmed in such a way that a group of samples were aligned along fiber-preferred direction (PD) and another group of samples were aligned along cross fiber-preferred direction (XD) (N = 4, grip-to-grip length: 25 mm, width: 5 mm). The samples were mounted with two stainless steel grips cushioned with emery paper. After 10 cycles of precondition at 10% strain, tissue samples were loaded to failure at a ramp speed of 400 μm/s.

Engineering stress was calculated by normalizing the force to the initial cross-sectional area; engineering strain was computed by normalizing the displacement to the initial grip-to-grip distance (gauge length). The maximum tensile modulus was estimated by finding the tangent value of the linear region of the stress-strain curve using linear regression. Failure stress and failure strain were also determined from the stress-strain data. To assess energy dissipation in tissue loading and unloading, the last cycle of preconditioning was used to estimate the tissue hysteresis, by normalizing the enclosed area of the loading and unloading curves (energy dissipation) to the area underneath the loading curve (energy input).

Shear testing. A pair of custom made shear plates was mounted onto the Mach-1 for shear mechanical testing on both the acellular myocardial scaffolds and the native myocardium (Figure 2.4-a). During the testing, tissue samples (N = 4 for each group), with PD direction aligned along with shear direction, were mounted between two shear plates by applying a minimum amount of cyanoacrylate glue (Figure 2.4-b). After ten cycles of preconditioning, the sample was loaded to a shear strain level of 40% (~10 kPa shear stress level for the native myocardium; ~400 Pa shear stress level for the acellular myocardial scaffolds). Shear stress was computed by normalizing the shear force to the contact area; shear strain was computed by normalizing the travel distance of the shear plate to the sample thickness. All samples were tested in a PBS bath at 37 ºC.

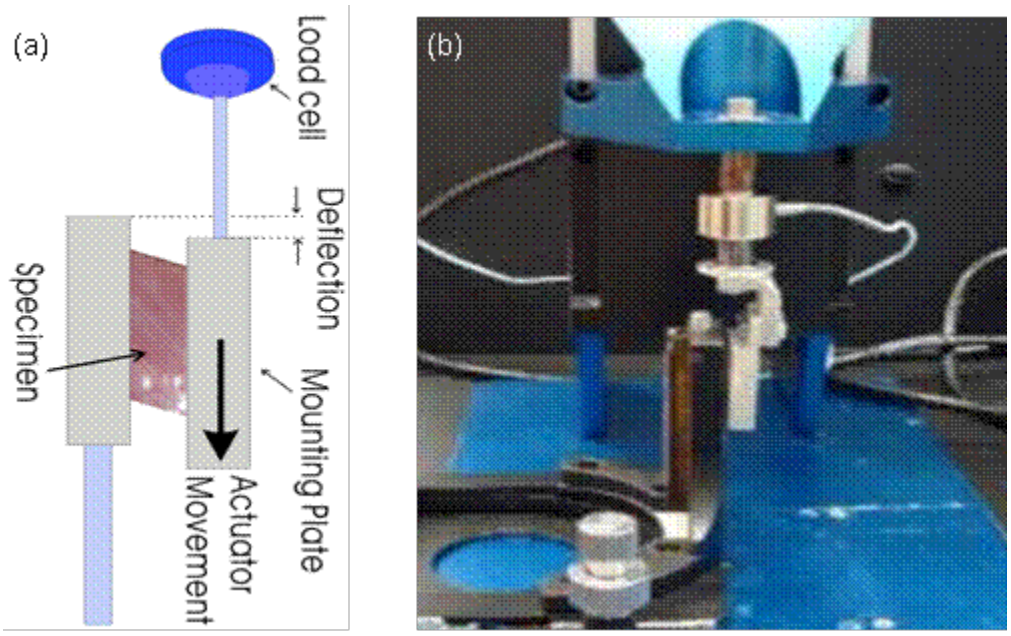

Figure 2.3 (a) Working principle of shear testing. (b) Shear testing device.

2.2.7 Statistical analysis

The experimental data were presented as mean ± standard deviation (STDEV). The Student's t-test was applied for two-group comparison (SigmaStat 3.0, SPSS, Chicago, IL). The differences were considered statistically significant when $p < 0.05$.

2.3 Results

2.3.1 Morphological, Histological, and SEM analyses

After 2.5 - 3 weeks of SDS treatment, the porcine native myocardium (NM) showed a bright white color typical of collagenous materials, indicating that thorough decellularization was achieved (Figure 2.4-b). Moreover, the frame-pin supporting system was found to be capable of preventing tissue contraction.

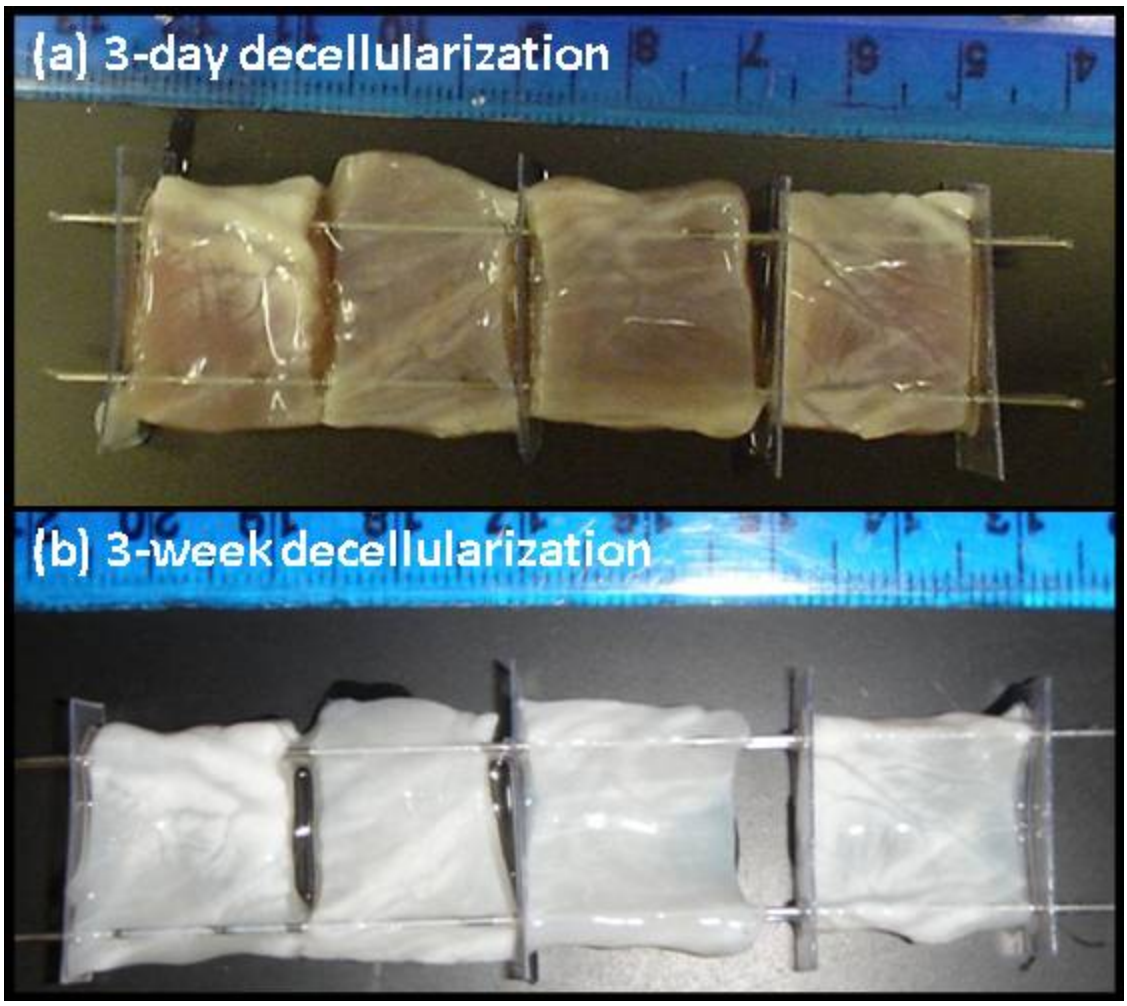

Figure 2.4 The frame-pin supporting system was found to further prevent tissue contraction in the decellularization procedure. The porcine myocardium showed bright white color after three weeks SDS treatment, indicating that thorough decellularization was achieved. (a) Sample morphology after 3-day decellularization; (b) Sample morphology after 3-week decellularization.

The dimensional comparison of myocardium samples before and after decellularization demonstrated that the acellular myocardial scaffolds (AMS) decreased in thickness (NM vs. AMS: 2.70 ± 0.23 mm vs. 2.27 ± 0.38 mm, $p = 0.039$), were larger in surface area (NM vs. AMS: 520.13 ± 46.94 mm^2 vs. 577.42 ± 44.51 mm^2, $p = 0.055$),

and showed only a small degree of overall contraction (NM vs. AMS: 1403.25 ± 232.36 mm^2 vs. 1314.74 ± 216.29 mm^2, p = 0.510) (Table 2.1 and Figure 2.5).

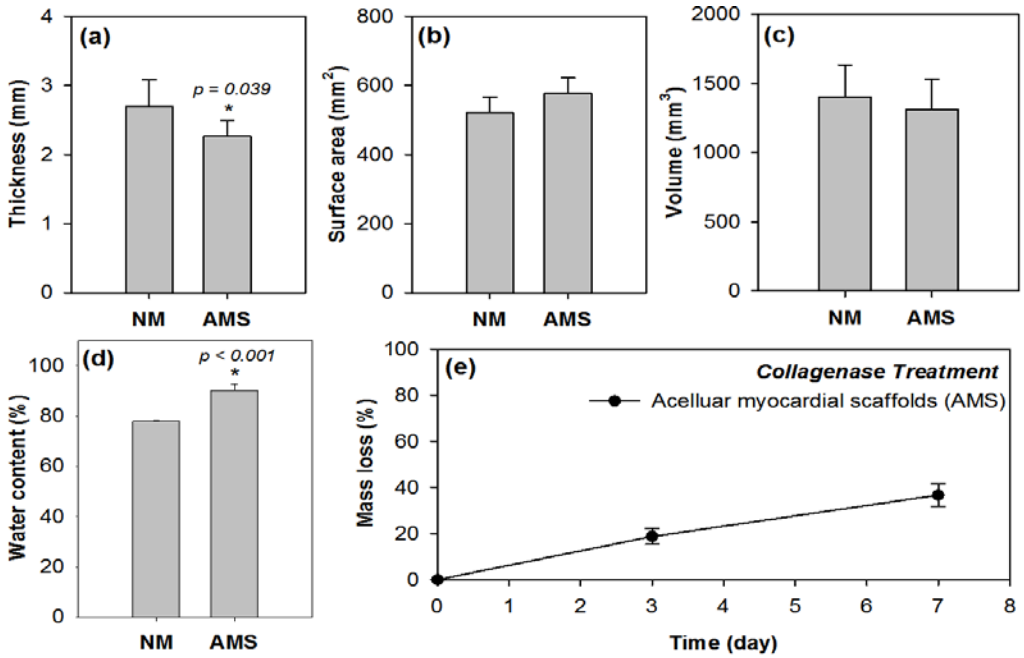

Figure 2.5 The dimensional comparison of myocardium samples before and after decellularization: (a) Thickness, (b) Surface area, and (c) Volume. (d) Water content of the native myocardium and the acellular myocardial scaffolds. (e) Mass loss of the acellular myocardial scaffolds at 3 days and 7 days in response to collagenase treatment.

Table 2.1 Parameters from structural characterizations and water content.

	Thickness (mm)	Surface Area (mm^2)	Volume (mm^3)	Pore Size (μm)	Water Content (%)
Native Myocardium	2.70±0.23	520.1±46.9	1403.25± 232.36	NA	77.99±0.46
Acellular Myocardial Scaffold	2.27±0.38*	577.4±44.5	1314.74± 216.29	21.4±16.8	90.21± 2.36*
p value	p = 0.039	p = 0.055	p = 0.510	NA	p < 0.001

(* indicates statistically significant difference between two groups (p < 0.05))

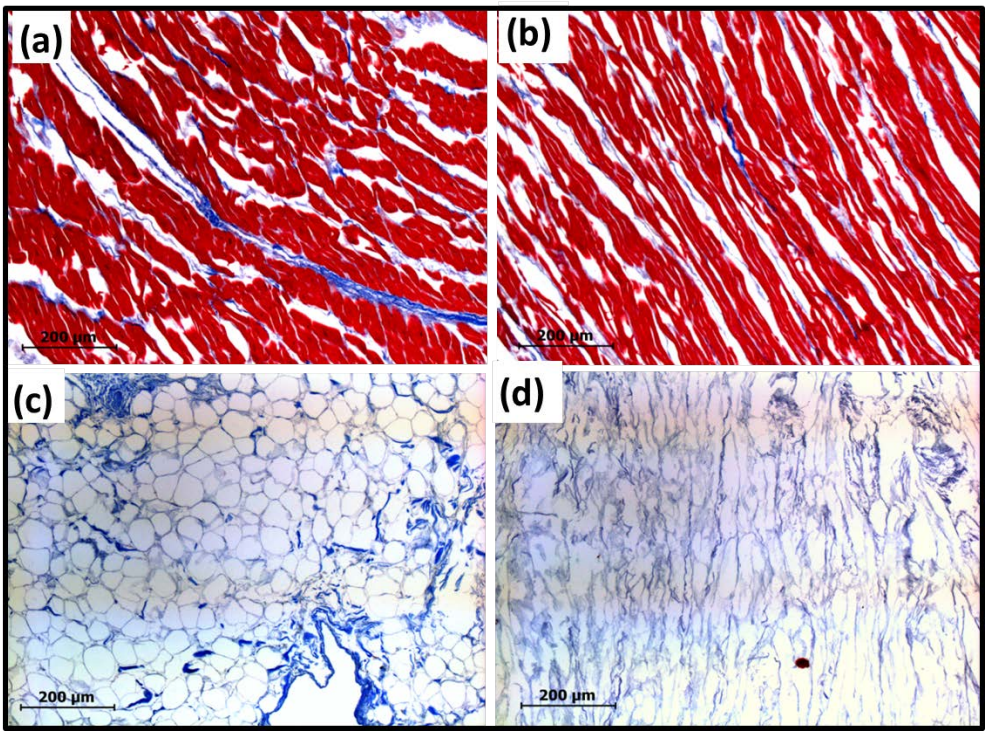

Figure 2.6 Mason's trichrome staining showed well preserved cardiomyocyte lacunae. (a) Cross-section of the native myocardium; (b) Longitudinal-section of the native myocardium; (c) Cross-section of the decellularized myocardium; (d) Longitudinal-section of the decellularized myocardium. Note - red: cardiomyocytes, blue: collagen.

Thorough removal of cardiomyocytes was confirmed by Mason's trichrome staining and the cardiomyocyte lacunae were found to be preserved, evidenced by cross-sectional and longitudinal histology (Figure 2.6).

The 3D topography of the acellular scaffolds further delineated the details of the well-preserved cardiomyocyte lacunae, which were characterized by an array of interconnecting open pores (Figure 2.7). The average pore size estimated from the SEM images was 21.4 ± 16.8 µm.

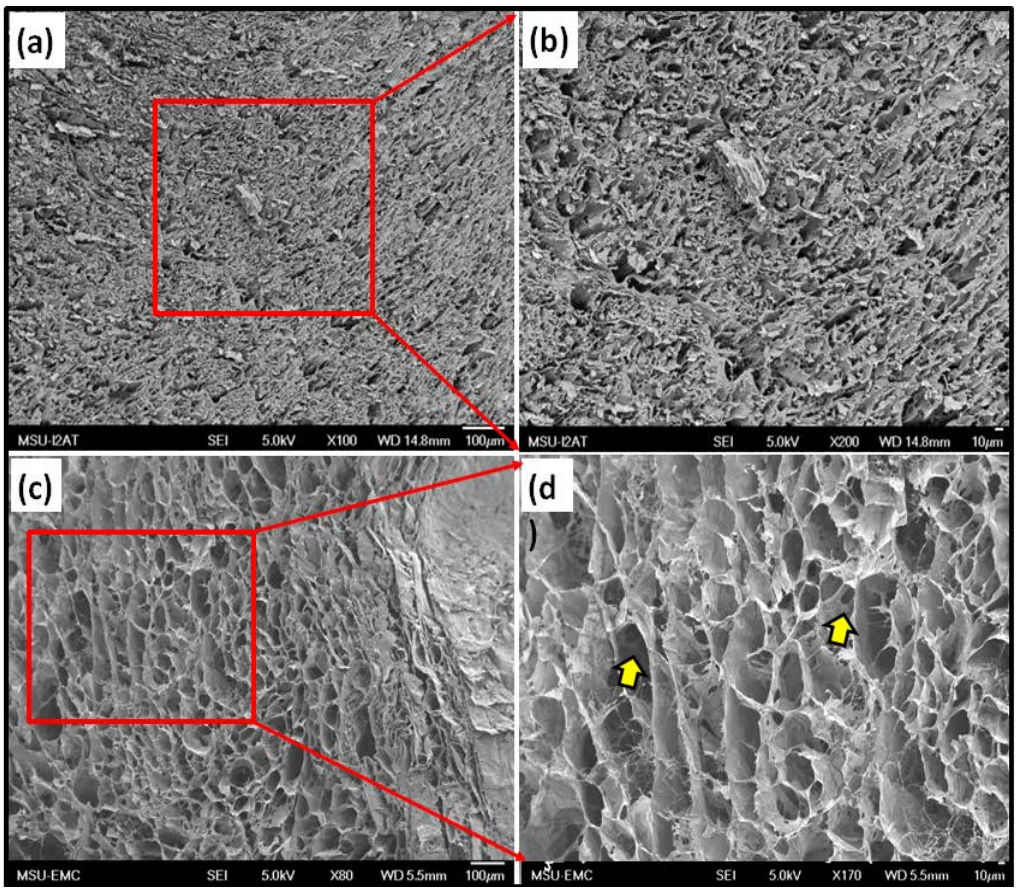

Figure 2.7 (a) Three-dimensional topography of the native myocardial scaffolds revealed by SEM; (b) Enlarged view of the cross-section; (c) Three-dimensional topography of the acellular myocardial scaffolds revealed by SEM; (d) Enlarged view of the cross-section; arrows highlight the interconnecting openings inside the aligned cardiomyocyte lacunae.

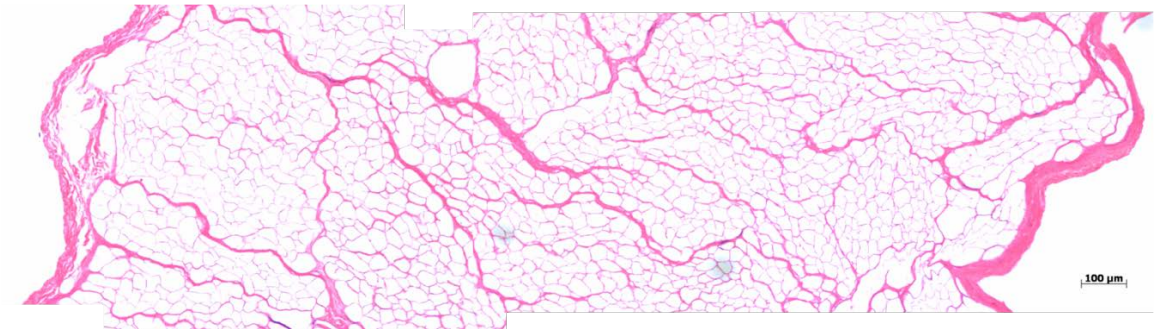

Figure 2.8 Edge-to-edge view of H&E staining showed that large pores distributed evenly across the 2 mm thick acellular scaffold.

Edge-to-edge views of transversal sections of acellular scaffolds showed that large pores were evenly distributed across the 2-mm thickness (Figure 2.8). Additionally, part of the vasculature channels was likely preserved. The channel-like structures in histology showed diameters approximately ranging from 100 to 400 μm, a size close to small vasculature (Figure 2.9-b, c, d: arrows).

The preservation of the vascular templates after decellularization was further validated by morphology revealed by SEM (Figure 2.10-a) and collagen type IV staining around the channel-like structure (Figure 2.10-c, d).

Under polarizing light, the collagen scaffolds in the native myocardium showed light extinguishing patterns that were corresponding to the collagen crimping pathways (Figure 2.11-a, b). In the acellular myocardial scaffolds, the light extinguishing patterns were found to be retained, implying the subtle collagen crimps survived the decellularization procedure (Figure 2.11-c, d).

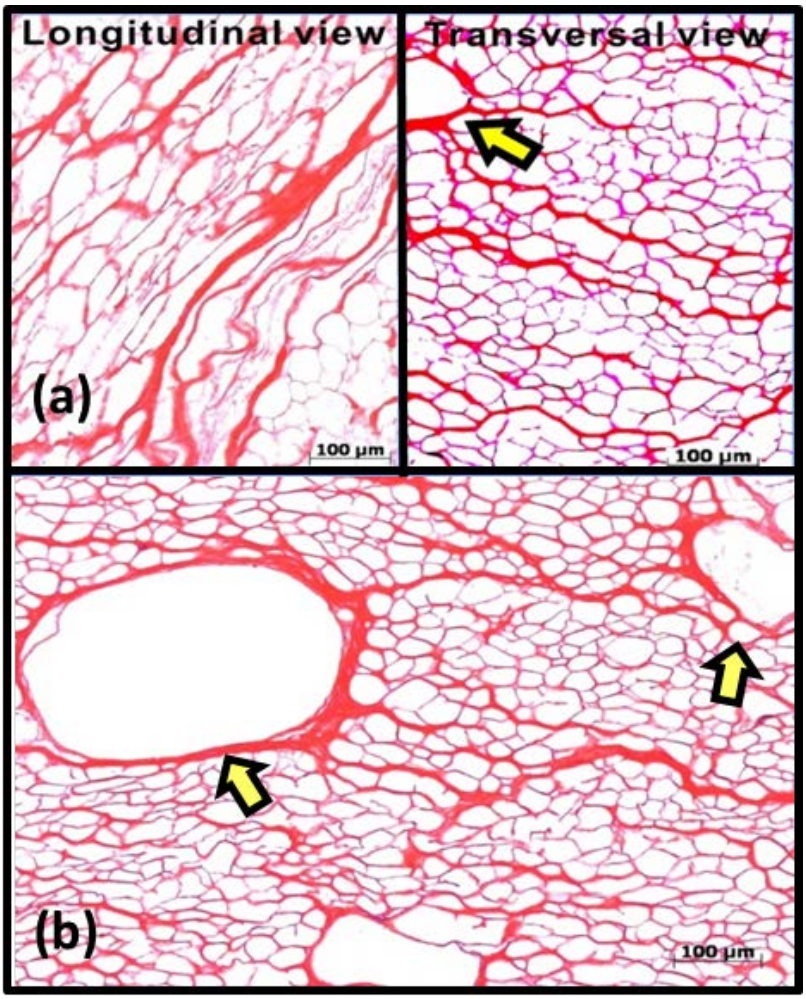

Figure 2.9 (a) H&E staining of the longitudinal and transversal views of the acellular scaffold showed that 3D lacunae housing cardiomyocytes were preserved (red: collagen). (d) Vasculature templates in the decellularized myocardial scaffold (H&E staining). Arrows indicate vasculature channels were preserved after decellularization.

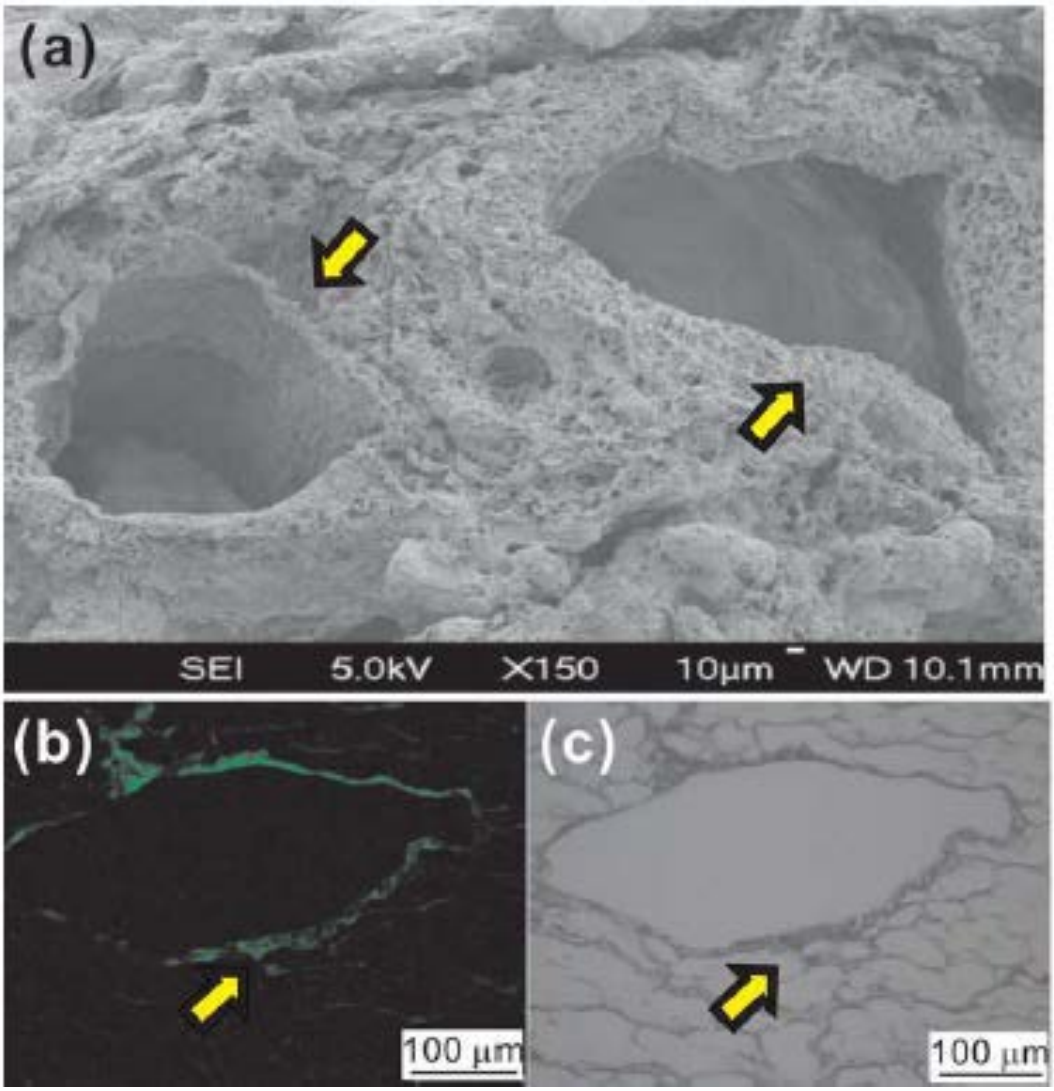

Figure 2.10 Preservation of vasculature structure was verified by (a) SEM and (b) Type IV collagen staining (green color) on the circular structure; (c) Transmission light image of the same region shown in (b). Arrows in (a), (b), and (c) indicate the existence of vasculature templates.

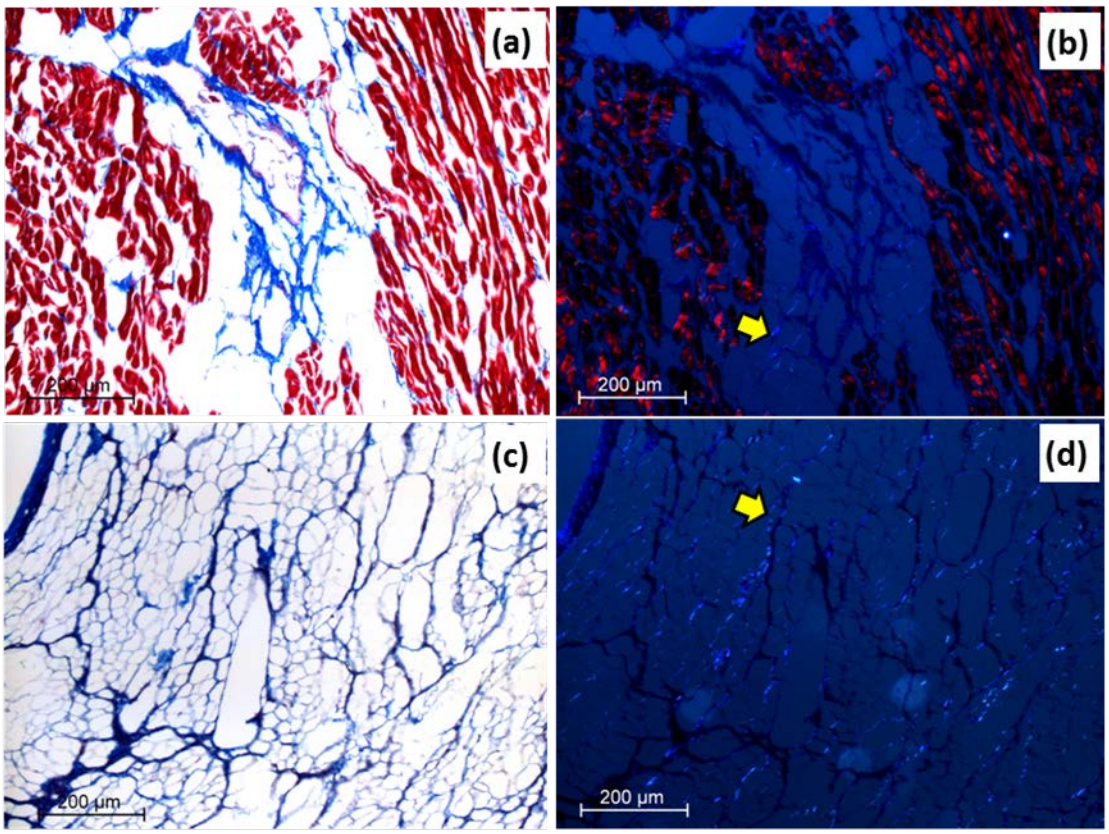

Figure 2.11 In polarizing light images, light extinguishing patterns of collagen network were found existing in both the native myocardium (b) and the acellular myocardial scaffolds (d). The light extinguishing patterns reflect collagen crimping pathways. The retaining of light extinguishing patterns in the acellular myocardial scaffolds implies the subtle collagen crimps survived the decellularization procedure.

The elastin structures in the acellular myocardial scaffolds were revealed by Movat's pentachrome staining (Figure 2.12). Both cardiac elastin and vasculature elastin, with their subtle structural features, were retained after the decellularization (Figure 2.12-c, d); for example, a circle of elastin lamina on the intima was observed, and the elastin fibers in the media and adventia maintained certain alignment and distribution. Furthermore, thorough removal of the cellular contents (e.g., smooth muscle cells) in blood vessels was also evidenced in the Movat's staining (Figure 2.12-c, d).

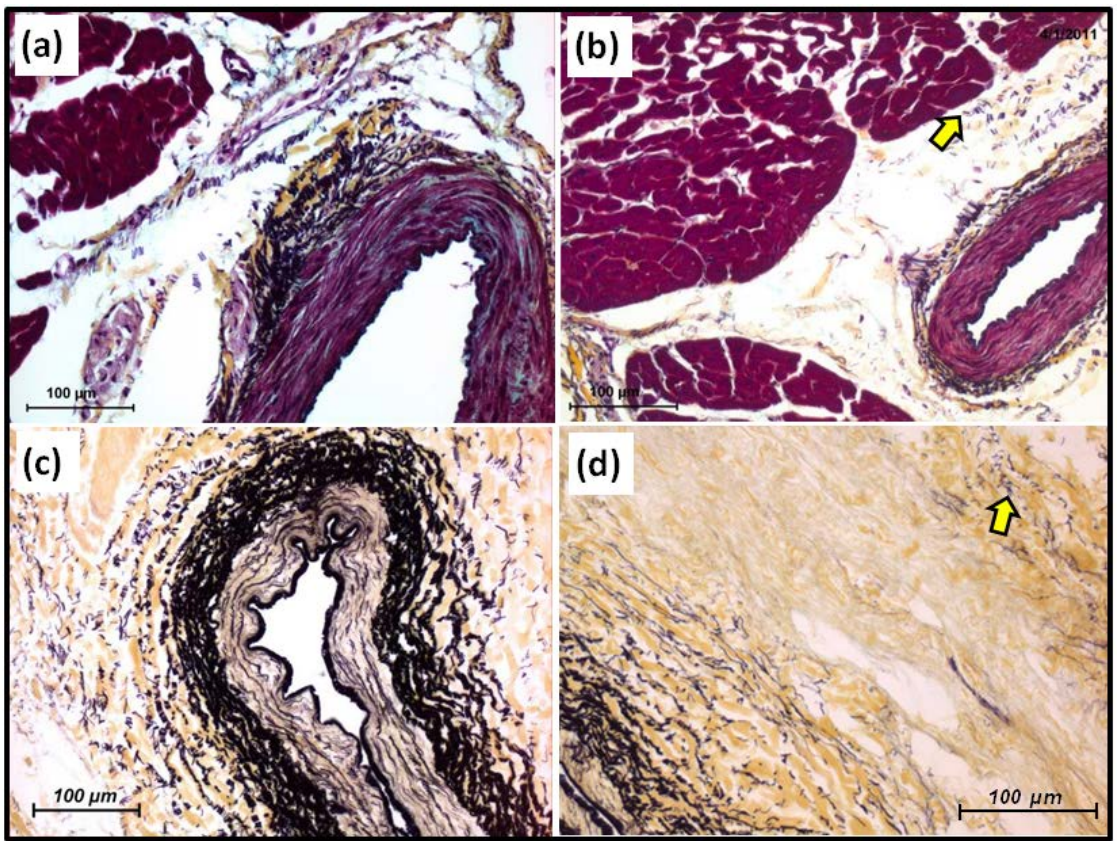

Figure 2.12 (a), (b) Movat's pentachrome staining of the native myocardium; (c), (d) Movat's pentachrome staining of the acellular myocardial scaffolds. Details of cardiac elastin and vascular elastin were revealed; cardiac elastin is highlighted by arrows. Note - Yellow: collagen, Pink/red: cardiomyocytes and smooth muscle cells, black: elastin, blue: proteoglycans/glycosaminoglycans.

2.3.2 DAPI Staining, DNA Assay, Porcine Antigen Characterization, DSC, and Enzymatic Resistance

DAPI staining of the acellular scaffold further verified that no nuclear chromatin

Quantitative DNA analysis showed that the decellularized scaffolds had a 98.59% reduction in DNA content compared with the native myocardium (from 275.4 $\pm$ 31.7 to 3.9 $\pm$ 0.5 ng DNA/mg wet tissue) (Figure 2.14).

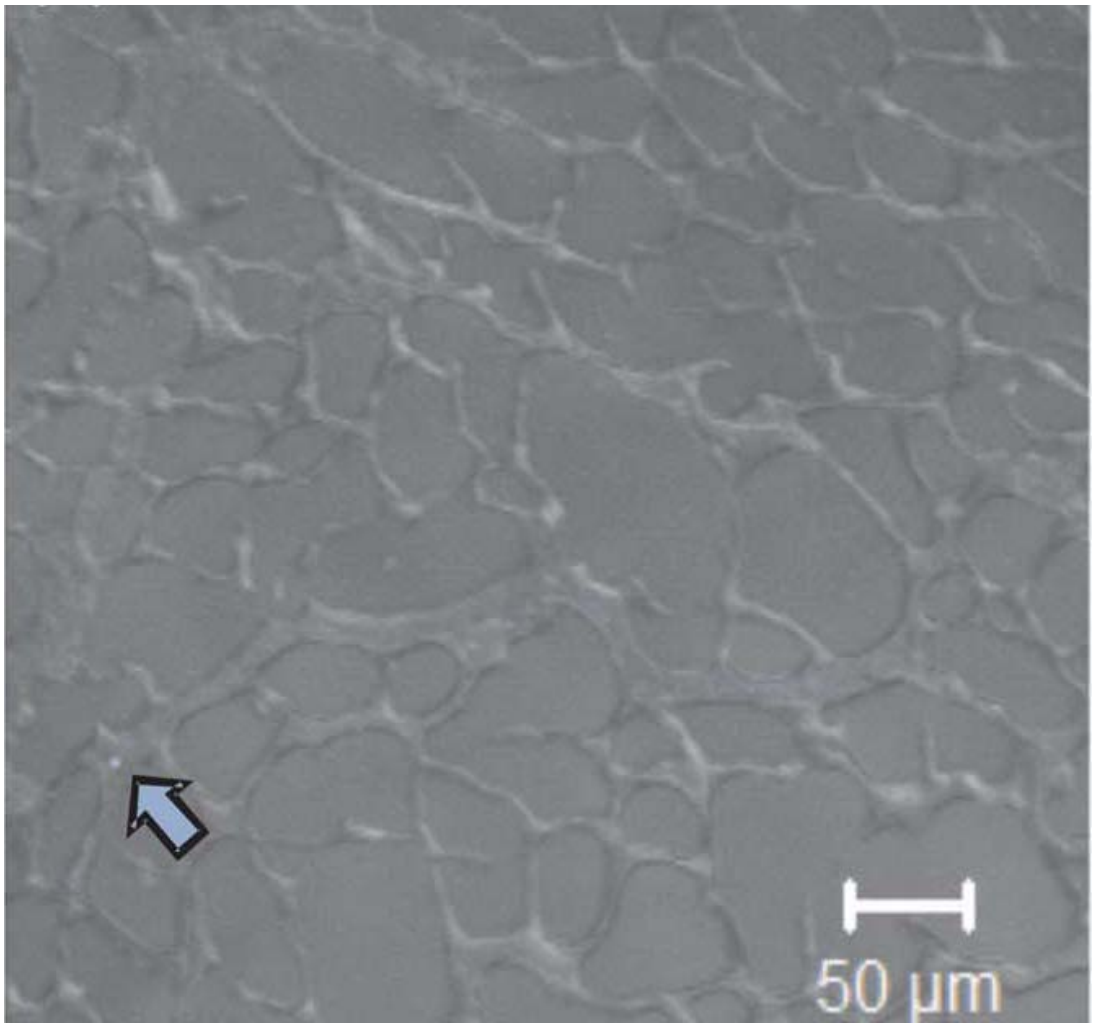

Figure 2.13 A combined image of the DAPI staining (blue color) and the transmission light image on the section of the decellularized scaffolds. Lack of DAPI staining verified that no nuclear chromatin fragments remained in the scaffolds. Arrow showed a minute spot of DAPI stain (blue color).

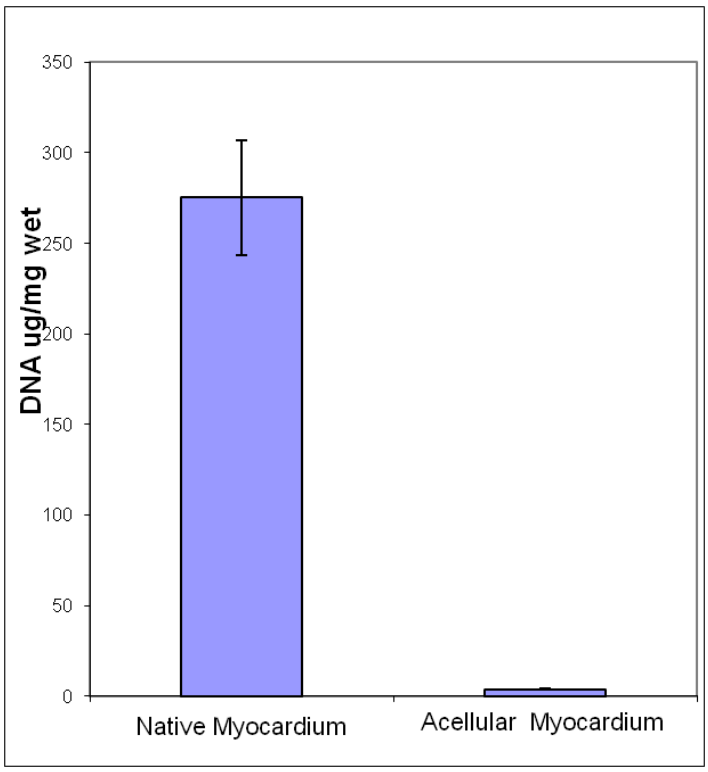

Figure 2.14 Quantitative DNA analysis showed that the decellularized scaffolds had a 98.59% reduction in DNA content compared with the native myocardium.

Results of α-Gal antigen staining showed that in native porcine myocardium, α-Gal antigen (brown color) was associated with myocardial fibroblasts, cardiomyocytes and blood vessels, while in the acellular myocardial scaffolds, α-Gal antigen is completely absent (Figure 2.15-c, d).

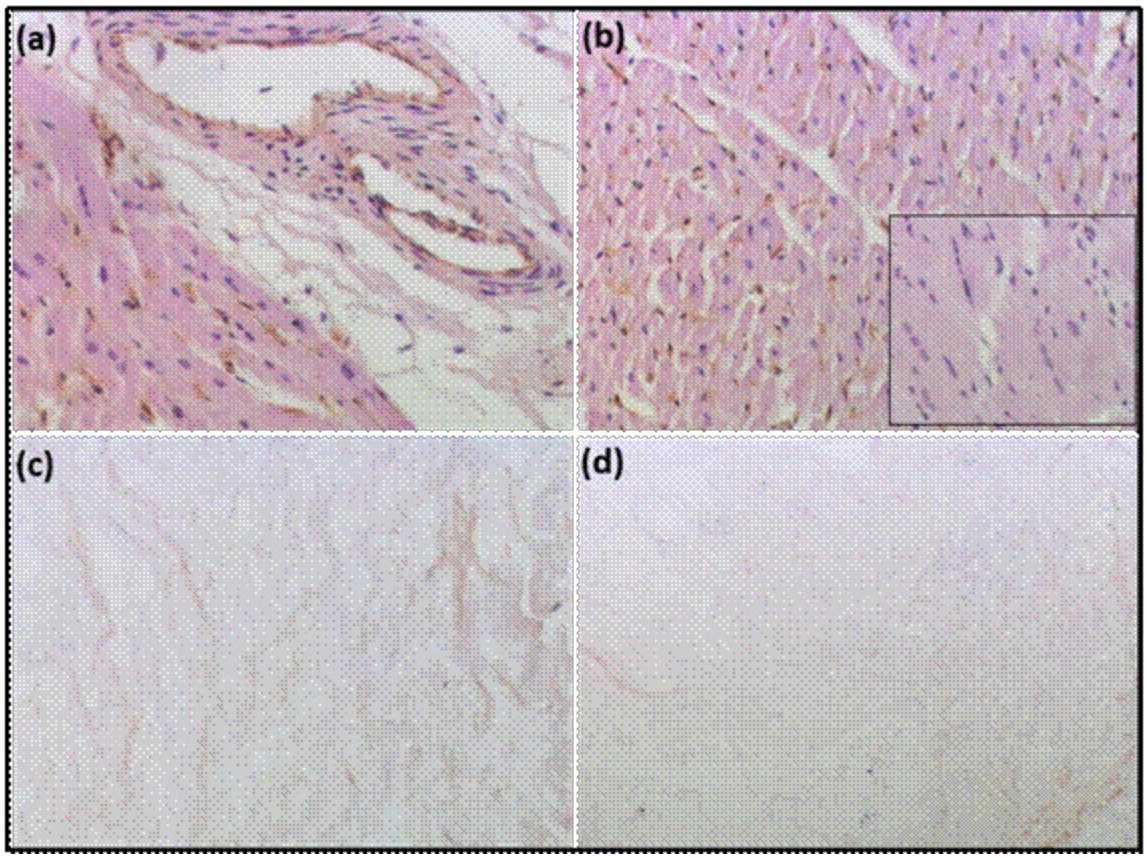

Figure 2.15 Immunohistochemical staining for α-Gal. (a), (b) Native porcine myocardium showed that α-Gal antigen was associated with myocardial fibroblasts, cardiomyocytes and blood vessels; insert shows a negative control where lectin was omitted. (c), (d) Acellular myocardial scaffold showed complete lack of staining for the α-Gal antigen.

The DSC analysis found that the acellular myocardial scaffolds have a T_d value of 70.28 ± 1.39 ºC, falling into the range of thermal denaturation temperature of typical collagenous scaffolds.[31] The collagenase treatment showed that the acellular myocardial scaffolds experienced 18.74% mass loss at 3 days and 36.65% mass loss at 7 days, demonstrating a steady biodegradation rate (Figure 2.5-e).[32] The acellular myocardial scaffolds also showed capability to attract and trap water, with a measured water content of 90.81 ± 0.46 % that was higher than the water content of native myocardium (77.99 ± 0.46 %) (Figure 2.5-d).

2.3.3 Tensile and Shear Properties of the Acellular Myocardial Scaffolds

Tensile mechanical behavior of the acellular myocardial scaffolds along both PD and XD directions is shown in Figure 2.16. Listed in Table 2.2 are maximum tensile modulus, failure stress, failure strain, and hysteresis of the acellular myocardial scaffolds along PD and XD directions. We found that the tensile mechanical behavior along PD direction was significantly stiffer than along the XD direction (Figure 2.16-a, Table 2.2). The acellular myocardial scaffolds showed much stiffer tensile properties when comparing with the native myocardium.[33] Moreover, the energy dissipation of the acellular myocardial scaffolds was in the range of collagenous tissues.[34] Unlike the differences observed in tensile behavior, the acellular myocardial scaffolds exhibited a weaker shear resistance (shear modulus at 40% strain: 5.16 ± 1.35 kPa), which was 8 times lower than the native myocardium (shear modulus at 40% strain: 42.99 ± 5.79 kPa) (Figure 2.16-b, c).

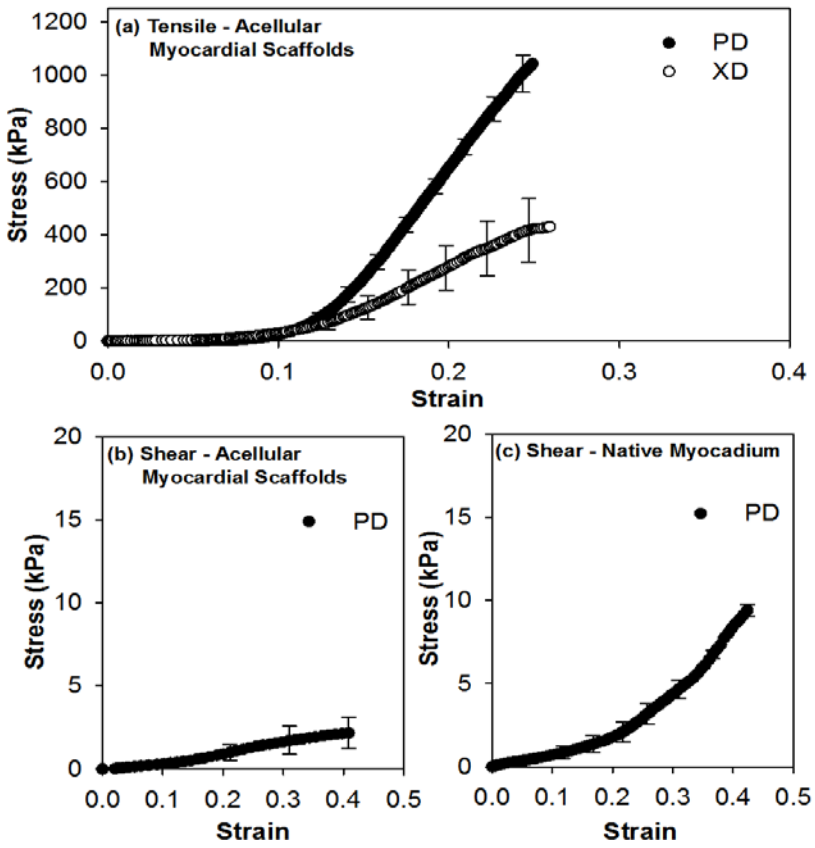

Figure 2.16 (a) Uniaxial tensile responses of the acellular myocardial scaffolds along PD and XD directions; samples were loaded up to failure. Shear mechanical responses of the acellular myocardial scaffolds (b) and the native myocardium (c); only PD direction was examined in shear testing.

Table 2.2 Mechanical parameters obtained from uniaxial tensile testing.

Acellular Myocardial Scaffolds	Maximum Tensile Modulus (kPa)	Tensile Failure Stress (kPa)	Tensile Failure strain (%)	Hysteresis (%)
Fiber preferred direction	9,498.3 ± 1,496.2	1,204.5 ± 40.8	24.99 ± 2.93	10.96 ± 0.37
Cross preferred direction	3,270.2 ± 797.8*	333.9 ± 76.2*	25.92 ± 3.47	12.54 ± 1.94
p value	$p = 0.006$	$p < 0.001$	$p = 0.781$	$p = 0.231$

(* indicates statistically significant difference between two groups ($p < 0.05$))

2.4 Discussion

We have successfully created acellular myocardial scaffolds from native porcine myocardium using an optimized decellularization protocol. The acellular myocardial scaffolds were found to preserve the unique ECM composition, 3D ultrastructure, cardiomyocyte lacunae, and vasculature templates. We found that the frame-pin supporting system additionally preserved the 3D cardiomyocyte ECM lacunae after decellularization which was clearly confirmed by cross-sectional and longitudinal views of histology (Figure 2.6) and topographic views of SEM (Figure 2.7). The pore size of the acellular myocardial scaffolds measured from SEM images showed a radius of 21.4 ± 16.8 μm, which matched transversal dimension of cardiomyocytes. Our edge-to-edge view of the cross section demonstrated that the open porous structure could maintain across a large area without collapse (Figure 2.8). It is evident that the cardiac collagen network appears to be a strong 3D structure, probably required for adequate cardiac functioning (extension of the cardiac ‘‘skeleton’’). We thus speculated that the capability of acellular myocardial scaffolds being able to maintain open pores is due to the inherent properties of myocardial ECM.[33] The quantification of the dimensional changes before and after decellularization showed the overall maintenance of tissue volume, adding more evidence in confirming the internal structural preservation (Figure 2.5, Table 2.1).

Another interesting feature revealed by our SEM study is the interconnecting openings inside the cardiomyocyte lacunae (highlighted by arrows in Figure 2.7-d). Those interconnecting passages were likely an important feature allowing continuity of cardiac muscle fibers both physically and functionally. The preservation of those subtle structures might benefit not only migration of the reseeded cells in tissue engineering maneuvers, but also the possible functional interaction of those cells. Note that the 3D

topographic views of cardiac ECM shown in Figure 2.7-c, d was remarkably similar to a ultrastructural study by Macchiarelli and Ohtani, in which they revealed the lacuna morphology in the NaOH-digested ventricle with SEM.[4] Besides, vasculature templates (vessel-like structure) were possibly preserved after decellularization, according to our histological observations (Figure 2.9), SEM (Figure 2.10-a), and collagen type IV staining (Figure 2.10-b, c).

Using polarizing light microscopy, we showed the existence of light extinguishing patterns in the collagen network of the native myocardium (Figure 2.11-b). As we know, the light extinguishing phenomenon under polarizing light resulted from the wavy pathways of collagen fiber bundles (collagen crimp) and the intrinsic birefringence property of collagen.[35] This observation was consistent with Hanley, et al.'s finding, which reported that collagen fibers in the native myocardium were wavy cords that were straightened considerably as the sarcomere length was increased from 1.85 ± 0.06 μm (near-resting length) to 2.30 ± 0.04 μm.[36] The retaining of light extinguishing patterns in the acellular myocardial scaffolds (Figure 2.11-d) revealed the preservation of collagen crimp, which suggests a likely beneficial feature for future scaffold-cardiomyocyte integration and functioning.

An important perservered feature we confirmed in this study was cardiac elastin and elastin in cardiac blood vessels (black color in Movat's Pentachrome staining, Figure 2.12). The preservation of cardiac elastin in the acellular scaffolds was also highlighted with a yellow arrow in Figure 2.12-c. Fomovsky et. al., recently pointed out that the myocardium contains collagen, cardiac elastin, proteoglycans, in which the mechanical contributions of cardiac elastin and proteoglycans are relatively poorly understood, and circumferential evidence suggests the need to better understand their mechanical

roles.[37] It was well known that in other dynamic tissues such as tendon/ligament, heart valves, and blood vessels, elastin fibers/sheets provide resilience by storing and releasing energy in favor of passive recoil (elasticity).[35] One possible mechanical role of cardiac elastin might be similar to the above mentioned dynamic tissues, i.e., assisting the cardiac contraction cycles by providing microscale resilience. There might be other functions still unknown about cardiac elastin; however, the existence of the cardiac elastin in the native myocardium is a self-evidence of importance from the structure-function point of view. Furthermore, the retaining of vascular elastin in blood vessel networks also provides a favorable platform for later revascularization. The conservation of elastin alignment and distribution in the medial layer and the retaining of elastin lamina on the intimal surface might provide important structural cues for smooth muscle cell differentiation and vascular channel endothelialization, respectively.

The efficiency of removal of cardiomyocytes has been demonstrated histologically by Mason's trichrome staining (Figure 2.6). Movat's pentachrome staining (Figure 2.12) further showed that smooth muscle cells and the endothelial layer in blood vessels were completely removed. Quantitative DNA analysis showed a 98.6% reduction in DNA content (Figure 2.14), which was considered satisfactory for tissue engineering applications and comparable to other decellularization studies.[38] α-Gal antigen staining (Figure 2.15-a, b) revealed that α-Gal antigen was associated with myocardial fibroblasts, cardiomyocytes and blood vessels, while acellular myocardial scaffolds completely lacked α-Gal antigen (Figure 2.15-c, d). The complete removal of all types of cells, DNA fragments, and α-Gal porcine antigen implied the great potential of the scaffolds in future cardiac regeneration applications.

The water content of the decellularized myocardial scaffolds was found to be higher than that of the native myocardium (AMS vs. NM: 90.21 ± 2.36 vs. 77.99 ± 0.46), reflecting a highly hydrophilic property of the acellular myocardial scaffolds. The high porosity of the acellular scaffolds explained the capability of the acellular scaffolds to attract and trap significant amounts of water. In the accelerating enzymatic degradation assay, we found that the decellularization treatment generated acellular myocardial scaffolds that were biodegradable and had a constant degradation rate (18.74 ± 3.44% at 3 days and 36.65 ± 4.95% at 7 days), which is similar to the mass loss in the PGG-fixed porcine pericardium and favors tissue remodeling in the recellularization phase.[32, 39]

As we determined in our previous study,[33] the stiffer mechanical behavior of the acellular myocardial scaffolds reflected the fact that the decellularization procedure turned a muscular tissue into scaffolds mainly consisting of collagen and elastin networks. The loss of shear resistance in the acellular myocardial scaffolds can be attributed to the highly porous structure. Ideally, for either patch application or whole heart tissue engineering, the passive mechanical properties should be re-established to a certain degree by refilling the empty niches of the acellular myocardial scaffolds with the appropriate types of cells. Two efforts are needed in restoration of the passive mechanics of myocardium: one is to lower the tensile properties by adding back cellular contents (matching the patch region with other parts of the ventricle) and another is to re-establish shear resistance to a physiological level. Recellularization and reformation of cell-ECM interaction might help re-establish mechanical properties. As we showed in our previous study,[33] recellularization promotes positive tissue remodeling and generated patch materials that are more mechanically similar to the native myocardium.

In short, the mechanical and structural parameters, such as tensile and shear properties, pore size of ECM lacunae, were reported here for the acellular myocardial ECM. From a biomimetic point of view, those characteristics might indicate useful mechanical and structural cues for the functionality of cardiomyocytes. It is possible that the cardiac scaffold design by polymeric or other approaches would be benefited by mimicking the physical and ultrastructural features reported in this study.[40] As an example, a biomaterial scaffold that has very low modulus might not be able to effectively transfer the contractile forces of cardiomyocytes. The future study will include biochemical characterizations of the ECM compositions, biological factors, and ligand integrity in the acellular myocardial scaffolds. It is also worthy to point out that the structural and biomechanical properties reported here are the characteristics of the remaining myocardial scaffolds after decellularization, which are prone to changes in the tissue remodeling processes either in the *in vitro* recellularization/conditioning, or after implantation.

2.5 Conclusions

An optimized decellularization protocol has been developed to obtain acellular myocardial scaffolds that preserved subtle components and features of the heart ECM. The aligned and interconnected myocardial niches provide nature-designed microenvironments for future recellularization. The preservation of collagen network, cardiac elastin, and vascular templates further confirmed the potential of porcine myocardial ECM as scaffolds for cardiac tissue engineering/regeneration. We demonstrated the complete removal of cells, DNA fragments, and α-Gal porcine antigens as well as a constant biodegradation rate rendered by our decellularization procedure.

Tensile and shear properties of the acellular myocardial scaffolds were also reported, together with structural parameters, providing useful information to porcine myocardial ECM and corresponding tissue engineering efforts (e.g., cardiac patch and whole heart tissue engineering).

2.6 References

1. Streeter, D., et al., Three-Dimensional Fiber Orientation in the Mammalian Left Ventricular Wall, in Cardiovascular System Dynamics. 1978, M.I.T Press. p. 73.

2. Streeter, D.D., Jr. and W.T. Hanna, *Engineering mechanics for successive states in canine left ventricular myocardium. II. Fiber angle and sarcomere length.* Circ Res, 1973. 33(6): p. 656-64.

3. Streeter, D.D., Jr., et al., *Fiber orientation in the canine left ventricle during diastole and systole.* Circ Res, 1969. 24(3): p. 339-47.

4. Macchiarelli, G. and O. Ohtani, *Endomysium in left ventricle.* Heart, 2001. 86(4): p. 416.

5. Gilbert, T.W., T.L. Sellaro, and S.F. Badylak, *Decellularization of tissues and organs.* Biomaterials, 2006. 27(19): p. 3675-83.

6. Ott, H.C., et al., *Perfusion-decellularized matrix: using nature's platform to engineer a bioartificial heart.* Nat Med, 2008. 14(2): p. 213-21.

7. Allen, R.A., et al., *Adrenal extracellular matrix scaffolds support adrenocortical cell proliferation and function in vitro.* Tissue Eng Part A. 16(11): p. 3363-74.

8. Crapo, P.M., T.W. Gilbert, and S.F. Badylak, *An overview of tissue and whole organ decellularization processes.* Biomaterials. 32(12): p. 3233-43.

9. Jackson, D.W., et al., *Freeze dried anterior cruciate ligament allografts. Preliminary studies in a goat model.* Am J Sports Med, 1987. 15(4): p. 295-303.

10. Jackson, D.W., et al., *Cruciate reconstruction using freeze dried anterior cruciate ligament allograft and a ligament augmentation device (LAD). An experimental study in a goat model.* Am J Sports Med, 1987. 15(6): p. 528-38.

11. Jackson, D.W., et al., *The effects of in situ freezing on the anterior cruciate ligament. An experimental study in goats.* J Bone Joint Surg Am, 1991. 73(2): p. 201-13.

12. Jackson, D.W., G.E. Windler, and T.M. Simon, *Intraarticular reaction associated with the use of freeze-dried, ethylene oxide-sterilized bone-patella tendon-bone allografts in the reconstruction of the anterior cruciate ligament.* Am J Sports Med, 1990. 18(1): p. 1-10; discussion 10-1.

13. Roberts, T.S., et al., *Anterior cruciate ligament reconstruction using freeze-dried, ethylene oxide-sterilized, bone-patellar tendon-bone allografts. Two year results in thirty-six patients.* Am J Sports Med, 1991. 19(1): p. 35-41.

14. Gulati, A.K., *Evaluation of acellular and cellular nerve grafts in repair of rat peripheral nerve.* J Neurosurg, 1988. 68(1): p. 117-23.

15. Dong, X., et al., *RGD-modified acellular bovine pericardium as a bioprosthetic scaffold for tissue engineering.* J Mater Sci Mater Med, 2009.

16. Prasertsung, I., et al., *Development of acellular dermis from porcine skin using periodic pressurized technique.* J Biomed Mater Res B Appl Biomater, 2008. 85(1): p. 210-9.

17. Reing, J.E., et al., *The effects of processing methods upon mechanical and biologic properties of porcine dermal extracellular matrix scaffolds.* Biomaterials. 31(33): p. 8626-33.

18. Gorschewsky, O., et al., *Quantitative analysis of biochemical characteristics of bone-patellar tendon-bone allografts.* Biomed Mater Eng, 2005. 15(6): p. 403-11.

19. Cox, B. and A. Emili, *Tissue subcellular fractionation and protein extraction for use in mass-spectrometry-based proteomics.* Nat Protoc, 2006. 1(4): p. 1872-8.

20. Xu, C.C., R.W. Chan, and N. Tirunagari, *A biodegradable, acellular xenogeneic scaffold for regeneration of the vocal fold lamina propria.* Tissue Eng, 2007. 13(3): p. 551-66.

21. Meyer, S.R., et al., *Comparison of aortic valve allograft decellularization techniques in the rat.* J Biomed Mater Res A, 2006. 79(2): p. 254-62.

22. Nakayama, K.H., et al., *Decellularized rhesus monkey kidney as a three-dimensional scaffold for renal tissue engineering.* Tissue Eng Part A. 16(7): p. 2207-16.

23. Lumpkins, S.B., N. Pierre, and P.S. McFetridge, *A mechanical evaluation of three decellularization methods in the design of a xenogeneic scaffold for tissue engineering the temporomandibular joint disc.* Acta Biomater, 2008. 4(4): p. 808-16.

24. Liao, J., E.M. Joyce, and M.S. Sacks, *Effects of decellularization on the mechanical and structural properties of the porcine aortic valve leaflet.* Biomaterials, 2008. 29(8): p. 1065-74.

25. Petersen, T.H., et al., *Tissue-engineered lungs for in vivo implantation.* Science. 329(5991): p. 538-41.

26. Hudson, T.W., S.Y. Liu, and C.E. Schmidt, *Engineering an improved acellular nerve graft via optimized chemical processing.* Tissue Eng, 2004. 10(9-10): p. 1346-58.

27. Sandrin, M.S. and I.F. McKenzie, *Gal alpha (1,3)Gal, the major xenoantigen(s) recognised in pigs by human natural antibodies.* Immunol Rev, 1994. 141: p. 169-90.

28. Strokan, V., et al., *Heterogeneous expression of Gal alpha1-3Gal xenoantigen in pig kidney: a lectin and immunogold electron microscopic study.* Transplantation, 1998. 66(11): p. 1495-503.

29. Azimzadeh, A., et al., *Comparative study of target antigens for primate xenoreactive natural antibodies in pig and rat endothelial cells.* Transplantation, 1997. 64(8): p. 1166-74.

30. Tedder, M.E., et al., *Stabilized collagen scaffolds for heart valve tissue engineering.* Tissue Eng Part A, 2009. 15(6): p. 1257-68.

31. Shanmugasundaram, N., et al., *Collagen-chitosan polymeric scaffolds for the in vitro culture of human epidermoid carcinoma cells.* Biomaterials, 2001. 22(14): p. 1943-51.

32. Sierad, L.N., et al., *Design and Testing of a Pulsatile Conditioning System for Dynamic Endothelialization of Polyphenol-Stabilized Tissue Engineered Heart Valves.* Cardiovasc Eng Technol. 1(2): p. 138-153.

33. Wang, B., et al., *Fabrication of cardiac patch with decellularized porcine myocardial scaffold and bone marrow mononuclear cells.* J Biomed Mater Res A. 94(4): p. 1100-10.

34. Roeder, B.A., et al., *Tensile mechanical properties of three-dimensional type I collagen extracellular matrices with varied microstructure.* J Biomech Eng, 2002. 124(2): p. 214-22.

35. Fung, Y.C., *Biomechanics: Mechanical Properties of Living Tissues*. 1981, New York: Springer-Verlag.

36. Hanley, P.J., et al., *3-Dimensional configuration of perimysial collagen fibres in rat cardiac muscle at resting and extended sarcomere lengths.* J Physiol, 1999. 517 (Pt 3): p. 831-7.

37. Fomovsky, G.M., S. Thomopoulos, and J.W. Holmes, *Contribution of extracellular matrix to the mechanical properties of the heart.* J Mol Cell Cardiol. 48(3): p. 490-6.

38. Baraki, H., et al., *Orthotopic replacement of the aortic valve with decellularized allograft in a sheep model.* Biomaterials, 2009. 30(31): p. 6240-6246.

39. Goo, H.C., et al., *Development of collagenase-resistant collagen and its interaction with adult human dermal fibroblasts.* Biomaterials, 2003. 24(28): p. 5099-113.

40. Guan, J., et al., *The stimulation of the cardiac differentiation of mesenchymal stem cells in tissue constructs that mimic myocardium structure and biomechanics.* Biomaterials. 32(24): p. 5568-80.

CHAPTER III

TISSUE ENGINEERED CARDIAC PATCH USING DECELLULARIZED MYOCARDIAL SCAFFOLD AND MESENCHYMAL STEM CELLS

3.1 Introduction

The myocardium is composed of tightly organized cardiomyocytes connected via gap junctions and highly vascularized and collagen-based extracellular matrix (ECM).[1, 2] Substantial progress has been made for more than ten years in myocardial tissue engineering, but there are still many challenges remaining,[3] such as the limitation of the amount of oxygen and nutrition the myocardial tissue can receive, difficulty in obtaining an ideal cell density, and immunological rejection.

As we mentioned previously, the goal of cardiac tissue engineering is to create a cardiac construct by seeding desired cells into the scaffold materials. Zimmermann embedded neonatal rat cardiomyocytes in a collagen gel scaffold and applied mechanical stimulation during *in vitro* culture to improve the contractile properties of the patch.[4] After implanation, they observed the integration of the patch with the native heart muscle, as well as the improvement of cardiac function. Leor et al. had developed the engineered myocardium by seeding fetal rat cardiomyocytes into the alginate sponges and implanted the engineered tissue into the infarcted rat heart.[5] They found that the scattered fetal cardiomyocytes in the graft were able to survive after implantation, whereas most of the alginate scaffold was packed with collagen fibers and scattered fibroblasts.[5] To further improve engrafted cell survival, various cell-supporting scaffold

materials have been examined,[6, 7] with pro-angiogenic factors and pro-survival factors integrated into scaffolds.[8, 9]

Instead of reseeding cells into a three-dimensional polymer scaffold, some research groups created cardiac tissue by growing cells into cell sheets or cell patches, which they believed provided a good environment for cell migration.[10] Okano created a cell sheet that was cultivated and detached from their culture substrate by using a thermo-sensitive polymer substrate.[11] Further *in vivo* study demonstrated that the cardiomyocytes in the cell sheet had survived after subcutaneous implantation for 1 year and the repaired rat hearts showed functional integration with the cell sheet and the host myocardium.[12]

Using the injectable biomaterials for cellular cardiomyoplasty is another promising strategy in cardiac regeneration. Once such biomaterials are injected into the scar tissue, the injected cells would contact intimately with the host tissue. More importantly, the injectable therapy can be administered using a less invasive procedure.[13] Christman developed an injectable scaffold using fibrin glue biomaterial to deliver myoblasts to the ischemic myocardium.[14] They reported that the fibrin significantly increased cell survival rate up to 5 weeks. Seliktar et al. created a new type of injectable biosynthetic material which is made by conjugating poly-ethylene glycol (PEG) with fibrinogen to form a liquid precursor.[15] Animal studies demonstrated that once this type of hydrogel was injected into infarct adult rat hearts together with neonatal rat cardiomyocytes or human embryonic stem cells (ESC) derived cardiomyocytes, cell survival was increased and the overall cardiac functionality was significantly improved after 30 days.[16]

More recently, whole organ regeneration has been studied due to a tremendous potential for the field of organ transplantation. In cardiac regeneration, Ott et al. obtained a whole rat heart ECM scaffold using the perfusion decellularization method; the decellularized whole rat heart maintained its 3D ECM structure, including the vasculature tubing skeleton, which was preserved by the presence of vascular basement membranes.[17] The next possible ambitious attempt is to apply this approach to larger xenogenous hearts, such as pig hearts that have similar size, anatomic geometry and vasculature systems as human.[18, 19] Another line of research using decellularized myocardium is this dissertation study, in which we are trying to harness the potential of acellular myocardial scaffolds as a template for cardiac patch tissue engineering as well as better understanding the mechanism of cell-myocardial ECM interactions.[20]

In this study, we investigated decellularized porcine myocardial scaffolds as a potential template for stem cell reseeding, cell differentiation, and cardiac tissue construct development. We hypothesize that the decellularized porcine myocardium scaffold preserves natural ultrastructural, mechanical, and compositional cues for cardiac tissue regeneration and would provide optimal microenvironments for stem cell reseeding, cardiomyocyte differentiation, and angiogenesis. This chapter describes how we created a cardiac patch using the decellularized pig myocardium scaffold and the bone marrow mononuclear cells (BMMCs), and assessed its potential for tissue remodeling.

3.2 Materials and Methods

3.2.1 Isolation of Porcine Bone Marrow Mononuclear Cells (BMMCs)

Bone marrow was extracted from femurs and tibias of fetal pigs. Both ends of each femur or tibia were cut and the bone marrow was washed out with phosphate-buffered saline (PBS) (Figure 3.1).

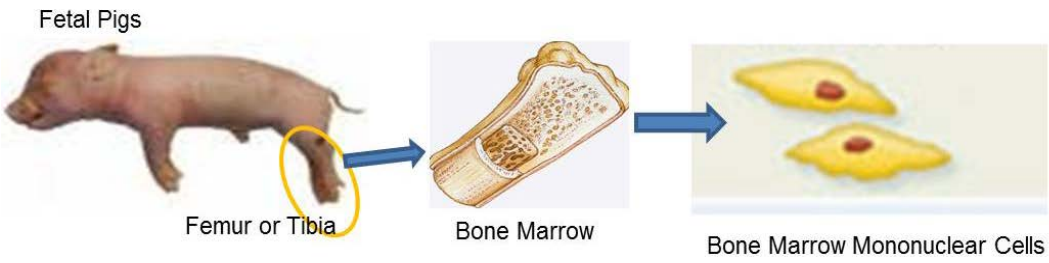

Figure 3.1 BMMCs were extracted from femurs and tibias of fetal pigs

Cells were centrifuged at 400 r/min for 10 min at 4°C, suspended by gentle pipetting, and cultured in mesenchymal stem cell (MSC) medium (Low-glucose Dulbecco's modified Eagle's medium (L-DMEM)) with 5% fetal bovine serum (FBS), Mesenchymal Stem Cell Growth Supplement (Sciencell), and 100 U/ml penicillin and 100 µg/ml streptomycin (Invitrogen) at 37°C in a humid 5% CO_2 air atmosphere. Three days later, nonadherent cells were removed by replacing the medium. After 10 days' culture, the adherent cells were resuspended after HyQTase (Fisher safety) treatment and re-plated at a density of $2 \times 10^4/cm^2$. The medium was changed every 3 days. Bone marrow mesenchymal stem cell population was verified by stem cell CD44 surface marker staining (Abcam).

3.2.2 Myogenic Differentiation and Reseeding

The second passage BMMCs were re-suspended after 0.25% trypsin treatment and washed twice with Tyrode's balanced salt solution (Sigma). The cells were re-suspended in mesenchymal stem cell medium and seeded into 175-mm flasks at a density of 2×10^3 cells/cm^2. Twenty-four hours after seeding, the medium was changed to differentiation medium (L-DMEM, 10% FBS, 5% porcine serum, 3 μmol/L 5-azacytidine (MP Biomedicals), and 100 U/ml penicillin and 100μg/ml streptomycin). After incubating for another 24 hrs, the cells were washed twice with Tyrode's balanced salt solution and the medium was changed to complete medium (L-DMEM, 10% FBS, 5% porcine serum, and 100 U/ml penicillin and 100μg/ml streptomycin). The medium was changed twice a week. Differentiation of BMMCs was verified by sarcomeric α-actinin staining (Sigma). After completing the protocol, aliquots of the cells were prepared for reseeding and immunohistochemistry study. Decellularized scaffolds were sterilized by 70% ethanol for 4 hours, reseeded with un-selected cells, mainly a mixture of non-differentiated and differentiated BMMCs (10^7 cells/ml), for 4 hrs under gentle agitation, and cultured in a rotating bioreactor with complete medium. The medium was changed twice every week.

3.2.3 Histological and Immunohistochemical Characterizations

Filmtracer™ LIVE/DEAD® Biofilm Viability Kit (Invitrogen) solution was prepared by adding 20 μl of the supplied 2 mM EthD-1 stock solution (Component B) to 10 ml of sterile, tissue culture–grade D-PBS, vortexing to ensure thorough mixing. The reagents were combined by transferring 5 μl of the supplied 4 mM calcein AM stock solution (Component A) to the 10 ml EthD-1 solution. The reseeded patch was incubated for 30 – 45 minutes at room temperature.

Specimens used for light microscopy were fixed in 2% paraformaldehyde solution for 2 hours, embedded in paraffin and stained with hematoxylin and eosin (H&E) and Masson's trichrome. For immunofluorescent staining, after rehydration and antigen retrieval with 0.05% Trypsin for 10 minutes at 37°C, sections were washed and incubated at 4°C for overnight with sarcomeric α-actinin (sigma), myosin heavy chain (MHC) (GenWay), and von Willebrand factor (vWF) (abcam) primary antibody. After the primary antibody, Cy3 AffiniPure Goat Anti-Mouse IgG (H+L), Cy5 AffiniPure Donkey Anti-Mouse IgM, and Alexa Fluor secondary antibodies (JacksonImmuno Research) were incubated at 37°C for 30 minutes to obtain fluorescent colors. The sections were then stained with Hoechst (Invitrogen) for cell nuclei. Immunohistological slides were observed with an inverted laser scanning confocal microscope (Zeiss LSM 510).

3.2.4 Biaxial Mechanical Testing

Tissue biaxial mechanical properties were characterized with a biaxial mechanical testing system (Figure 3.2-a).[21] Briefly, a square specimen was trimmed from the native myocardium/engineered patch with one edge of the square aligned with fiber-preferred direction (PD) and the other edge aligned with cross fiber-preferred direction (XD). Each side of the square specimen was mounted onto four stainless steel hooks that were attached to two loops of 000 polyester sutures. Biaxial loading was then applied along muscle/scaffold PD and XD direction of the specimen (Figure 3.2-b). Since the test loaded the planar tissue specimen biaxially with four loading points on each side, membrane tension was used for testing protocol control and data report. By definition, Lagrangian membrane tension refers to force per unit initial length of the specimen edge and is calculated by the following equation: (Lagrangian Membrane Tension) = (Applied

Force)/(Initial Edge Length). For calculating the real time biaxial stretches, four fiducial graphite markers were affixed to the center of the square specimen with cyanoacrylate adhesive and monitored via a CCD camera. After a 10-cycle preconditioning, the specimen was subjected to biaxial test utilizing an equibiaxial protocol of T_{PD}:T_{XD} = 60:60 N/m, where T_{PD} and T_{XD} were the applied tensions along PD and XD, respectively. Due to possible tissue tear at the hook sites at higher tension levels, specimens were loaded up to a maximum tension of 60 N/m. Tissue extensibility was characterized by maximum stretch along PD (λ_{PD}) and maximum stretch along XD (λ_{XD}) at equibiaxial tension of 60 N/m.

3.2.5 Uniaxial Mechanical Testing

A uniaxial machine (Mach-1, Biosyntech, MN) was used to determine tissue material properties including failure strength and strain. After biaxial testing, tissue strips were cut along the PD and were mounted with two stainless steel grips cushioned with emery paper. The tissue was preconditioned for 10 cycles at a ramp speed of 0.1 mm/s. All of the samples were then elongated to failure at the same ramp speed. Stress-strain data in the linear region were fit with linear regression. The tissue extensibility was defined as the intersecting point made by the extrapolation of the linear region with the strain axis, and tensile modulus was determined by finding the tangent of the linear fit. Moreover, failure strength and failure strain were determined from the stress-strain curve. All samples were tested in a PBS bath at 37 ºC.

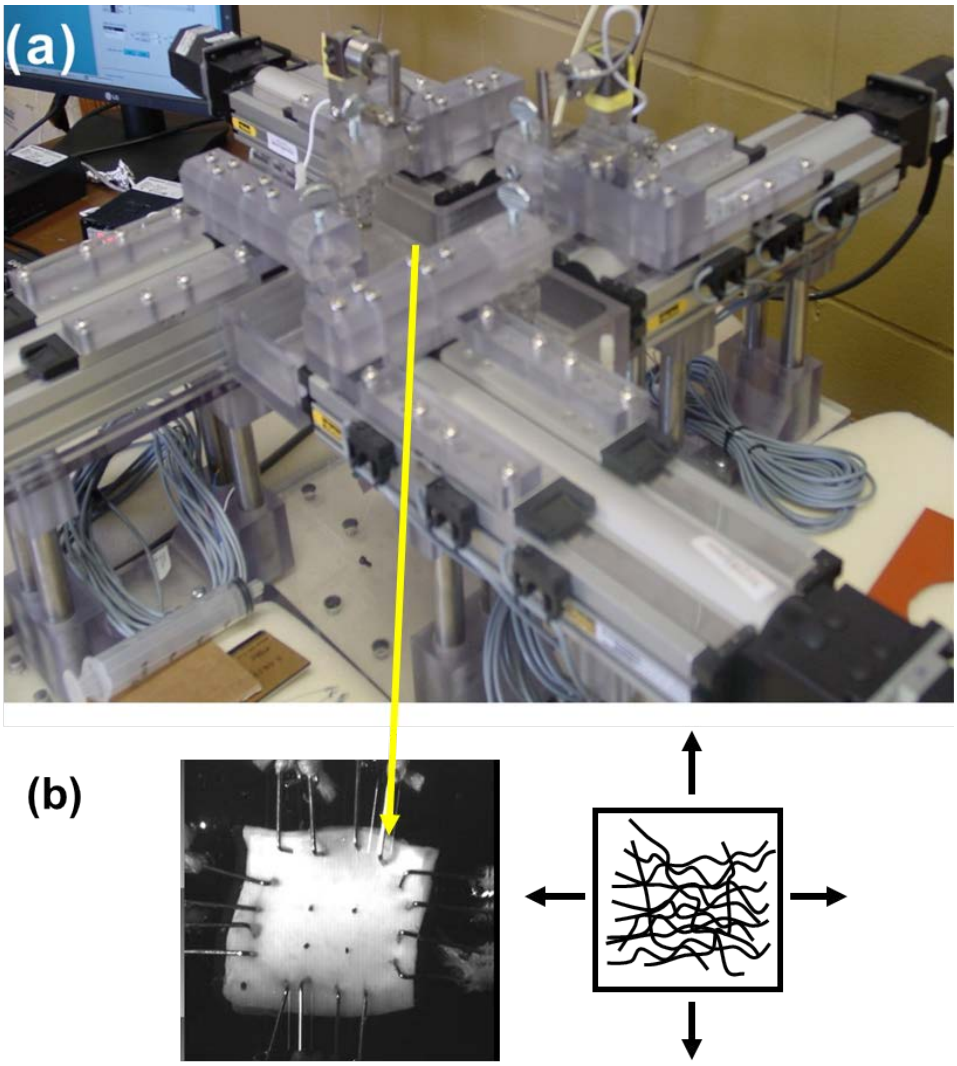

Figure 3.2 (a). Tissue biaxial testing system; (b) The square sample was trimmed from the native myocardium/engineered patch. Biaxial loading was then applied along muscle/scaffold fiber preferred direction (PD) and cross preferred direction (XD) of the specimen.

3.2.6 Statistical Analysis

The experimental data were presented as mean ± standard deviation. One Way Analysis of Variances (ANOVA) was used for statistical analysis, with Holm-Sidak test being used for post hoc pair wise comparisons and comparisons versus the control group (SigmaStat 3.0, SPSS Inc., Chicago, IL). The differences were considered statistically significant when p is less than 0.05.

3.3 Results

3.3.1 Recellularization and Phenotype Characterizations

One week after primary culture, BMMCs developed long spindle-shaped cell morphology (Figure 3.3-a). BMMC surface antigen profile was positive for CD44 (Figure 3.3-b,c). After 5-azacytidine treatment, sarcomeric α-actinin staining showed positive results (Figure 3.4-a, b). The cardiomyocyte differentiation rate was estimated to be ~24% according to the ratio of cells stained positive for sarcomeric α-actinin (Figure 3.4-a).

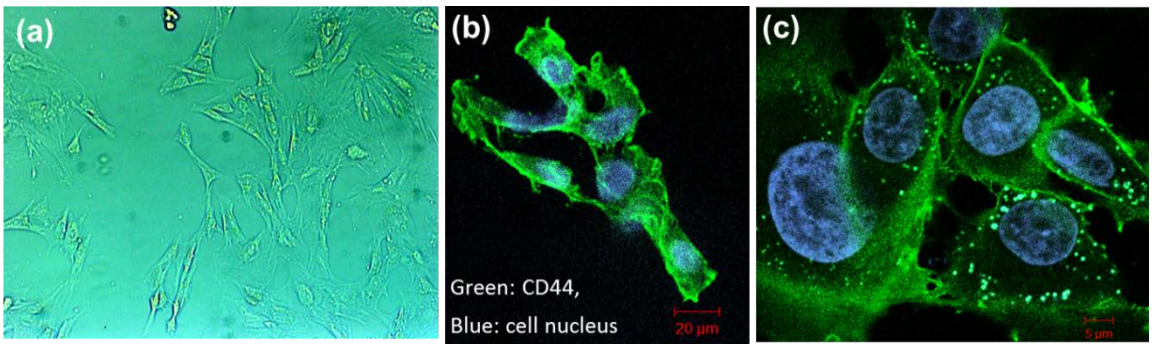

Figure 3.3 (a) BMMCs after one week primary culture under light microscope. (b,c) Positive staining for stem cell marker CD44 (green color).

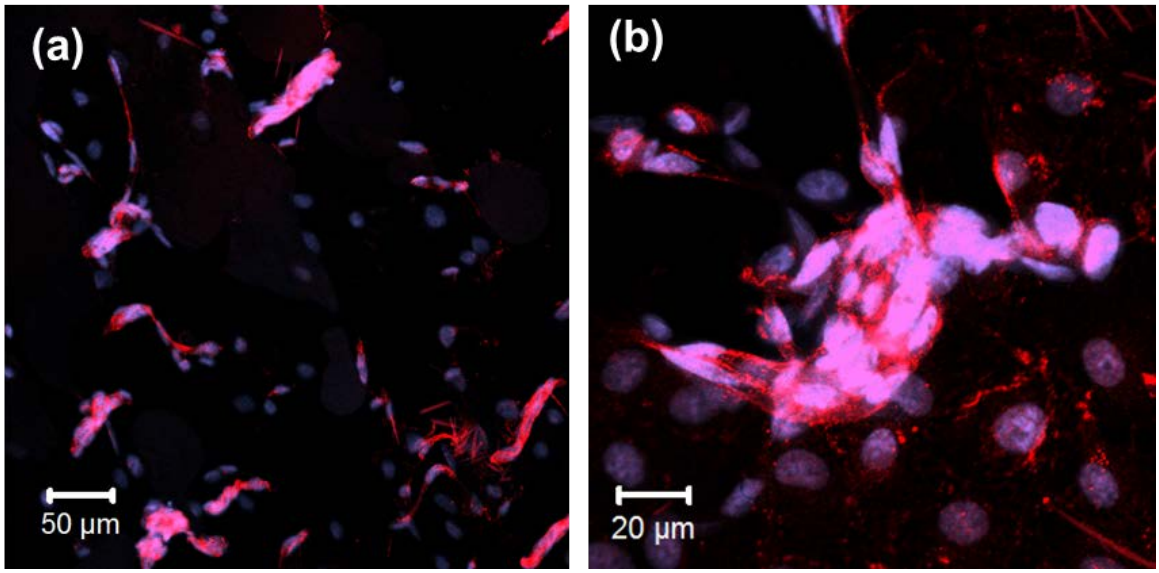

Figure 3.4 Cardiomyocyte differentiation after treated with 5-azacytinine; red staining: sarcomeric α-actin.

The transversal section of acellular myocardial scaffold had an average pore size of 19.5 ± 17.9 μm, which matched the transversal dimension of cardiomyocytes. Edge-to-edge views of transversal sections of acellular scaffolds showed that large pores were distributed evenly across the ~2 mm thickness (Figure 3.5-a). A thorough recellularization was verified by Mason's trichrome staining in both the 2-week (Figure 3.5-b) and 4-week constructs (Figure 3.5-c). In the 2-week construct, cells were found to infiltrate and distribute within the myocardial scaffold. We divided the edge-to-edge section evenly into three regions (2 edge regions and 1 middle region) and measured the cell density in each region. Cell densities of the 3 regions in the 2-week constructs were $(2.00 \pm 0.02) \times 10^3/mm^2$, $(1.24 \pm 0.20) \times 10^3/mm^2$, and $(1.69 \pm 0.16) \times 10^3/mm^2$, respectively. Cell densities of the 3 regions in the 4-week constructs were $(2.50 \pm 0.28) \times 10^3/mm^2$, $(1.85 \pm 0.43) \times 10^3/mm^2$, and $(3.11 \pm 0.13) \times 10^3/mm^2$, respectively. In both the 2- and 4-week construct, cell density was evenly distributed, but was found much higher than that of the 2-week construct.

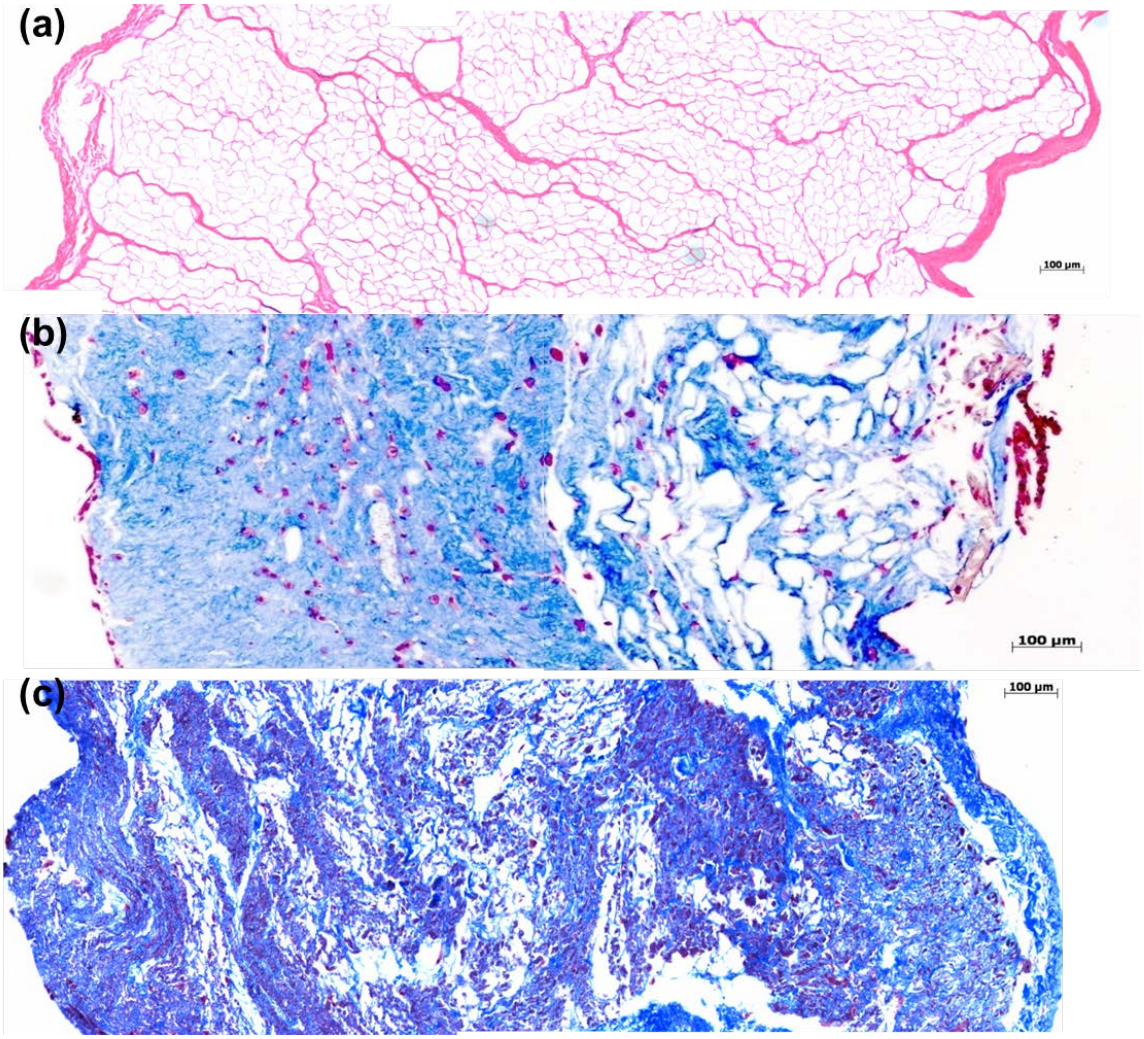

Figure 3.5 (a) Edge-to-edge view of H&E staining showed that large pores distributed evenly across the 2 mm thick acellular scaffold. (b) thorough recellularization was found after 2 weeks, in which cells were found to infiltrate and distribute within the myocardial scaffold. (c)Tissue remodeling were observed in the 4 weeks recellularization tissue construct; even cell distribution was still observed and cell density was found much higher than that of the 2-week construct.

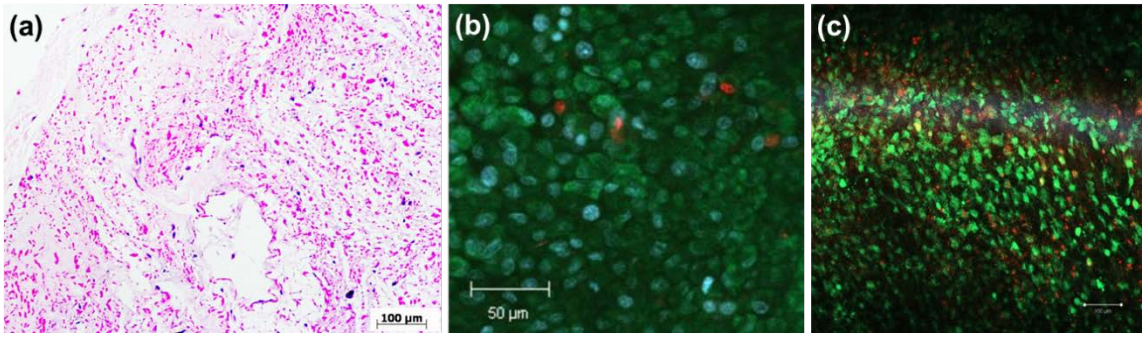

Figure 3.6 (a) Thorough and relatively dense reseeding was observed in tissue construct after 4 week culture (H&E staining). Live/dead cell staining on 4-week tissue construct: (b) surface of tissue construct and (c) side view of cross-sectional cut. Green: living cells; Red: dead cells.

Cell viability was verified by live/dead cell staining (Figure 3.6-b, c). A side view of the cross-sectional cut of the construct showed that most cells were alive (Figure 3.6-c). However, a ~27% dead cell ratio inside the construct was higher than that on the surface (Figure 3.6-b, c).

Immunohistological staining studies showed that the reseeded cells exhibited cardiomyocyte-like phenotype and expressed sarcomeric α-actinin, myosin heavy chain, and cardiac troponin T (Figure 3.7-b, d, f). Moreover, vWF factor was found around vessel-like structures, implying possible endothelialization inside vasculature channels (Figure 3.7-g).

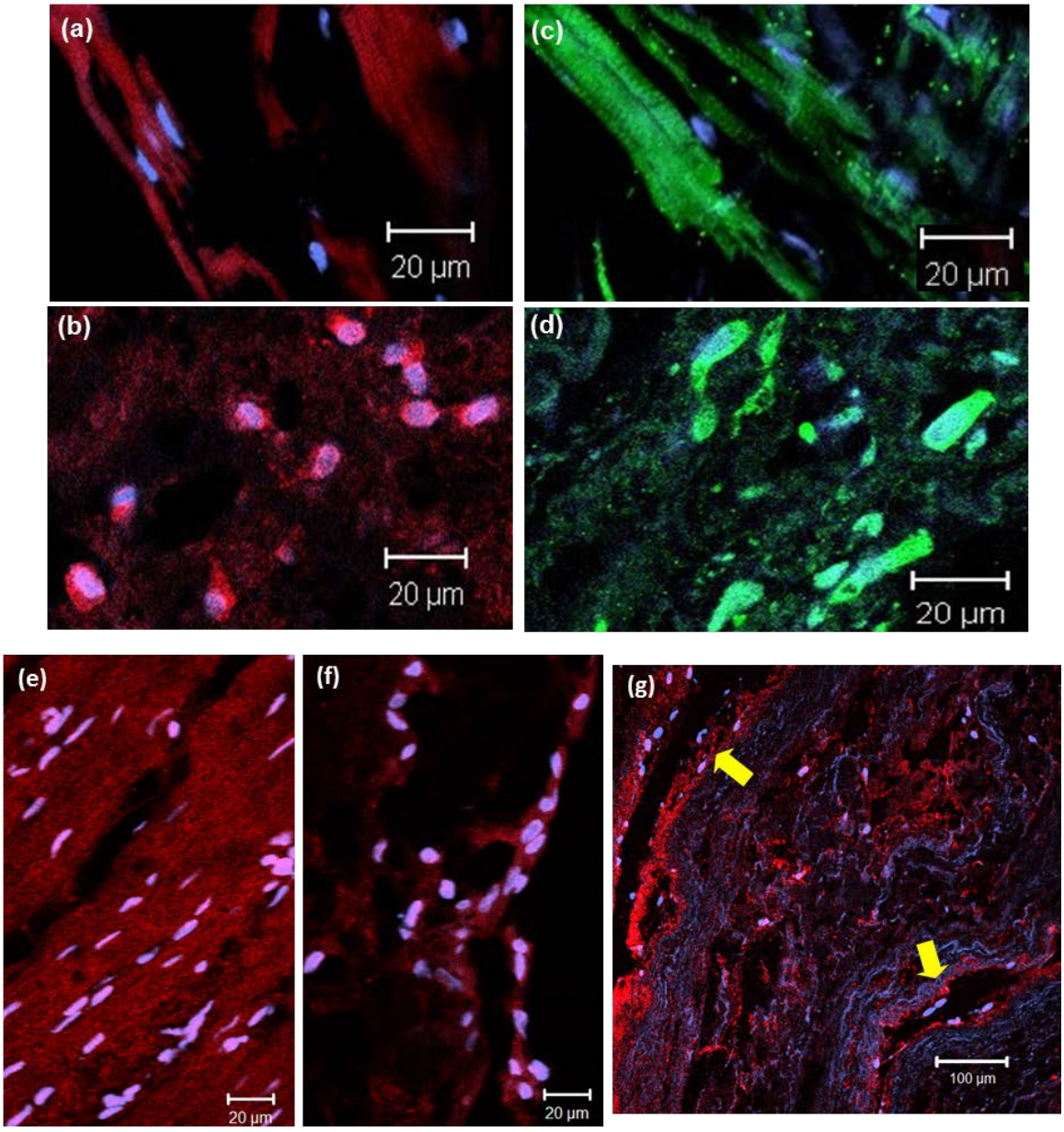

Figure 3.7 Sarcomeric a-actinin staining (red) in the native myocardium (a) and the reseeded patch (b); myosin heavy chain staining (green) in the native myocardium (c) and the reseeded patch (d); cardiac troponin T staining (red) in the native myocardium (e) and the reseeded patch (f) vWF factor (red) was shown in the reseeded patch (g). Cell nucleus: blue.

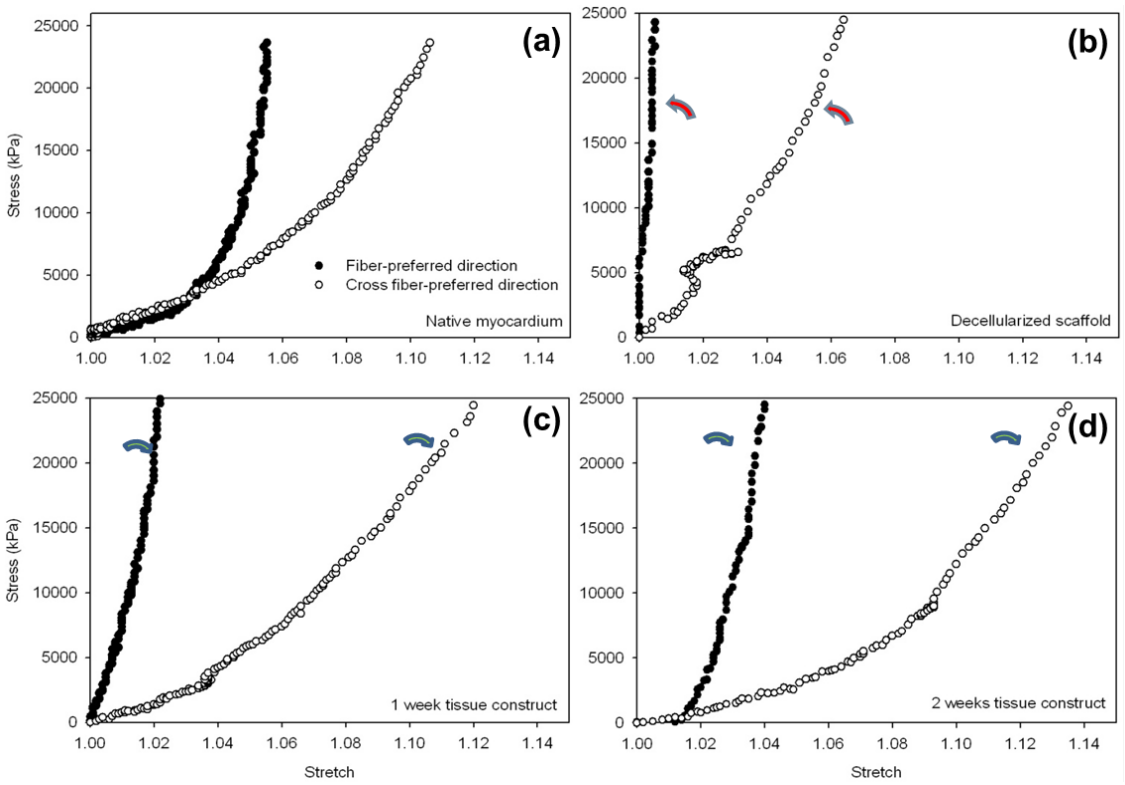

Figure 3.8 Biaxial mechanical properties. (a) Native myocardium showed anisotropic nonlinear behavior in which muscle fiber-preferred direction (PD) is stiffer than cross fiber-preferred direction (XD). (b) PD and XD directions showed stiffer stress–strain curves in decellularized myocardial scaffold. (c) 1 week reseeded cardiac patch. (d) 2 weeks reseeded cardiac patch. Tissue remodeling caused a recovery of the biaxial mechanical properties after 1-week and 2-week recellularization. The 1-week and 2-week tissue constructs kept nonlinear anisotropic behavior and tissue extensibility more close to native myocardium along both PD and XD directions.

3.3.2 Mechanical Properties

We found that both native myocardium and acellular scaffold showed anisotropic nonlinear behavior (Figure 3.8-a, b), in which muscle fiber-preferred direction was stiffer than cross fiber-preferred direction (Figure 3.8-a). After the removal of muscle cells, both PD and XD directions showed stiffer stress-strain curves (Figure 3.8-b). We later found that tissue remodeling caused a recovery of the biaxial mechanical properties after 1-week and 2-week recellularization (Figure 3.8-c, d). The 1-week and 2-week tissue

constructs kept nonlinear anisotropic behavior and tissue extensibility closer to native myocardium along both PD and XD directions (Table 3.2; Figure 3.8-c, d).

The stiffer mechanical properties of the decellularized myocardial scaffolds were also verified by uniaxial testing results (Figure 3.9-a, b). Similar to biaxial characterization, after 1-week and 2-week cultures, constructs showed a recovering tendency (Figure 3.9-a, b). Tensile modulus, tissue extensibility, and failure stress are listed in Table 3.1 for native myocardium, decellularized scaffold, 1-week, and 2-week tissue constructs.

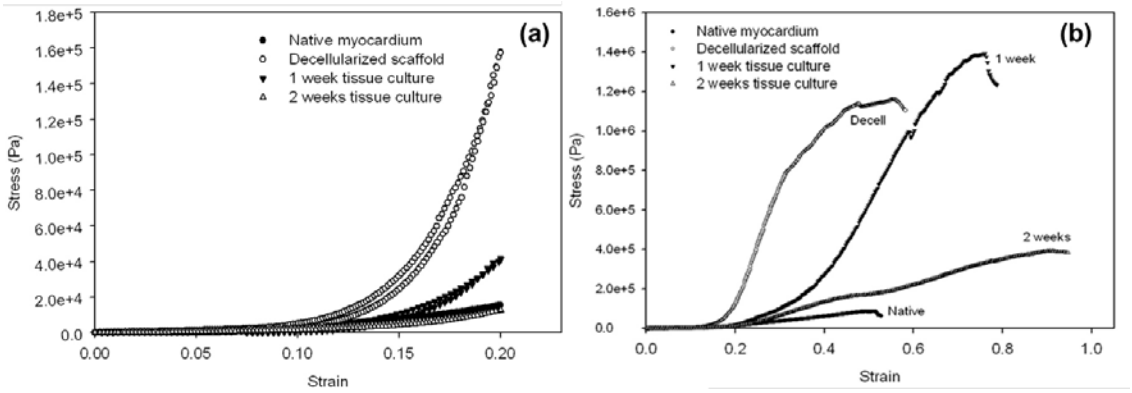

Figure 3.9 Both (a) uniaxial mechanical properties and (b) tissue failure properties show a recovering tendency after 1-week and 2-week cultures. Note that both loading and unloading stress–strain curves were shown in (a).

Table 3.1 Biaxial and uniaxial mechanical properties of native myocardium, decellularized scaffold, and patch constructs.

	Biaxial Mechanical Properties		Uniaxial Mechanical Properties		
	Maximum stretch (PD)	Maximum stretch (XD)	Tensile modulus (kPa)	Extensibility (strain)	Failure stress (kPa)
Native	1.083 ± 0.029	1.145 ± 0.048	223.3 ± 49.2	0.199± 0.050	67.5 ± 25.1
Acellular Scaffold	1.004± 0.006*	1.150 ± 0.008	5218.7± 1723*	0.169± 0.003	903.0 ± 363.5
Reseed 1 week	1.060 ± 0.006	1.150 ± 0.053	3593.2± 838.9*	0.198± 0.074	914.0 ± 673.2
Reseed 2 weeks	1.040 ± 0.037	1.210 ± 0.009	760.6 ± 69.7	0.216± 0.012	482.5 ± 85.6

* denotes significant difference when compared with native myocardium ($p < 0.05$).

3.4 Discussion

In this exploratory study, we chose BMMCs as our reseeding cell source. The isolated BMMCs had strong self-renewal ability and 70% of the cells were mesenchymal stem cells and positive for CD44, a cell-surface glycoprotein of mesenchymal stem cells (MSCs).[22] BMMCs were previously reported to have the ability to differentiate into cardiomyocyte phenotype under specific culture conditions as well as in healthy and infarcted myocardium (e.g., injection in animal models).[23-27] BMMCs were found to secrete angiogenic cytokines that promote blood flow recovery in a murine hind limb ischemia model.[28]

5-azacytidine is a member of the cytosine analogue, which had been reported to have the ability to change cell phenotypes by activating novel gene expressions both *in vitro* and *in vivo*.[29] It was reported that after 5-azacytidine treatment, about 30% cardiomyocyte differentiation took place in the culture.[30, 31] We showed that, after BMMCs were treated with 5-azacytidine for 24 hours, the treated cells exhibited cardiomyocyte phenotype and were positive for sarcomeric α-actinin (Figure 3.4). The

successful recellularization of the 5-azacytidine treated BMMCs verified our hypothesis that the acellular porous myocardial scaffold provided an optimal recellularization microenvironment.

Reseeded cells were found to have infiltrated and proliferated well in the tissue construct (Figure 3.5). The cell density in the 4-week construct was higher than the 2-week construct. From the live/dead staining results, it was shown that the proliferation rate of the reseeded cells remained high in the 4-week *in vitro* culture. The cells were found distributed evenly across the 2 mm thick patch, indirectly proving the interconnectivity of 3D myocyte lacunae after decellularization. As we know, thorough and uniform recellularization at high cell density was a prerequisite for the later success of functional cardiac tissue constructs. Note that our reseeding data showed thorough reseeding, but the level of uniformity and cell density may be insufficient and require further investigation to improve our reseeding technique.

Phenotypic characterizations showed that cells in the engineered patch were positive for sarcomeric α-actinin, MHC, and cardiac troponin T (Figure 3.7-b, d, f), which suggested a differentiation into a myocyte-like phenotype. Another interesting finding was that vasculature templates (vessel-like structure) were possibly preserved after decellularization, according to our histological observations. In the engineered patch, vWF expression (endothelial marker) was verified at locations with vessel-like histological structure (Figure 3.7-g). Moreover, Hoechst staining showed the cell nuclei aligned along the inner surface of the vessel-like structure. The above observations revealed that possible endothelialization took place around the vasculature templates, implying a potential for angiogenesis in the engineered patch. However, the detailed mechanism is unclear. We speculated that undifferentiated mesenchymal stem cells might

be the underlying mechanism of endothelialization along the vasculature channels in the engineered patches.

Our biaxial and uniaxial mechanical testing results also provided potential mechanistic insight into how reseeded cells remodeled the engineered scaffolds. After the removal of cardiomyocytes, mechanical properties of the remaining ECM, consisting of mainly collagen, were measured. It was thus understandable that both PD and XD directions showed stiffer curves. The preservation of anisotropic properties (Figure 3.8-b) was due to the orientation of ECM lacunae, which aligned most collagen fibers along the muscle fiber-preferred direction (note that muscle cells were removed). The increase of cellular content explained the recovery of the biaxial mechanical properties after reseeding for 1 week and 2 weeks (Figure 3.8-c, d). The uniaxial testing results also demonstrated obvious tissue remodeling in the 2-week constructs, which exhibited greater tissue extensibility and lower failure stress (Figure 3.9-b; Table 3.2). Overall, the mechanical properties of the reseeded scaffolds showed a recovering trend along with the culture time, as expected from the increased cellular content (Figure 3.9). It had been reported that the "passive stiffness" of the myocardium is a major determinant of overall cardiac function.[32, 33] Thus, it was of importance to have an engineered cardiac patch that matched the mechanical properties of native myocardium. We have found that the mechanical properties of the two-week scaffold were close to the native myocardium; however, further studies are needed in order to obtain higher cell density, cell interconnection, and electrophysiological properties.

3.5 Conclusions

In this study, we have successfully recellularized the acellular myocardial scaffold. The reseeded cells were found to infiltrate and proliferate in the tissue constructs. Immunohistological staining studies showed that the reseeded cells demonstrated cardiomyocyte-like phenotype and possible endothelialization was found in locations close to vasculature channels, indicating angiogenesis potential. Both biaxial and uniaxial mechanical testing showed a stiffer mechanical response of the acellular myocardial scaffolds; however, tissue extensibility and tensile modulus were found to recover in the constructs along with the culture time, as expected from increased cellular content. To better improve the reseeding density, cell alignment and interconnection, and facilitating mesenchymal stem cell differentiation, we initiated a bioreactor design that could provide coordinated mechanical and electrical stimulations (Chapter 4).

3.6 References

1. Rakusan, K., et al., *Morphometry of human coronary capillaries during normal growth and the effect of age in left ventricular pressure-overload hypertrophy.* Circulation, 1992. 86(1): p. 38-46.

2. Korecky, B., C.M. Hai, and K. Rakusan, *Functional capillary density in normal and transplanted rat hearts.* Can J Physiol Pharmacol, 1982. 60(1): p. 23-32.

3. Zimmermann, W.H., et al., *Heart muscle engineering: an update on cardiac muscle replacement therapy.* Cardiovasc Res, 2006. 71(3): p. 419-29.

4. Zimmermann, W.H., et al., *Tissue engineering of a differentiated cardiac muscle construct.* Circ Res, 2002. 90(2): p. 223-30.

5. Leor, J., et al., *Bioengineered cardiac grafts: A new approach to repair the infarcted myocardium?* Circulation, 2000. 102(19 Suppl 3): p. III56-61.

6. Ishii, O., et al., *In vitro tissue engineering of a cardiac graft using a degradable scaffold with an extracellular matrix-like topography.* J Thorac Cardiovasc Surg, 2005. 130(5): p. 1358-63.

7. Ozawa, T., et al., *Optimal biomaterial for creation of autologous cardiac grafts.* Circulation, 2002. 106(12 Suppl 1): p. I176-82.

8. Kutschka, I., et al., *Collagen matrices enhance survival of transplanted cardiomyoblasts and contribute to functional improvement of ischemic rat hearts.* Circulation, 2006. 114(1 Suppl): p. I167-73.

9. Dvir, T., et al., *Prevascularization of cardiac patch on the omentum improves its therapeutic outcome.* Proc Natl Acad Sci U S A, 2009. 106(35): p. 14990-5.

10. Shimizu, T., et al., *Two-dimensional manipulation of cardiac myocyte sheets utilizing temperature-responsive culture dishes augments the pulsatile amplitude.* Tissue Eng, 2001. 7(2): p. 141-51.

11. Shimizu, T., et al., *Cell sheet-based myocardial tissue engineering: new hope for damaged heart rescue.* Curr Pharm Des, 2009. 15(24): p. 2807-14.

12. Furuta, A., et al., *Pulsatile cardiac tissue grafts using a novel three-dimensional cell sheet manipulation technique functionally integrates with the host heart, in vivo.* Circ Res, 2006. 98(5): p. 705-12.

13. Orlando, G., et al., *Regenerative medicine as applied to solid organ transplantation: current status and future challenges.* Transpl Int. 24(3): p. 223-32.

14. Christman, K.L., et al., *Injectable fibrin scaffold improves cell transplant survival, reduces infarct expansion, and induces neovasculature formation in ischemic myocardium.* J Am Coll Cardiol, 2004. 44(3): p. 654-60.

15. Williams, C.G., et al., *Variable cytocompatibility of six cell lines with photoinitiators used for polymerizing hydrogels and cell encapsulation.* Biomaterials, 2005. 26(11): p. 1211-8.

16. Habib, M., et al., *A combined cell therapy and in-situ tissue-engineering approach for myocardial repair.* Biomaterials. 32(30): p. 7514-23.

17. Ott, H.C., et al., *Perfusion-decellularized matrix: using nature's platform to engineer a bioartificial heart.* Nat Med, 2008. 14(2): p. 213-21.

18. Badylak, S.F., D. Taylor, and K. Uygun, *Whole-organ tissue engineering: decellularization and recellularization of three-dimensional matrix scaffolds.* Annu Rev Biomed Eng. 13: p. 27-53.

19. Wainwright, J.M., et al., *Preparation of cardiac extracellular matrix from an intact porcine heart.* Tissue Eng Part C Methods. 16(3): p. 525-32.

20. Wang, B., et al., *Fabrication of cardiac patch with decellularized porcine myocardial scaffold and bone marrow mononuclear cells.* J Biomed Mater Res A. 94(4): p. 1100-10.

21. Grashow, J.S., A.P. Yoganathan, and M.S. Sacks, *Biaixal stress-stretch behavior of the mitral valve anterior leaflet at physiologic strain rates.* Ann Biomed Eng, 2006. 34(2): p. 315-25.

22. Vogel, W., et al., *Heterogeneity among human bone marrow-derived mesenchymal stem cells and neural progenitor cells.* Haematologica, 2003. 88(2): p. 126-33.

23. Wollert, K.C. and H. Drexler, *Mesenchymal stem cells for myocardial infarction: promises and pitfalls.* Circulation, 2005. 112(2): p. 151-3.

24. Makino, S., et al., *Cardiomyocytes can be generated from marrow stromal cells in vitro.* J Clin Invest, 1999. 103(5): p. 697-705.

25. Toma, C., et al., *Human mesenchymal stem cells differentiate to a cardiomyocyte phenotype in the adult murine heart.* Circulation, 2002. 105(1): p. 93-8.

26. Mangi, A.A., et al., *Mesenchymal stem cells modified with Akt prevent remodeling and restore performance of infarcted hearts.* Nat Med, 2003. 9(9): p. 1195-201.

27. Shake, J.G., et al., *Mesenchymal stem cell implantation in a swine myocardial infarct model: engraftment and functional effects.* Ann Thorac Surg, 2002. 73(6): p. 1919-25; discussion 1926.

28. Kinnaird, T., et al., *Local delivery of marrow-derived stromal cells augments collateral perfusion through paracrine mechanisms.* Circulation, 2004. 109(12): p. 1543-9.

29. Chiu, C.P. and H.M. Blau, *5-Azacytidine permits gene activation in a previously noninducible cell type.* Cell, 1985. 40(2): p. 417-24.

30. Tomita, Y., et al., *Application of mesenchymal stem cell-derived cardiomyocytes as bio-pacemakers: current status and problems to be solved.* Med Biol Eng Comput, 2007. 45(2): p. 209-20.

31. Fukuda, K., *Regeneration of cardiomyocytes from bone marrow: Use of mesenchymal stem cell for cardiovascular tissue engineering.* Cytotechnology, 2003. 41(2-3): p. 165-75.

32. Holmes, J.W., T.K. Borg, and J.W. Covell, *Structure and mechanics of healing myocardial infarcts.* Annu Rev Biomed Eng, 2005. 7: p. 223-53.

33. Humphery, J.D., *Cardiovascular Solid Mechanics*. 2002: Springer Verlag.

CHAPTER IV

DESIGN A BIOREACTOR WITH COORDINATED MECHANICAL AND ELECTRICAL STIMULATIONS

4.1 Introduction

Based on previous studies, major challenges in fabricating functional myocardial tissue constructs include: (i) thorough cell reseeding in a thick construct,[1-5] (ii) low contractile force incompetent to contribute to normal cardiac function,[6, 7] (iii) poor electrophysiological function,[8, 9] (iv) unmatched mechanical properties,[2] and (v) poor neovascularization.[2, 9]

Besides the scaffold materials and cell sources, it has been shown that tissue culture microenvironment, such as cell culture medium, growth factors, physical stimulations, etc., can affect the cell proliferation, differentiation, and migration, and consequently the biological, mechanical, and electrical properties of the construct.[10] As a means, the bioreactor is often used in tissue engineering to provide necessary conditions during *in vitro* culture, with the hope of developing tissue constructs with high cell density, ideal construct properties, and deposition of the extracellular matrix.[11]

For tissue engineered cardiac patch, two types of simulations can be employed to assist in the development of tissue construct: one is uniaxial stretching and another one is electrical current stimulation. Uniaxial stretching is commonly applied in tissue culture to improve the structural and functional properties of the engineered tissue; it is found that the reseeded cells can be guided to form aligned morphology. In an *in vitro* study,

Zhuang et al.[12] has reported that 10% cyclic uniaxial stretch produced upregulation of connexin-43 and N-cadherin in the intercellular junctions and increased the propagation velocity. Yamada et al. have also reported that the cyclic stretch (10%) upregulates expression of both the electrical junction protein (connexin-43) and the mechanical junction proteins (plakoglobin, desmoplakin, and N-cadherin) via integrin-dependent activation of focal adhesion kinase (FAK).[13, 14] Zimmerman et al. found that the encapsulated neonatal rat cardiomyocytes in the gel formed an intensively interconnected, longitudinally oriented cardiac muscle bundles under uniaxial stretching, and the tissue construct showed contractile properties similar to the native myocardium.[15] Another benefit of the cyclic stretch is to help nutrients to diffuse into a thick construct.

For electrical stimulation, Radisic and Vunjak-Novakovic observed that spontaneous construct beating took place in a construct reseeded with rat cardiomyocytes (collagen sponge) under ~5 volt and 1 Hz electrical stimuli.[16, 17] In Ott's study,[18] electrical stimulation of 5-20 volt (10 ms) pulse was also applied using epicardial leads in the perfusion recellularization procedure of the acellular rat heart. However, synergistic effects of both the mechanical and electrical stimulations have not been fully reported up to now.

We hypothesize that a higher differentiation rate and cell organization might be achieved by providing multifaceted stimulations to the myocardial scaffold-based tissue construct. The purpose of this project is to design and build a novel bioreactor that provides both the mechanical stimulus and electrical stimulus for facilitating cardiac patch tissue engineering.

4.2 Bioreactor Design and Fabrication

4.2.1 Bioreactor design

The bioreactor was designed using Solidworks 3D CAD software (Solidworks Corp., Concord, MA). The structural elements of the device were machined from abrasion-resistant acrylic and polysulfone that provided excellent thermal and chemical stability. The bioreactor consisted of one tissue culture chamber, in which maximal four pieces of tissue constructs (25 mm × 25 mm × ~3mm) could be mounted between a fixed clamp and a movable clamp (Figure 4.3). Ti-corn blue sutures (# 0) were used for connecting the sample with two clamps. The cover of the tissue culture chamber is fabricated with 1/4" thick clear polycarbonate (Small Parts, Inc.). A hole in 2 cm diameter was made on the cover and sealed with the PIFE membrane with 0.2 μm pore size (Millipore) to enable air transporting (Figure 4.3).

Linear movement was be applied by the movable arm that was driven by an Xslide assembly and a stepper motor (Velmex) (Figure 4.3). Electrodes were made from Teflon-coated silver wire (75 μm diameter, A-M Systems) (Figure 4.1). The frequency and amplitude of the cyclic stretch were controlled by a custom written LabView program. Teflon insulation was stripped from the end of the wire and the naked wires were stuck into the two opposite edges of the tissue construct. To simulate what myocardial tissue experiences, electrical pulses were applied when each unloading cycle started (Figure 4.1). Similarly, the frequency and amplitude of the electrical pulses were controlled by the LabView program, which was capable of delivering multiple protocols of mechanical stretching and various waveforms of electrical stimulation (Figure 4.4).

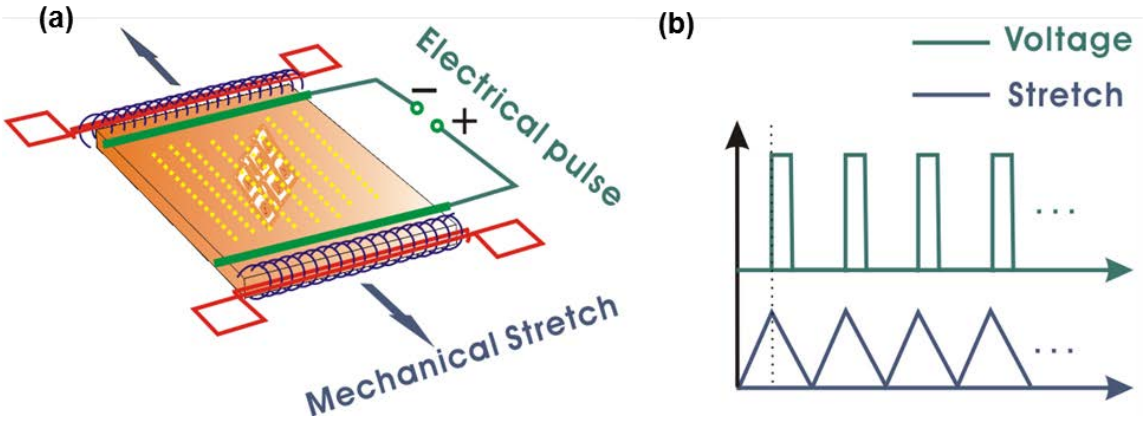

Figure 4.1 (a) Schematic illustration of the multifaceted stimulations. Scaffold fiber PD direction (yellow dash line) was aligned along the stretch direction to promote cardiomyocyte alignment. (b) Wave forms of the applied mechanical stretch and electrical pulses.

4.2.2 Bioreactor Validation and Performance

The bioreactor and conditioning system have been tested in more than 20 experiments. We found that the system ensured good cell viability under sterile conditions for an extended period of time, and experiments showed excellent reproducibility. Other advantages of the designed multi-stimulation bioreactor are easy sample mounting, visibility of the sample chamber, and flexibility in implementing complicated protocols.

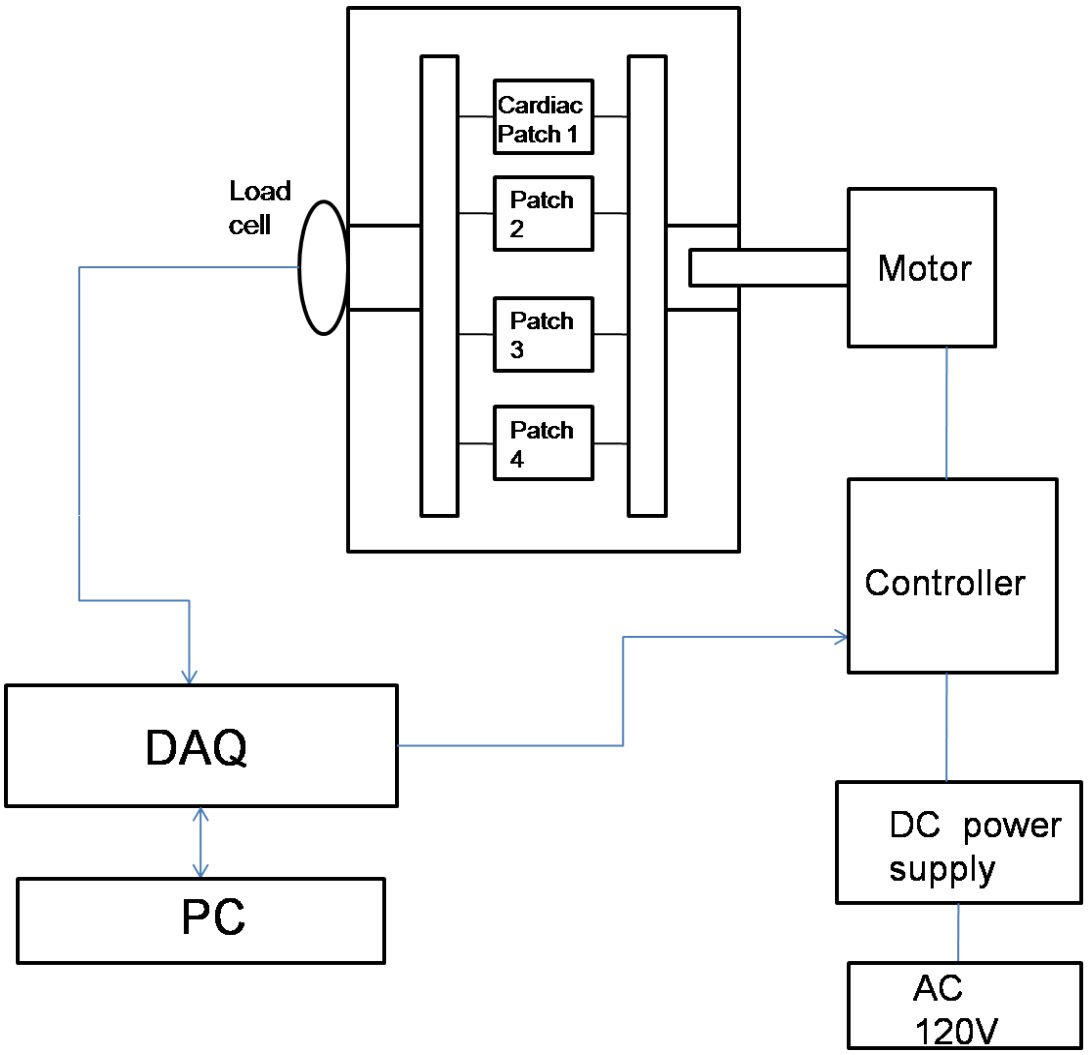

Figure 4.2 The design diagram of the multi-stimulation bioreactor.

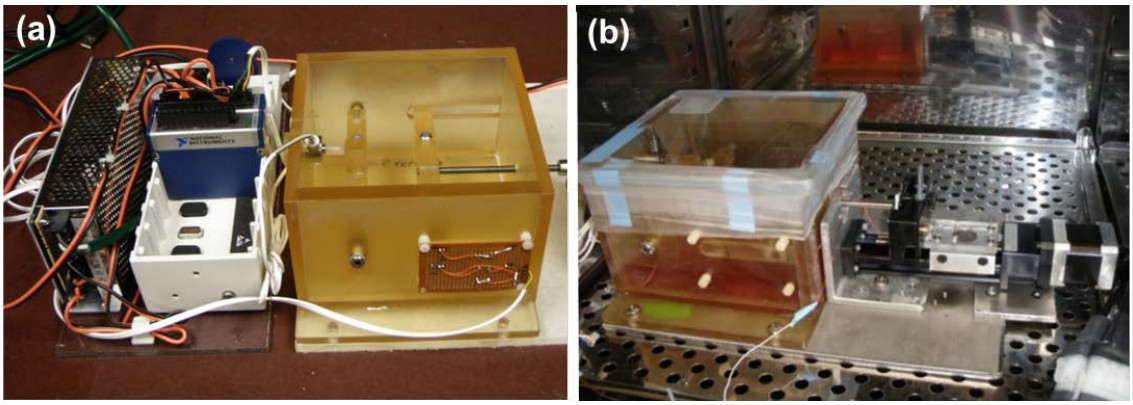

Figure 4.3 (a) The prototype of the multi-stimulation bioreactor. (b) The bioreactor placed in the incubator.

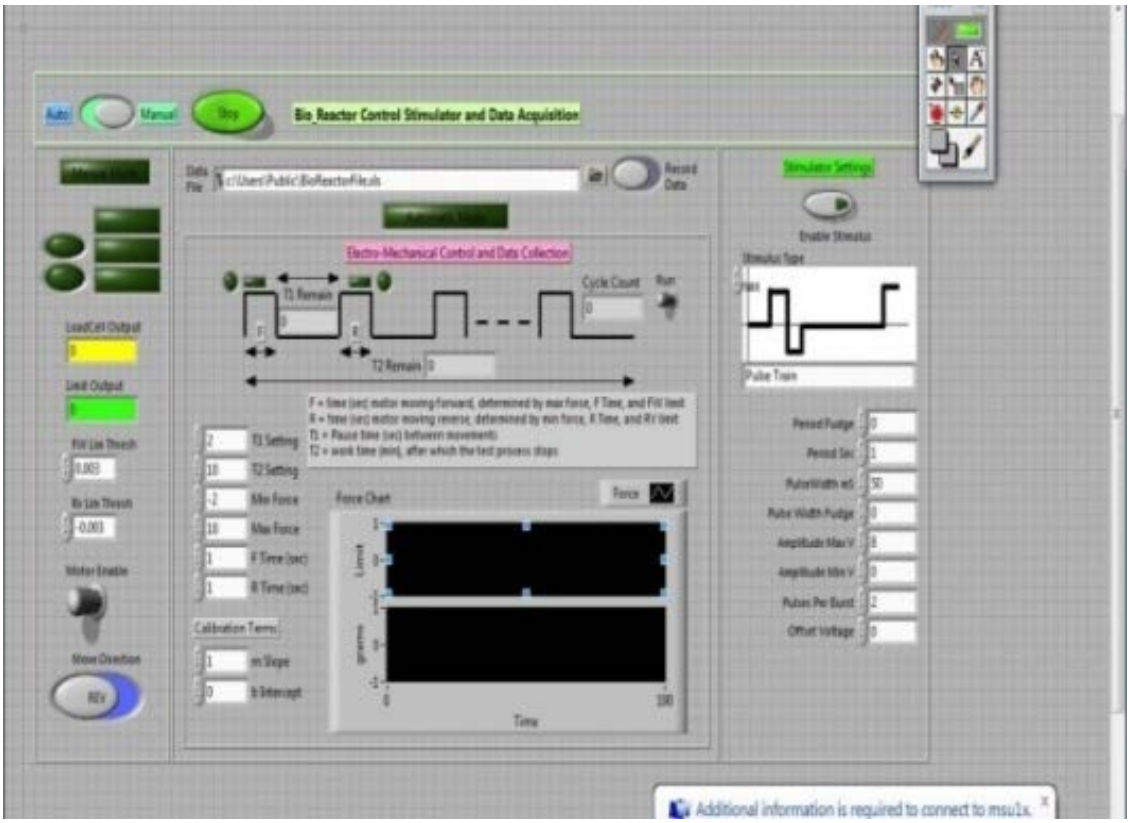

Figure 4.4 User interface of the custom written LabView program.

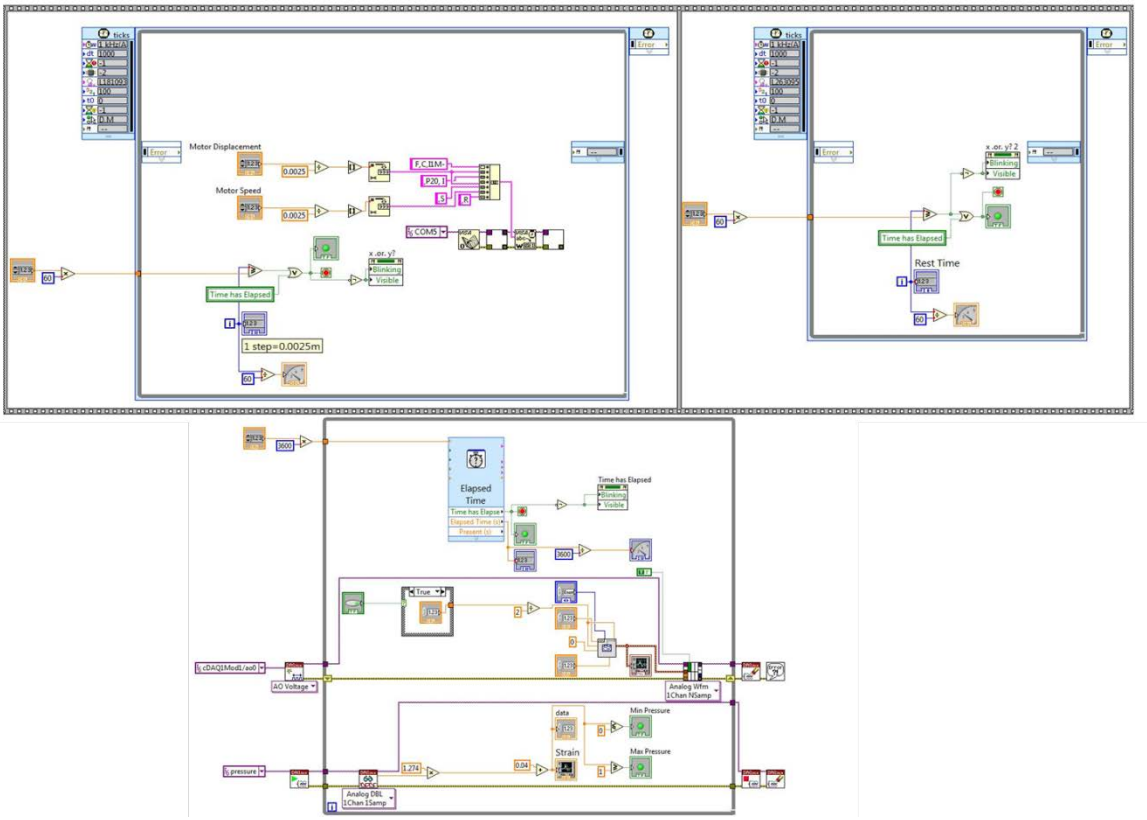

Figure 4.5 Block view of the custom written LabView program.

4.3 Discussion

In this project, the multi-stimulation bioreactor has been successfully built; the bioreactor is able to periodically stretch the tissue construct, as well as apply electrical pulses to stimulate cell differentiation and construct development. In our design, the stretch level, the stretching speed (stepper motor speed), the waveform and frequency of the electrical current, the time length of stimulations, and the construct rest time are all digitally controlled by the custom written Labview program.

The rotating bioreactor in our previous studies allowed better oxygenation of the recellularized scaffolds than the static tissue culture; however, the recellularization efficiency and cell differentiation rate are still relatively low. We therefore designed the multi-stimulation bioreactor to provide both the mechanical and electrical stimulations to

facilitate tissue construct development. This multi-stimulation bioreactor can also provide opportunities to understand the synergistic effects of the combined mechanical and electrical stimulations in cardiac tissue engineering, which has not been reported yet.

To drive the cyclic stretching motion, a stepper motor was used due to its ability to be precisely controlled and easily programed. The applied strain was calculated by normalizing the displacement of the movable arm to the original distance of the two sample mounting arms. The use of the clamp to clamp displacement in strain estimation was not an ideal method to accurately measure the tissue construct strains. Future improvement will be real time tracking of markers on tissue construct using a CCD camera (A high resolution web camera also is a good option).

Effective sterilization is an essential step for tissue culture, especially for a bioreactor that has many complicated components and was constructed for repeated use. The most commonly used sterilization methods include wet heat, dry heat, solvents, radiation, and microwave.[19, 20] For our application, a combined method that uses both 70% ethanol sterilization and UV light sterilization was adopted. Furthermore, each part of the clamps and sample hooks could be disassembled for easy cleaning and sterilizing after each experiment. Our bioreactor tissue culture experiments demonstrated that the sterile conditions could be maintained for an extended period of time (evidenced by viable and proliferating cells), and all the procedures and results were reproducible.

Temperature is another important parameter in bioreactor applications. Heat exchange has to be carefully designed to maintain the bioprocess at a constant temperature. In this design, we placed both the culture chamber and the stepper motor inside the incubator. We noticed that the heat generated by the stepper motor in long hours of operation largely affected the motor performance and resulted in undesired

motor movements. This problem was solved by designing a water refrigeration system, in which cold copper coils were wrapped around the step motor and cooling water was circulated by a rotation pump outside of the incubator. The water refrigeration system dissipated the heat generated by the step motor effectively, and the temperature was maintained in a reasonable range without causing any motor malfunction.

4.4 Conclusions

We have successfully built a bioreactor that is able to apply both mechanical and electrical stimulations for facilitating tissue construct development. In Chapter 5, we will assess the effectiveness and efficiency of this multi-simulation bioreactor in promoting stem cell differentiation and tissue remodeling.

4.5 References

1. Robinson, K.A., et al., *Extracellular matrix scaffold for cardiac repair.* Circulation, 2005. 112(9 Suppl): p. I135-43.

2. Carrier, R.L., et al., *Cardiac tissue engineering: cell seeding, cultivation parameters, and tissue construct characterization.* Biotechnol Bioeng, 1999. 64(5): p. 580-9.

3. Birla, R.K., G.H. Borschel, and R.G. Dennis, *In vivo conditioning of tissue-engineered heart muscle improves contractile performance.* Artif Organs, 2005. 29(11): p. 866-75.

4. Birla, R.K., et al., *Myocardial engineering in vivo: formation and characterization of contractile, vascularized three-dimensional cardiac tissue.* Tissue Eng, 2005. 11(5-6): p. 803-13.

5. Borschel, G.H., et al., *Tissue-engineered axially vascularized contractile skeletal muscle.* Plast Reconstr Surg, 2006. 117(7): p. 2235-42.

6. Zimmermann, W.H. and T. Eschenhagen, *Cardiac tissue engineering for replacement therapy.* Heart Fail Rev, 2003. 8(3): p. 259-69.

7. Zimmermann, W.H., I. Melnychenko, and T. Eschenhagen, *Engineered heart tissue for regeneration of diseased hearts.* Biomaterials, 2004. 25(9): p. 1639-47.

8. Bursac, N., et al., *Novel anisotropic engineered cardiac tissues: studies of electrical propagation.* Biochem Biophys Res Commun, 2007. 361(4): p. 847-53.

9. Bursac, N., et al., *Cardiac muscle tissue engineering: toward an in vitro model for electrophysiological studies.* Am J Physiol, 1999. 277(2 Pt 2): p. H433-44.

10. Vogel, V. and M. Sheetz, *Local force and geometry sensing regulate cell functions.* Nat Rev Mol Cell Biol, 2006. 7(4): p. 265-75.

11. Radisic, M., et al., *Biomimetic approach to cardiac tissue engineering.* Philos Trans R Soc Lond B Biol Sci, 2007. 362(1484): p. 1357-68.

12. Zhuang, J., et al., *Pulsatile stretch remodels cell-to-cell communication in cultured myocytes.* Circ Res, 2000. 87(4): p. 316-22.

13. Yamada, K., et al., *Distinct pathways regulate expression of cardiac electrical and mechanical junction proteins in response to stretch.* Circ Res, 2005. 97(4): p. 346-53.

14. Shanker, A.J., et al., *Matrix-protein-specific regulation of Cx43 expression in cardiac myocytes subjected to mechanical load.* Circ Res, 2005. 96(5): p. 558-66.

15. Zimmermann, W.H., et al., *Engineered heart tissue grafts improve systolic and diastolic function in infarcted rat hearts.* Nat Med, 2006. 12(4): p. 452-8.

16. Radisic, M., et al., *High-density seeding of myocyte cells for cardiac tissue engineering.* Biotechnol Bioeng, 2003. 82(4): p. 403-14.

17. Radisic, M., et al., *Medium perfusion enables engineering of compact and contractile cardiac tissue.* Am J Physiol Heart Circ Physiol, 2004. 286(2): p. H507-16.

18. Ott, H.C., et al., *Perfusion-decellularized matrix: using nature's platform to engineer a bioartificial heart.* Nat Med, 2008. 14(2): p. 213-21.

19. Sanborn, M.R., S.K. Wan, and R. Bulard, *Microwave sterilization of plastic tissue culture vessels for reuse.* Appl Environ Microbiol, 1982. 44(4): p. 960-4.

20. Miyagawa, K., et al., *Purification, characterization, and application of an acid urease from Arthrobacter mobilis.* J Biotechnol, 1999. 68(2-3): p. 227-36.

CHAPTER V

APPLICATION OF COORDINATED MECHANICAL AND ELECTRICAL STIMULATIONS

5.1 Introduction

The myocardium is highly oriented in structure, and possesses unique electrophysiological and mechanical properties.[1] The ideal engineered cardiac construct should generate contractile and functional equivalent of the native myocardium, which can provide proper thickness, optimal structure, and matched mechanical properties.[2-4] Moreover, the construct should contain a high density of cells, facilitate cell remodeling, stimulate the formation of vasculature, and ideally be able to propagate electrical impulses.[5-9]

In Chapter 2 and 3, we have shown that in the acellular myocardial scaffolds, the 3D cardiomyocyte lacunae and ECM networks were preserved after decellularization, and the MSCs reseeded scaffold was able to promote cardiomyocyte-like differentiation and tissue positive remodeling represented by a recovering trend in tissue mechanical property.[10] To further improve the effectiveness and efficiency of the cardiac patch engineering using the acellular myocardial scaffolds and MSCs, we have designed and fabricated a novel bioreactor to provide multi-stimulations to the tissue construct (Chapter 4).

In this study, we investigate the effects of the applied mechanical and electrical stimulations on tissue construct development during *in vitro* culture. The acellular

myocardial scaffolds were reseeded with rat MSCs and subjected to bioreactor conditioning. The *in vitro* conditioning parameters we have examined include stretching level, electrical stimulation, and tissue culture times. We hypothesize that the combined mechanical and electrical stimulations will more efficiently promote the cell proliferation, cardiomyocyte differentiation, and tissue remodeling of the engineered cardiac patch.

5.2 Materials and Methodologies

5.2.1 MSC Culture, Cell Reseeding, and *In Vitro* Conditioning Protocols

MSC culture. Well characterized Lewis rat mesenchymal stem cells (MSCs, fourth passage) were obtained from the Stem/Progenitor Cell Standardization Core (SPCS) at the Texas A&M Health Science Center (NIH/NCRR grant). These cells were re-suspended in mesenchymal stem cell medium (L-DMEM, 10% FBS, 100 U/ml penicillin and 100μg/ml streptomycin) and seeded into 175-mm flasks at a density of 2×10^3 cells/cm^2. The medium was changed twice a week. Aliquots of the cells were prepared for reseeding and differentiation.

Cell reseeding. The acellular scaffolds (25 mm × 25 mm × ~3 mm) were mounted between a fixed clamp and a movable clamp using the surgical suture (Figure 5.1). Then the acellular scaffolds were sterilized in 70% ethanol in the tissue culture chamber for 2 hours and rinsed with sterilized PBS for four times. Before reseeding, the whole tissue culture chamber with the scaffolds was sterilized with UV light for 20 minutes. After completing the sterilization protocols, each scaffold was injected with a total of 1 ml MSC solution at a concentration of 10^6 cells/ml. A 1-ml syringe with 26G Permanent needle (BD, Inc.) was used for injection, and 1-ml MSCs were injected evenly at nine

injection points (~0.1ml/point) that located as a 3 x 3 array within the middle region of the square sample (Figure 5.2). After reseeded with the MSCs, the tissue constructs were cultured in the 5-azacytidine differentiation medium (L-DMEM, 10% FBS, cardiac myocyte growth supplement (Sciencell), 3 μmol/L 5-azacytidine (MP Biomedicals), 100 U/ml penicillin and 100μg/ml streptomycin). After incubating for 24 hrs, the medium was changed to the complete medium (L-DMEM, 10% FBS, cardiac myocyte growth supplement (Sciencell), 100 U/ml penicillin and 100μg/ml streptomycin).

In vitro conditioning protocols. To compare the influence of mechanical and electrical stimulations on the tissue engineered cardiac patch, we randomly divided all the acellular scaffolds into five groups (8 samples in each group, 4 for biological function characterizations and 4 for mechanical testing). The five groups are: (i) the control group in static culture; (ii) 20% strain stimulation; (iii) 5 Volt electrical stimulation; (iv) 20% strain + 5 Volt electrical stimulations; and (v) 40% strain + 5 Volt electrical stimulations (Figure 5.3). For the static culture control group (group (i)), samples were injected with MSCs at the same density, sitting in the same culture chamber without mechanical or electrical stimulations; for tissue constructs subjected to only the stretch conditioning (groups (ii)), samples were mounted between the fixed clamp and the movable clamp inside the tissue culture chamber; for only the electrical stimulation (group (iii)), the electrodes were mounted on the sample and no clamp stretch was applied; for group (iv) and (v), the stretch and electrical stimulations were simultaneously applied. Note that, for the applied stimulations, both the triangular strain waveform and electrical square wave pulse were set at a frequency of 1 Hz, which simulates the physiological frequency experienced by the heart muscles.

Figure 5.1 Tissue culture chamber showed the tissue constructs mounted onto the fixed arm and the movable arm

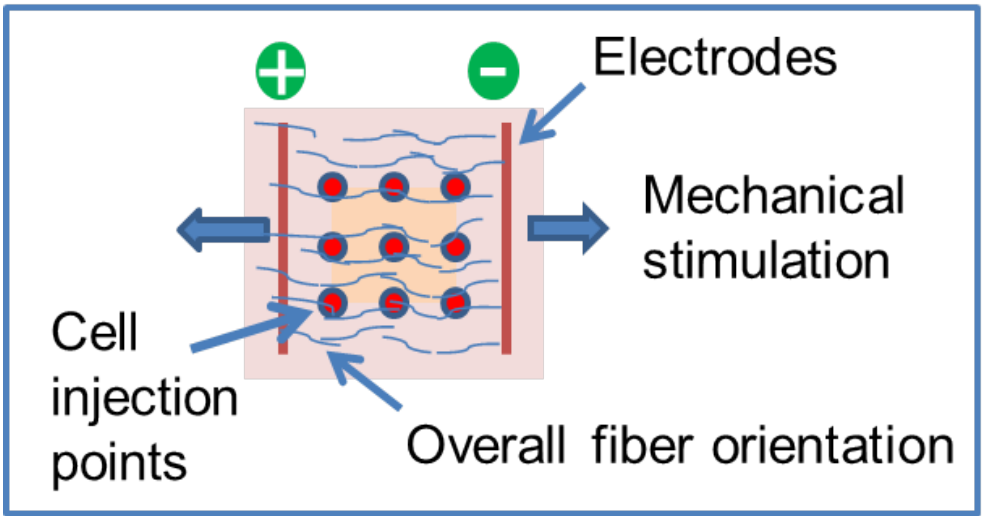

Figure 5.2 Schematic illustration of the engineered scaffold subjected to cell injection, mechanical, and electrical stimulations.

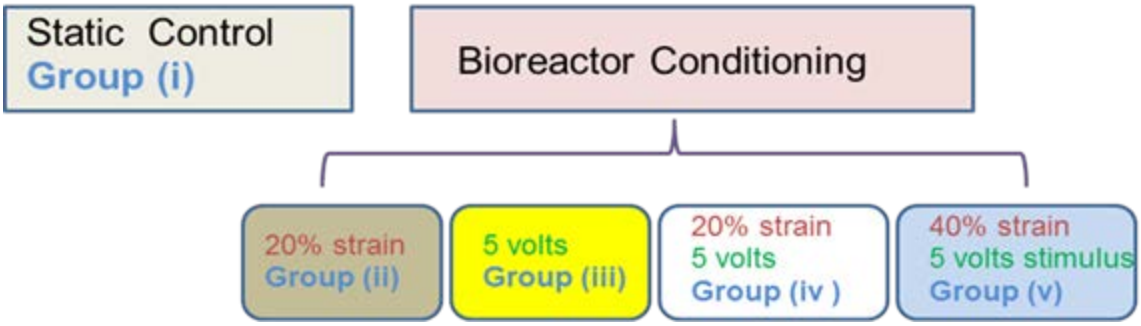

Figure 5.3 Experimental design for the *in vitro* bioreactor condition study

5.2.2 Cell Viability, Histology, and Immunohistochemical Characterizations

Live/Dead assay was carried out to assess the cell viability in the tissue construct. Filmtracer™ LIVE/DEAD® Biofilm Viability Kit (Invitrogen) solution was prepared by adding 20 µl of the supplied 2 mM EthD-1 stock solution (Component B) to 10 ml of sterile tissue culture–grade D-PBS. The reagents were combined by transferring 5 µl of the supplied 4 mM calcein AM stock solution (Component A) to the 10 ml EthD-1 solution. The reseeded patch was incubated for 20 minutes at room temperature. Hematoxylin and eosin (H&E) staining and Masson's trichrome staining were performed for assessing the cell density and distribution. Samples were fixed in 2% paraformaldehyde solution for 2 hours, embedded in paraffin, and subjected to sectioning. The sample slides were then stained with H&E or Masson's trichrome and imaged with bright field light microscopy.

For immunofluorescent staining, after rehydration and antigen retrieval with 0.05% Trypsin for 10 min at 37°C, sections were washed and incubated at 4°C overnight with primary antibodies targeting sarcomeric α-actinin (Sigma), myosin heavy chain (GenWay), cardiac troponin T (abcam), von Willebrand factor (vWF) (abcam), Connexin-43 (Sigma), and N-Cadherin (Sigma). Secondary antibodies, Cy3 AffiniPure goat anti-mouse IgG, Cy5 Affini-Pure donkey anti-mouse IgM, Alexa Fluor secondary

antibodies, goat anti-mouse IgG, DyLight 649 AffiniPure Donkey Anti-Mouse IgM, and DyLight 549 AffiniPure Donkey Anti-Mouse IgG (JacksonImmuno Research), were then applied at room temperature for 1 hour to obtain fluorescent colors. At last, all sections were stained with Hoechst (Invitrogen) for cell nuclei. Immunohistological slides were observed with an inverted laser scanning confocal microscope (Zeiss LSM 510). Negative controls were prepared by following the same protocols with the omission of all the primary antibodies.

5.2.3 Biaxial and Uniaxial Mechanical Testing

Biaxial and uniaxial mechanical properties of the tissue constructs were characterized with the biaxial testing system and the uniaxial machine (Mach-1, Biosyntech, MN). The detailed testing protocols were described in Chapter 3.

5.2.4 Statistical Analysis

The experimental data were presented as mean ± standard deviation. One Way Analysis of Variances (ANOVA) was used for statistical analysis, with Holm-Sidak test being used for post hoc pair wise comparisons and comparisons versus the control group (SigmaStat 3.0, SPSS Inc., Chicago, IL). The differences were considered statistically significant when p is less than 0.05.

5.3 Results

5.3.1 Effects of the *in vitro* Conditioning Protocols on Construct Recellularization

H&E and Live/Dead cell staining after 2-day tissue culture showed that the cell density, distribution, and viability were affected by the *in vitro* bioreactor condition protocols (Figure 5.4). H&E staining showed that the cell densities in 20% strain

stimulation group (group (ii)), 5 Volt electrical stimulation group (group (iii)), and 20% strain + 5 Volt combined stimulations (group (iv)) are higher than the static control group (group (i)). The Live/Dead staining results further proved this observation, and the ratio of living cells in the bioreactor conditioning groups (group (ii, iii, iv)) was also higher than the static control group (group (i)).

Compared with the static control group (group (i)), higher cell density and a degree of cell alignment were observed in the 20% strain stimulation group (group (ii)); high cell density was also found in the 5 Volt electrical stimulation group (group (iii)), though there was no cell alignments existing in this group. In the combined stimulation group (group (iv)), much higher cell density was observed and the reseeded cells exhibited better morphology, alignment, and cell viability (Figure 5.4 - g, h; Table 5.1).

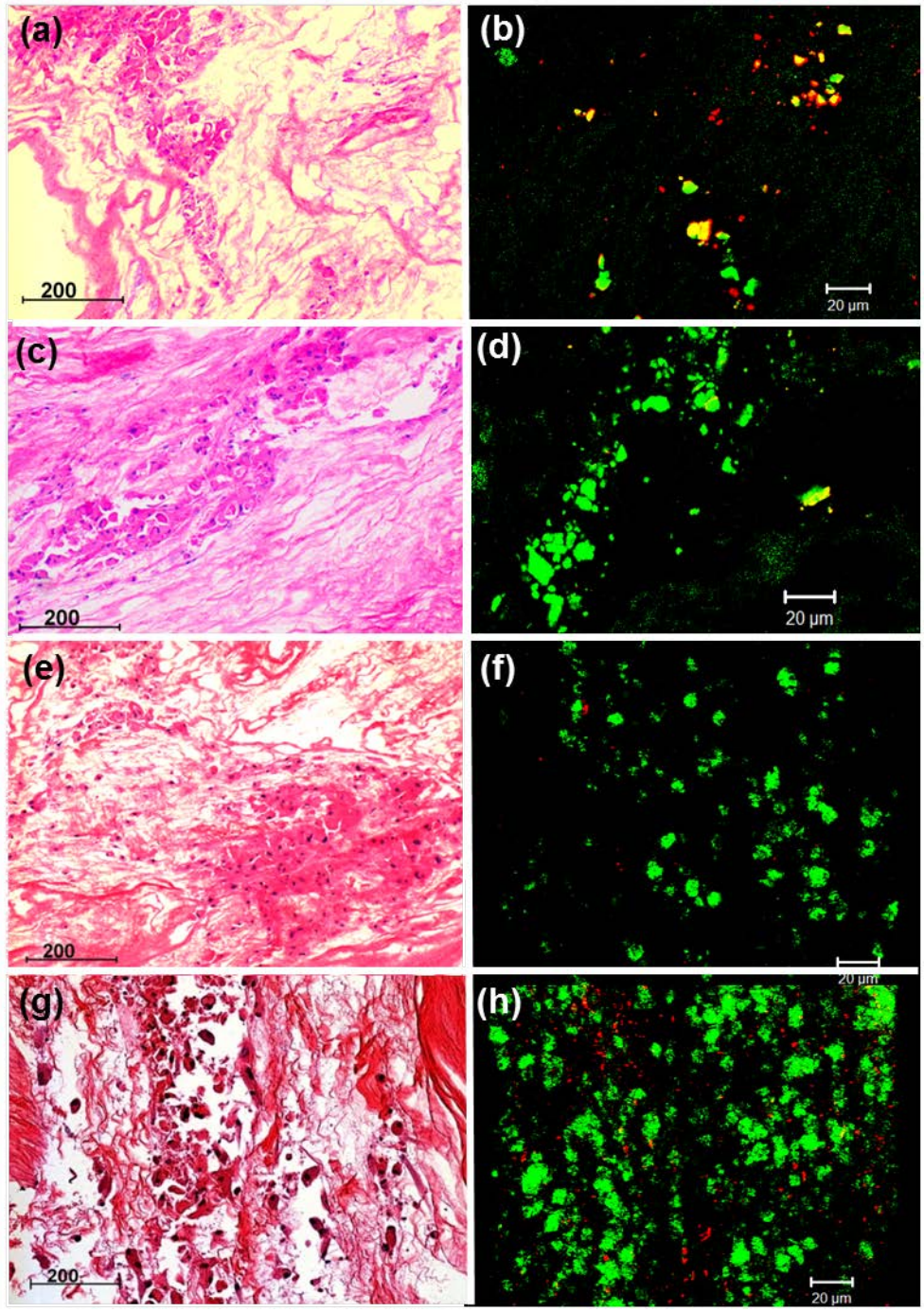

Figure 5.4 (a) H&E and (b) Live/Dead staining of the static control group (group (i)); (c) H&E and (d) Live/Dead staining of the 20% strain stimulation group (group (ii)); (e) H&E and (f) Live/Dead staining of the 5 Volt electrical stimulation group (group (iii)); (g) H&E and (h) Live/Dead staining of the 20% strain + 5 Volt stimulation group (group (iv)).). Images were taken from the constructs after 2-day's tissue culture.

Table 5.1 Cell density and ratio of living cells of the static control group

	Groups (i)	Groups (ii)	Groups (iii)	Groups (iv)
Reseeded cell density (cells/cm^3)	0.72×10^6	2.69×10^6	2.83×10^6	3.38×10^6
Ratio of liveing cells	51.43%	80.35%	80.98%	79.38%

*(group (i)), 20% strain stimulation group (group (ii)), 5 Volt electrical stimulation group (group (iii)), and 20% strain + 5 Volt stimulation group (group (iv)).

It could be seen from the above observation that the combined stimulation (20% strain + 5 Volt, group (iv)) resulted in better construct recellularization. We further assessed the cell morphologies of the combined simulation groups (group (iv): 20% strain + 5 Volt; group (v): 40% strain + 5 Volt) after 1-day, 2-day, and 4-days tissue cultures. Mason's trichrome staining showed that, with only 1-day combined stimulations (20% strain + 5 Volt), the reseeded cells showed good alignment (Figure 5.5-a). After 2-day of the combined stimulations (20% strain + 5 Volt), the cells showed a higher cell density, morphology of cell aggregation, and better alignment (Figure 5.5-c); this trend was even more obvious in the 4-day combined stimulation group (20% strain + 5 Volt) (Figure 5.5-e). However, we did not observe the similar phenomenon in group (v), in which 40% strain + 5 Volt stimulations were delivered.

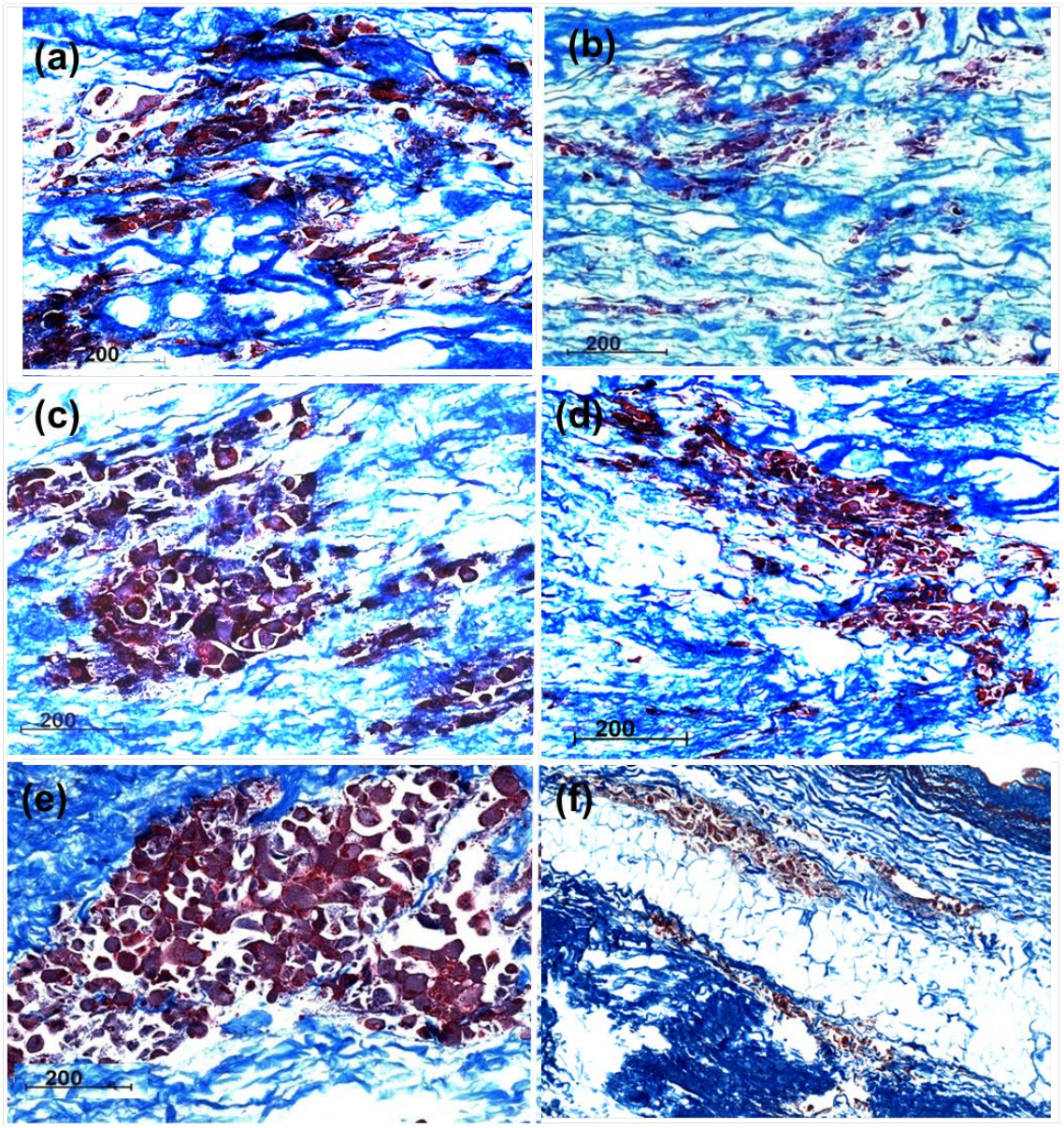

Figure 5.5 Mason's trichrome staining: (a) Group (iv) and (b) group (v) after 1-day bioreactor conditioning; (c) group (iv) and (d) group (v) after 2-day bioreactor conditioning; (e) group (iv) and (f) group (v) after 4-day bioreactor conditioning. Group (iv) delivers 20% strain + 5 Volt stimulations; group (v) delivers 40% + 5 Volt stimulations.

5.3.2 Cell Phenotype Characterizations

Up to now, we have found that a combination of 20% strain and 5 volt electrical simulation (group (iv)) generated the best recellularization result when compared with

other conditioning protocols. Cell phenotypes in the tissue construct subjected 20% + 5 Volt combined stimulations were thus characterized using immunohistological stainings. Figure 5.6 showed that the differentiated cells demonstrated cardiomyocyte-like phenotype, by expressing sarcomeric α-actinin, myosin heavy chain, and cardiac troponin T (Figure 5.6-a, b, c). The existence of electrical gap junctions and mechanical gap junctions were also verified by positive staining of the connexin-43 and N-cadherin, respectively (Figure 5.6-d, e). Another notable observation was that cells expressing von Willebrand factor (vWF) were lining around the vasculature channels (Figure 5.6-f), implying possible endothelialization around vasculature channels. There was no positive staining in all the negative controls, which indicates the immunohistological images (Figure 5.6) showed specific staining.

5.3.3 Biaxial Mechanical Properties

The following eight categories were subjected to biaxial mechanical testing: (a) native myocardium, (b) decellularized myocardial scaffold, (c) 2-day *in vitro* condition (group (iv): 20% strain + 5 Volt), (d) 4-day *in vitro* condition (group (iv): 20% strain + 5 Volt), (e) 2-day *in vitro* condition (group (v): 40% strain + 5 Volt), (f) 4-day *in vitro* condition (group (v): 40% strain + 5 Volt), (g) 2-day static control (group (i)), and (h) 4-day static control (group (i)).

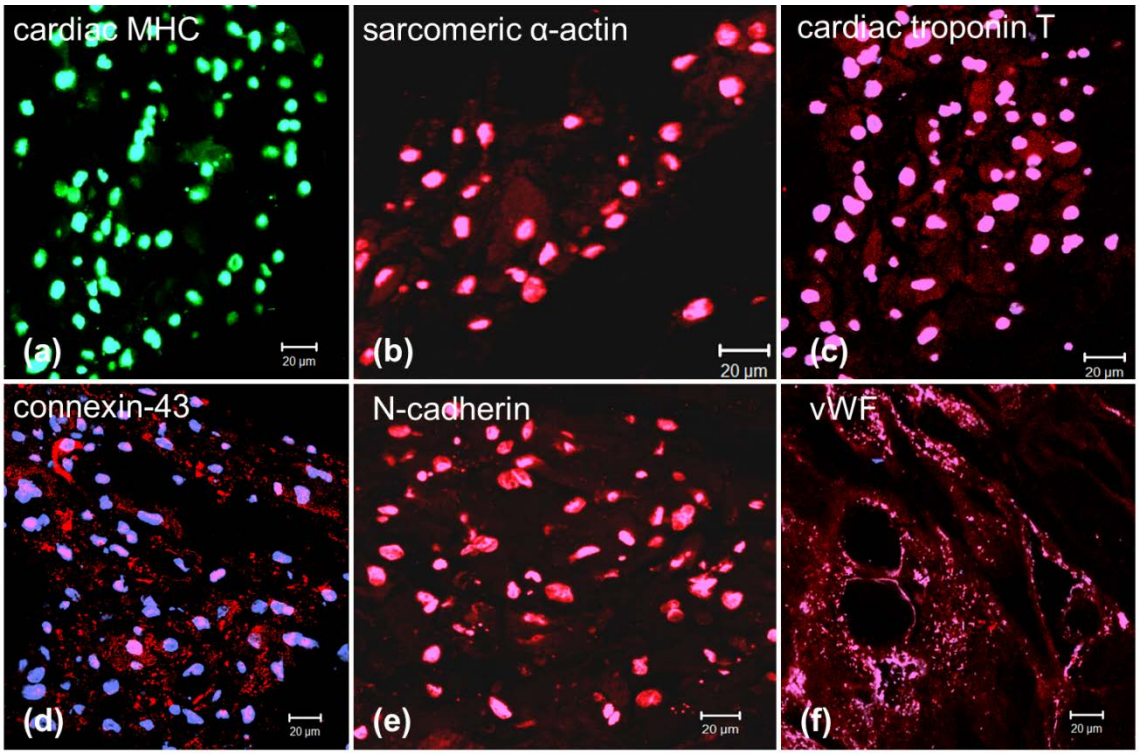

Figure 5.6 Immunohistological staining of tissue constructs after 2-day bioreactor conditioning (group (iv): 20% strain + 5 Volt). The reseeded cells exhibited cardiomyocyte-like phenotype by expressing (a) myosin heavy chain (MHC), (b) sarcomeric α-actinin, and (c) troponin T; electrical gap junctions and mechanical gap junctions were verified by (d) connexin-43 and (e) N-cadherin staining; (f) expression of vWF factor was also observed around vessel-like structures.

The biaxial tissue responses of the eight groups were evaluated and the averaged stress-strain curves were plotted in Figure 5.7. The tissue extensibilities were compared by the maximum stretches in PD direction and XD direction (Table 5.2). Both PD and XD directions of the decellularized myocardium scaffold showed stiffer stress-strain responses ($p < 0.01$) (Figure 5.7-b compared with Figure 5.7-a).

By examining the stress-strain curves in Figure 5.7-c, d, e, f, g, h, we found that panel (d), i.e., 4-day *in vitro* condition with 20% strain and 5 Volt electrical simulations (group (iv)), showed the nonlinear anisotropic mechanical behavior very close to the

biaxial behavior of the native myocardium (Figure 5.7-d compared with Figure 5.7-a). We noticed that group (v) with combination of 40% strain and 5 volt electrical simulation resulted in an isotropic biaxial behavior (Figure 5.7-e, f), which is not desirable in terms of mimicking the biomechanical behavior of the native myocardium (Figure 5.7-a). The 2-day and 4-day static control groups (Figure 5.7-g, h) showed a small trend of softening when compared with the decellularized scaffold group (Figure 5.7-b), which can be explained by the remodeling of the injected cells.

5.3.4 Tensile Mechanical Properties

Tensile mechanical behavior of the native myocardium, decellularized scaffold, tissue construct of group (iv) (20% strain and 5 Volt) after 2-day and 4-day *in vitro* conditioning, and static control after 2-day and 4-day culture were shown in Figure 5.8. Listed in Table 5.3 are maximum tensile modulus, failure stress, and failure strain.

We found that the decellularized myocardial scaffolds showed much stiffer tensile properties when compared with the native myocardium. After 2-day and 4-day bioreactor conditioning, tissue constructs of group (iv) (20% strain and 5 Volt) showed a very large recovering trend. The maximum tensile modulus and failure stress of group (iv) (20% strain and 5 Volt) after 4-day culture are significantly lower than the decellularized scaffolds, but the failure strain is significantly higher than the decellularized scaffold. Here we summarized the comparison of 4-day group (iv) vs. decellularized scaffold - maximum tensile modulus: 0.502 ± 0.073 vs. 11.941 ± 1.274 MPa, $p < 0.01$; failure stress: 0.313 ± 0.059 vs. 1.099 ± 0.034 MPa, $p = 0.01$; failure strain: 0.835 ± 0.061 vs. 0.191 ± 0.054, $p < 0.01$.

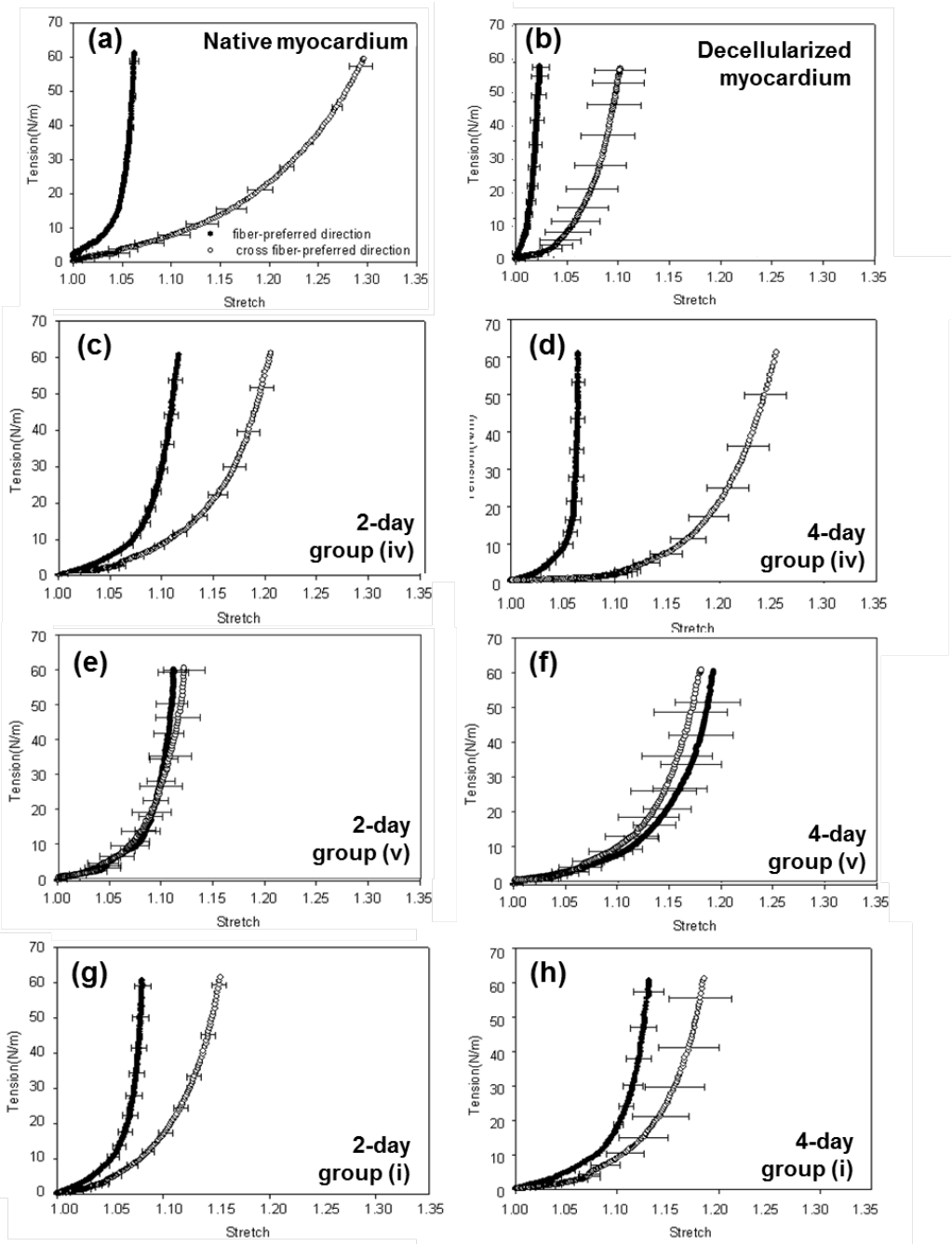

Figure 5.7 Biaxial mechanical behavior: (a) native myocardium, (b) decellularized myocardial scaffold, (c) 2-day *in vitro* condition (group (iv): 20% strain + 5 Volt), (d) 4-day *in vitro* condition (group (iv): 20% strain + 5 Volt), (e) 2-day *in vitro* condition (group (v): 40% strain + 5 Volt), (f) 4-day *in vitro* condition (group (v): 40% strain + 5 Volt), (g) 2-day static control (group (i)), and (h) 4-day static control (group (i)).

Table 5.2 Biaxial mechanical properties of the native myocardium, decellularized scaffold, and tissue construct of group (i, iv, v) after 2-day and 4-day culture.

	Native	Decell	2-Day			4-Day		
			Group (i)	Group (iv)	Group (v)	Group (i)	Group (iv)	Group (v)
Maximum Stretch (PD)	1.062±0.004	1.024±0.008	1.080±0.008	1.115±0.007	1.111±0.015*	1.131±0.015*	1.065±0.006	1.192±0.031*
Maximum Stretch (XD)	1.293±0.012	1.102±0.025*	1.154±0.006*	1.203±0.012*	1.121±0.019*	1.186±0.030*	1.254±0.0208	1.181±0.035*

* denotes significant difference when compared with the native myocardium ($p < 0.05$).

Table 5.3 Uniaxial mechanical properties of native myocardium, decellularized scaffold, and tissue construct of group

	Native	Decell	Group (i)		Group (iv)	
			2-Day	4-Day	2-Day	4-Day
Tensile Modulus (MPa)	0.565±0.167	11.941±1.274	0.816±0.112	0.757±0.206	0.642±0.009	0.502±0.073
Failure Stress (MPa)	0.132±0.060	1.099±0.034	0.636±0.034	0.381±0.071	0.399±0.069	0.313±0.059
Failure Strain	0.384±0.035	0.191±0.054	0.756±0.007	0.701±0.162	0.765±0.063	0.835±0.061

(i): static control group and group (iv): 20% strain + 5 Volt after 2-day and 4-day culture.

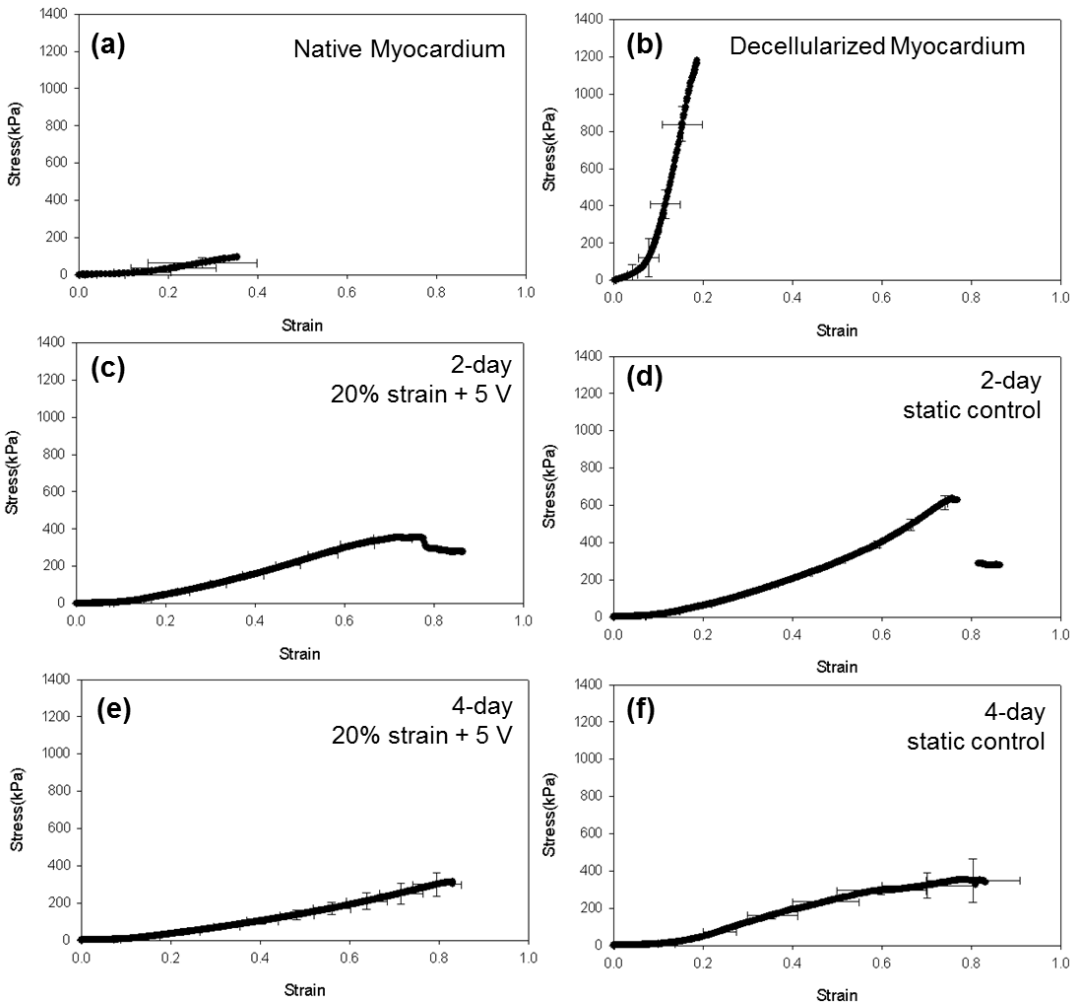

Figure 5.8 Uniaxial tensile mechanical behavior: (a) native myocardium; (b) decellularized myocardial scaffold; tissue constructs of group (iv) (20% strain + 5 Volt) after (c) 2-day and (e) 4-day conditioning; tissue constructs of group (i) (static control) after (d) 2-day and (f) 4-day culture.

5.4 Discussion

Previous studies have demonstrated that either *in vitro* electrical or mechanical stimulation can improve the structural and functional properties of the tissue engineered cardiac construct.[11-13] However, synergistic effects of biochemical treatment with both mechanical and electrical simulations on cardiac constructs have not been reported up to now.

To obtain the tissue engineered cardiac patch with a high cell density, we employed a needle injection method for cell implanting with a total cell amount of 1×10^6 cells/scaffold in this study. The scaffold was injected at nine points (~0.1 ml/point) that separated evenly within the central $1cm^2$ square region to ensure that the implanted cells could be distributed evenly. However, due to the porous structure of the acellular myocardial scaffold, a small amount of leakage happened during the process of the cell injection. For this kind of situation, we injected the leaked medium back into the same region of the acellular patch. The success of the cell injection was evidenced by our histology, which showed that the cell density of the 2-day static control is around 0.72×10^6 cells/cm^3

To further explore the effects of electrical stimulation alone, mechanical stimulation alone, and the combined mechanical and electrical stimulations on cell proliferation and alignment, we compare the cell density, alignment, and viability after 2-day *in vitro* culture among the static control (group (i)), 20% strain stimulation (group (ii)), 5 Volt electrical stimulation (group (iii)), and 20% strain + 5 Volt combined stimulations (group (iv)). Cell density of the control group after 2-day culture was 0.72×10^6 cells/cm^3, and no obvious cell alignment was found. In the bioreactor conditioning groups, cell densities are 2.69×10^6 cells/cm^3 (group (ii)), 2.83×10^6 cells/cm^3 (group (iii)), and 3.38×10^6 cells/cm^3 (group (iv)) (Figure 5.4), which demonstrated that the combined mechanical and electrical stimulations (group (iv)) obviously promoted the proliferation rate of the reseeded cells. Cell alignment was found in both group (ii) and group (iv), but there was no obvious cell alignment in group (iii), which revealed that the mechanical stimulation likely assisted in cell alignment during *in vitro* conditioning (Figure 5.4).

Previous studies have shown that cyclic mechanical stimulation can assist in the cell alignment, stimulate ECM formation,[14, 15] and improve the cardiomyocytes development and function.[16, 17] Our findings were consistent with the previous studies focusing on mechanical stimulation. We further noticed that the cell density of the combined stimulations (20% strain + 5 Volt, group (iv)) are higher than the 20% strain stimulation (group (ii)), which might indicate that adding the electrical stimulation can further promote the stem cell proliferation. Electrical stimulation is believed to be able to induce transient calcium levels which will in turn further improve the amount and organization of sarcomeres in the tissue.[18] Besides, electrical stimulation has been found to facilitate cell proliferation and promote the formation and localization of electric gap junctions.[19, 20] Our results showed that synergistic treatment with both mechanical and electrical simulations further promoted the proliferation and viability of the reseeded cells.

The immunohistologic results of the combined simulations (20% strain + 5 Volt, group (iv)) further proved the synergistic effects of multi-stimulation on stem cell differentiation (Figure 5.6). Our results indicated that the differentiated cells clearly demonstrated cardiomyocyte-like phenotypes, by abundantly expressing sarcomeric α-actinin, myosin heavy chain, and cardiac troponin T (Figure 5.6-a, b, c). The existence of electrical gap junctions and mechanical gap junctions were also verified by positive staining of the connexin-43 and N-cadherin, respectively (Figure 5.6-d, e). As we know, connexin-43 is the major electrical gap junction protein, and N-cadherin is the fascia adherens junction protein in heart muscles. Those junction proteins play important roles to synchronize and coordinate the myocardium contraction; the myocardium contracts synchronously since ion currents conducted through the tissue by intercellular gap

junctions, which directly couple the cytoplasmic compartments of adjacent cells.[21, 22] Yamada et al. found that mechanical stretch could upregulate the expression of both electrical and mechanical junction proteins.[12] Zhuang et al. also proved that *in vitro* pulsatile linear stretch could upregulate the expression of both electrical and mechanical junction proteins.[11] Our study further demonstrated that the combined mechanical and electrical stimulations facilitated the formation of electrical gap junctions and mechanical junctions (electrical gap junctions even showing a weak alignment (Figure5.6-d)).

Endothelialization and cell nuclei alignment around vasculature networks were also revealed by vWF staining (Figure 5.6-f). In Chapter 3, we reported that possible endothelialization took place in the cardiac patch around the vasculature templates after 2-week *in vitro* culture.[10] This study validated our previous finding only in a more efficient fashion, i.e., endothelialization took place only after 2-day *in vitro* conditioning (20% strain + 5 Volt), further implying the potential of application in angiogenesis. In a clinical setting, patients will have to wait for cell expansion, tissue culture, and cell reconstruction until a functional regenerated tissue can be applied in surgical treatment.[23] Our results showed that the synergistic simulations might be beneficial for solving the above inconvenience by reducing the waiting time.

To understand the effects of the physiological level of strain and higher strain on tissue constructs, we compared the tissue constructs subjected to 20% strain + 5 Volt stimulations to the tissue constructs conditioned with 40% strain + 5 Volt stimulations (Figure 5.5). In the group with 20% strain + 5 Volt stimulations (group (iv)), the cell proliferation, cell morphology, and cell alignment were much higher than those in the group conditioned with 40% strain + 5 Volt stimulations (group (v)) (Figure 5.5). The

40% strain seemed too high for conditioning purposes and likely was the reason of poor recellularization in group (v).

Biaxial testing results also showed that the 20% strain + 5 Volt stimulations (group (iv)) generated best nonlinear anisotropic tissue behavior and tissue remodeling trend (Figure 5.7-c,d); especially in the 4-day *in vitro* conditioning of group (iv), which resulted in a biaxial stress-strain behavior very similar to that of the native myocardium (Figure 5.7-a,d). Note that the 40% strain + 5 Volt stimulations (group (v)) caused the tissue construct to lose anisotropy, indicating that the excessive stretching (40% strain) might disrupt the ECM network and hence resulted in an isotropic tissue biaxial behavior (Figure 5.7-e, f). The uniaxial testing results (Figure 5.8) also demonstrated positive tissue remodeling taking place in group (iv) (20% strain + 5 Volt) (Figure 5.8-c, e; Table 5.3).

5.5 Conclusions

In this study, we found that the recellularization, cardiomyocyte differentiation, and tissue remodeling were more effectively and efficiently promoted by the combined mechanical and electrical stimulations (20% strain + 5 Volt, group (iv)). The benefit of this combination of stimulations (20% strain + 5 Volt) was evidenced by good cell viability, proliferation, differentiation, positive tissue remodeling, and a trend of angiogenesis within a short period of time (2 - 4 days). We also found that 40% strain stimulation (40% strain + 5 Volt, group (v)) resulted in the loss of tissue anisotropic behavior, a phenomenon likely related to the ECM network disruption caused by the over-stretching. Note that only a few combinations were examined in this study due to excessive workload. Future investigation is warranted to identify the optimal tissue engineering protocol in order to fabricate the functional cardiac patch.

5.6 References

1. Zimmermann, W.H., et al., *Heart muscle engineering: an update on cardiac muscle replacement therapy.* Cardiovasc Res, 2006. 71(3): p. 419-29.

2. Wall, S.T., et al., *Theoretical impact of the injection of material into the myocardium: a finite element model simulation.* Circulation, 2006. 114(24): p. 2627-35.

3. Chen, Q.Z., et al., *Characterisation of a soft elastomer poly(glycerol sebacate) designed to match the mechanical properties of myocardial tissue.* Biomaterials, 2008. 29(1): p. 47-57.

4. Simpson, D., et al., *A tissue engineering approach to progenitor cell delivery results in significant cell engraftment and improved myocardial remodeling.* Stem Cells, 2007. 25(9): p. 2350-7.

5. Radisic, M., et al., *Biomimetic approach to cardiac tissue engineering.* Philos Trans R Soc Lond B Biol Sci, 2007. 362(1484): p. 1357-68.

6. Leor, J., et al., *Bioengineered cardiac grafts: A new approach to repair the infarcted myocardium?* Circulation, 2000. 102(19 Suppl 3): p. III56-61.

7. Kellar, R.S., et al., *Cardiac patch constructed from human fibroblasts attenuates reduction in cardiac function after acute infarct.* Tissue Eng, 2005. 11(11-12): p. 1678-87.

8. Assmus, B., et al., *Transplantation of Progenitor Cells and Regeneration Enhancement in Acute Myocardial Infarction (TOPCARE-AMI).* Circulation, 2002. 106(24): p. 3009-17.

9. Schachinger, V., et al., *Transplantation of progenitor cells and regeneration enhancement in acute myocardial infarction: final one-year results of the TOPCARE-AMI Trial.* J Am Coll Cardiol, 2004. 44(8): p. 1690-9.

10. Wang, B., et al., *Fabrication of cardiac patch with decellularized porcine myocardial scaffold and bone marrow mononuclear cells.* J Biomed Mater Res A. 94(4): p. 1100-10.

11. Zhuang, J., et al., *Pulsatile stretch remodels cell-to-cell communication in cultured myocytes.* Circ Res, 2000. 87(4): p. 316-22.

12. Yamada, K., et al., *Distinct pathways regulate expression of cardiac electrical and mechanical junction proteins in response to stretch.* Circ Res, 2005. 97(4): p. 346-53.

13. Shanker, A.J., et al., *Matrix-protein-specific regulation of Cx43 expression in cardiac myocytes subjected to mechanical load.* Circ Res, 2005. 96(5): p. 558-66.

14. Rubbens, M.P., et al., *Quantification of the temporal evolution of collagen orientation in mechanically conditioned engineered cardiovascular tissues.* Ann Biomed Eng, 2009. 37(7): p. 1263-72.

15. Akhyari, P., et al., *Mechanical stretch regimen enhances the formation of bioengineered autologous cardiac muscle grafts.* Circulation, 2002. 106(12 Suppl 1): p. I137-42.

16. Zimmermann, W.H., et al., *Engineered heart tissue grafts improve systolic and diastolic function in infarcted rat hearts.* Nat Med, 2006. 12(4): p. 452-8.

17. Fink, C., et al., *Chronic stretch of engineered heart tissue induces hypertrophy and functional improvement.* FASEB J, 2000. 14(5): p. 669-79.

18. Huang, G., et al., *The role of cardiac electrophysiology in myocardial regenerative stem cell therapy.* J Cardiovasc Transl Res. 4(1): p. 61-5.

19. Wikswo, J.P., Jr., S.F. Lin, and R.A. Abbas, *Virtual electrodes in cardiac tissue: a common mechanism for anodal and cathodal stimulation.* Biophys J, 1995. 69(6): p. 2195-210.

20. McDonough, P.M. and C.C. Glembotski, *Induction of atrial natriuretic factor and myosin light chain-2 gene expression in cultured ventricular myocytes by electrical stimulation of contraction.* J Biol Chem, 1992. 267(17): p. 11665-8.

21. Akar, F.G., et al., *Mechanisms underlying conduction slowing and arrhythmogenesis in nonischemic dilated cardiomyopathy.* Circ Res, 2004. 95(7): p. 717-25.

22. Kostin, S., et al., *Connexin 43 expression and distribution in compensated and decompensated cardiac hypertrophy in patients with aortic stenosis.* Cardiovasc Res, 2004. 62(2): p. 426-36.

23. Tatsuya Shimizu, M.Y., Akihiko Kikuchi, Teruo Okano, *Tissue engineering for myocardial regeneration*, in *J Artif Organs*. 2002. p. 6.

CHAPTER VI

SUMMARY, LIMITATIONS, AND FUTURE STUDIES

6.1 Summary

In this project, we successfully developed the acellular porcine myocardial scaffold with well-preserved ECM structure and subtle components and features, which can be a promising scaffold material in thick cardiac patch regeneration. We demonstrated the complete removal of cells, DNA fragments, and α-Gal porcine antigens in the acellular myocardial scaffolds, as well as a constant biodegradation rate rendered by our decellularization procedure. Our histological staining and SEM results all demonstrated that the natural ultrastructure and compositional cues were well preserved. The preservation of cardiac collagen network and cardiac elastin were confirmed; furthermore, the aligned and interconnected myocardial niches can provide nature-designed microenvironments for recellularization. We also demonstrated that vasculature templates were preserved after decellularization and were later resellularized with cells that expressed vWF, an endothelial marker. To better understand the mechanical properties of the acellular myocardial scaffolds (myocardial ECM), we characterized the uniaxial, biaxial, and shear properties of the acellular myocardial scaffolds and compared those properties with the native myocardium. We found that the tensile mechanical behavior along the PD direction was significantly stiffer than along the XD direction. The acellular myocardial scaffolds showed much stiffer tensile properties when comparing with the native myocardium. Unlike the stiffer behavior observed in uniaxial and biaxial

testings, the acellular myocardial scaffolds exhibited a weaker shear resistance, which was 8 times lower than the native myocardium.

To assess the recellularizion potential, we firstly reseeded the acellular myocardial scaffolds with BMMCs using a rotating bioreactor, and observed that the scaffolds showed good cell repopulation, proliferation, viability, and differentiation in about 2 weeks. Both uniaxial and biaxial mechanical data demonstrated the positive tissue remodeling in the reseeded construct. To improve reseeding density, cell alignment and interconnection, and stem cell differentiation, we have built a multi-stimulation bioreactor that is able to apply coordinated mechanical and electrical stimulations to the tissue construct. We found that the recellularization, cardiomyocyte differentiation, and tissue remodeling were more effectively and efficiently promoted by the combined mechanical and electrical stimulations (20% strain + 5 Volt), which produced tissue construct with good cell viability, proliferation, differentiation, mechanical properties mimicking native myocardium, and a trend of angiogenesis within a short period of time (2 - 4 days). In short, the clinical product that we envision will benefit from the natural architecture of myocardial ECM, which has the potential to promote stem cell differentiation, cardiac regeneration, and angiogenesis. The hopes and expectations are that our novel approach will ultimately impact thousands of patients who have suffered significant damage from a prior myocardial infarction.

6.2 Limitations and Future Studies

The decellularization protocol that we currently use generates acellular myocardial scaffolds with thorough decellularization and ECM preservation; however, it takes a relatively long treatment time (~2.5 weeks). We will further optimize the

decellularization protocol in order to achieve effective decellularization within a shorter time period. Other than ultrastructural and mechanical characterizations, the acellular scaffolds will be quantitatively assessed to evaluate the retention of glycosaminoglycans and adhesion proteins such as fibronectin and laminin through immunohistochemistry, ELISA and/or western blot analysis. Retention of growth factor after decellularization will also be evaluated quantitatively using ELISA.[1]

By employing the method of cell injection for recellularization, better cell density, alignment, and interconnection were achieved in a relatively short period of time; however, the cell density that we achieved so far was still low, and there was no evidence of strong cell-to-cell connections in a relatively large range. To obtain an ideal cardiac patch with high cell density, even distribution, and cell-to-cell connections, better reseeding methodologies will be assessed in the future. In current stage, we only applied the Immunohistochemical staining to track the cell phenotypic development; in the future, gene expression levels in tissue construct will be characterized using qRT-PCR analyses. Electrophysiological properties of the engineered patch will also be determined using the microelectrode array technique. If the tissue electrophysiological properties exist, the microelectrode array technique is able to quantify the electrical parameters, such as the excitation threshold, conduction velocity, average amplitude, and maximum capture rate. Another limitation worthy to point out is that, in this dissertation, only BMMCs and MSCs were used for assessing recellularization potential and tissue construct development. In future studies more cell sources, such as embryonic stem cells, cardiomyocytes, induced pluripotent stem cells can be assessed.

Further improvement of the multi-stimulation bioreactor is also a must. The strain control was currently realized by calculating the ratio of the clamp-to-clamp

displacement over the original clamp-to-clamp distance. A more accurate way is the use of real time tissue strain tracking system, in which a CCD camera or high resolution web camera is integrated into the bioreactor system and provide the real time strain measurement and control. It is also a worthwhile effort to monitoring the real time tension level in the tissue construct. Load cells can be mounted into the bioreactor to oversee the mechanical forces experienced by the construct during the tissue remodeling process.

Finally, we will use a well-established rat model to assess the effectiveness of the engineered cardiac patch in cardiac regeneration.[2-4] The reliability and reproducibility of rat left coronary artery (LCA) ligation model guarantee the creation of an acute myocardial infarction within 48 hours.[2, 3, 5] The repairing capacity of the engineered patch can be monitored in real time with echocardiography. If the rat experiment shows the improvement of ventricular functionality and excellent cardiac tissue regeneration, large animal experiment such as pig model will be pursued to further move the study toward eventual clinical trials.[6]

6.3 References

1. Soto-Gutierrez, A., et al., *A whole-organ regenerative medicine approach for liver replacement.* Tissue engineering.Part C, Methods, 2011. 17(6): p. 677-686.

2. Wei, H.J., et al., *Bioengineered cardiac patch constructed from multilayered mesenchymal stem cells for myocardial repair.* Biomaterials, 2008. Epub.

3. Leor, J., et al., *Bioengineered cardiac grafts: A new approach to repair the infarcted myocardium?* Circulation, 2000. 102(19 Suppl 3): p. III56-61.

4. Ozawa, T., et al., *Optimal biomaterial for creation of autologous cardiac grafts.* Circulation, 2002. 106(12 Suppl 1): p. I176-82.

5. Fujimoto, K.L., et al., *An elastic, biodegradable cardiac patch induces contractile smooth muscle and improves cardiac remodeling and function in subacute myocardial infarction.* J Am Coll Cardiol, 2007. 49(23): p. 2292-300.

6. Gilbert, T.W., T.L. Sellaro, and S.F. Badylak, *Decellularization of tissues and organs.* Biomaterials, 2006. 27(19): p. 3675-83.

APPENDIX A

PEER-REVIEWED JOUNAL PUBLICATIONS

1. Bo Wang, Ali Borazjani, Mina Tahai, Amy L. de Jongh Curry, Dan T. Simionescu, Jianjun Guan, Filip To, Steve H. Elder, and Jun Liao. “Fabrication of Cardiac Patch with Decellularized Porcine Myocardial Scaffold and Bone Marrow Mononuclear Cells.” J Biomed Mater Res A. 94(4), 1100-10, 2010

2. Jun Liao, Lauren B. Priddy, Bo Wang, Joseph Chen, and Ivan Vesely. “Ultrastructure of Porcine Mitral Valve Chordae Tendineae.” Journal of Heart Valve Disease, 18(3), 292-299, 2009

3. Corin Williams, Jun Liao, Erinn M. Joyce, Bo Wang, Jennie B. Leach, Michael S. Sacks, and Joyce Y. Wong. “Structural and Mechanical Properties of Decellularized Rabbit Carotid Arteries.” Acta Biomaterialia, 5(4):993-1005, 2009

4. Dan T. Simionescu, Joseph Chen, Michael Jaeggli, Bo Wang, Jun Liao. “Form Follows Function: Advances in Trilayered Structure Replication for Aortic Heart Valve Tissue Engineering." Journal of Healthcare Engineering (in press).

5. Guangjun Wang, Bo Wang, Yi Su, Jun Liao, and David L. Monts. “Application of Raman spectroscopy to tissue-engineered myocardial scaffold.” Applied Spectroscopy (accepted).

6. Bo Wang, Mary E. Tedder, Clara E. Perez, Guangjun Wang, Amy L. de Jongh Curry, Filip To, Steve H. Elder, Lakiesha N. Williams, Dan T. Simionescu, and Jun Liao. “Advanced Structural and Biomechanical Characterizations of Porcine Myocardial Extracellular Matrix.” Journal of Materials Science: Materials in Medicine. (in review)

7. Bo Wang, Alayne Stewart White, Guangjun Wang, Filip To, Amy Curry, and Jun Liao. “Myocardial Scaffold-based Cardiac Tissue Engineering: Application of Coordinated Mechanical and Electrical Stimulations.” Tissue Engineering: Part A (in preparation)

APPENDIX B

CONFERENCE PRESENTATIONS

1. Bo Wang, Clara Esteban Perez, Alayne Stewart White, Filip To, Amy Curry, and Jun Liao. "Myocardial Scaffold-based Cardiac Tissue Engineering: Application of Coordinated Mechanical and Electrical Stimulations." The 9th World Biomaterials Congress (WBC), Chengdu, China, June 1-5, 2012.

2. Bo Wang, Clara Esteban Perez, Alayne Stewart White, Filip To, Amy Curry, and Jun Liao. "Myocardial Scaffold-based Cardiac Tissue Engineering: Application of Coordinated Mechanical and Electrical Stimulations." TERMIS North America 2011 Annual Conference and Exposition, Houston, TX, December 11-14, 2011

3. Bo Wang, Dustin McCallum, Lakiesha Williams, and Jun Liao. "Evaluation of Valuation of Acellular Mitral Valve Scallolds: Anterial Leaflet, Posterial Leaflet, and Chorade Tendinea." ASME 2011 Summer Bioengineering Conference, Famington, PA, June 22-25, 2011

4. Bo Wang, Dustin McCallum, Lakiesha Williams, and Jun Liao. "Evaluation of Acellular Mitral Valve Scaffolds: Anterior Leaflet, Posterior Leaflet, and Chordae Tendineae" BMES Annual Fall Meeting, Hartford, Conn., October 12-15,2011

5. Dan Koback, Ali Borazjani, Sourav Patnaik, Katherine King, Bo Wang, Lakiesha Williams, Jun Liao. "Biomechanical Properties of the Decellularized Human Amnion." BMES Annual Fall Meeting, Hartford, Conn., October 12-15,2011

6. Bo Wang, Clara Esteban Perez, Alayne Stewart White, Filip To, Amy Curry, and Jun Liao. "Design a Bioreactor with Coordinated Mechanical and Electrical Stimulations for Cardiac Patch Tissue Engineering" BMES Annual Fall Meeting, Hartford, Conn., October 12-15,2011

7. Bo Wang, Robbin Bertucci, Zhenqing Li, Lakiesha Williams, Jianjun Guan and Jun Liao. "Effect of Thermosensitive Hydrogel Injection on Mechanical and Ultrastructural Properties of Porcine Myocardium" BMES Annual Fall Meeting, Hartford, Conn., October 12-15,2011

8. Bo Wang, Dustin McCollum, Mary E. Tedder, Dan T. Simionescu, Filip To, Amy L. de Jongh Curry, Lakiesha Williams, and Jun Liao. "The Structural and Biomechanical Properties of Porcine Myocardial Extracellular Matrix." BMES Annual Fall Meeting, Austin, TX, October 7-10, 2010

9. Bo Wang, Ali Borazjani, Jianjun Guan, Amy Curry, Dan T. Simionescu, Filip To, Steve Elder, and Jun Liao, "Decellularized Porcine Myocardium as a Scaffold for Cardiac Regeneration" S 6th Symposium on Biologic Scaffolds for Regenerative Medicine, Napa Valley, CA, April 25 - 27, 2010.

10. Bo Wang, Ali Borazjani, Jianjun Guan, Steve Elder, Amy Curry, Dan T. Simionescu, and Jun Liao, "Fabrication of Tissue-engineered Cardiac Patch with Decellularized Porcine Myocardial Scaffold." Society for Biomaterials Annual Meeting and Exhibition, San Antonio, San Antonio, TX, April 22-25, 2009

11. Bo Wang, Ali Borazjani, Jianjun Guan, Steve Elder, and Jun Liao, “Fabrication of Cardiac Patch with Decellularized Myocardial Scaffold and Mesenchymal Stem Cells.” ASME International Mechanical Engineering Congress & Exposition, Boston, MA, November 2- 6, 2008

12. Bo Wang, Ali Borazjani, Anna Hood, Jianjun Guan, Steve Elder, and Jun Liao, “Tissue Engineered Cardiac Patch using Decellularized Myocardial Scaffold and Mesenchymal Stem Cells.” BMES Annual Fall Meeting, St. Louis, MO, October 2-4, 2008

13. Bo Wang, Ali Borazjani, Jianjun Guan, Steve Elder, and Jun Liao. “Fabrication of Cardiac Patch with Decellularized Myocardial Scaffold and Mesenchymal Stem Cells.” Bio-Inspired Design Conference 2008, Starkville, MS, August 19-22, 2008